Aerodynamic design of a gas turbine rotor blade for the KTH test turbine

William Wiberg and Nicholas Anton

LUNDS UNIVERSITET
Lunds Tekniska Högskola

2013

Division of Thermal Power Engineering
Department of Energy Sciences
Lund Institute of Technology
SE-221 85 Lund, Sweden

Abstract

The purpose of the thesis was to design a new rotor blade for the KTH test turbine according to present design guidelines for gas turbines manufactured at Siemens Industrial Turbomachinery in Finspång. Stage one of a real gas turbine was used as a reference for the aerodynamic design providing a starting point for the project. Using similar gas conditions the new rotor blade was optimized with regard to metal angles and pitch/chord ratio at reference scale. With a satisfying geometry the new blade was scaled back to test turbine size. The blade design could be evaluated and modified using several different in house codes: MAC1, used for meanline design, Beta2 for through flow design, CATO for airfoil design and Multall for 3D design. During the project certain reference specifications restricted the design and had to be considered. ANSYS CFX was used to analyze the final geometry in great detail not possible in any of the other software. The new blade was first analyzed at reference scale and then once again evaluated in Beta2, Multall06 and ANSYS CFX at test turbine scale. As a consequence of generally having low Reynolds number in model tests the results are not entirely comparable with the real case. Effects of transition using different transition models were assessed providing valuable information about the expected differences.

Acknowledgements

This thesis would not have been possible without the help of several dedicated employees at the department of aerodynamics at Siemens Industrial Turbomachinery in Finspång. Especially our supervisor Lars Hedlund who has provided expert guidance and shared much of his extensive knowledge of turbine design during the work, Christoph Mau and Tobias Pihlstrand for their CFX support, Ken Flydalen for providing much needed guidance with design software and answers to many complex questions and Navid Mikaillian for sharing his knowledge of the test turbine.

We would also like to thank Mats Annerfeldt for the fantastic opportunity to write our thesis at the department, Magnus Genrup for initializing the contact and introducing us to exciting world of turbines, Jens Fridh and Johan Dahlqvist at KTH for letting our work become a part of the project TurboAero.

Abstract ..... **i**
Acknowledgements ..... **ii**
List of figures ..... **v**
List of tables ..... **vii**
Nomenclature ..... **viii**
Preface ..... **xi**
Background **1**
1 Theory **2**
1.1 Basic principles 2
1.1.1 Introduction to the gas turbine 2
1.1.2 The ideal gas turbine cycle – Brayton cycle 2
1.1.3 The Euler work equation 6
1.1.4 Velocity triangles 7
1.1.5 Blade geometry 8
1.1.6 Key parameters 9
1.1.7 Degree of reaction 11
1.1.8 Velocity distribution and curvature 12
1.1.9 Zweifel 13
1.2 Vortex theory 14
1.3 Secondary flows 16
1.4 Losses 17
2 The design process **20**
2.1 1D Mean line design 21
2.2 2D Through flow design 21
2.3 2D Airfoil design 22
2.4 3 D Flow analysis – CFD 22
3 Software **24**
3.1 1D Meanline – MAC1 24
3.2 2D Through flow – Beta2 24
3.3 Airfoil design – CATO 24
3.4 3D analysis 24
3.4.1 Multall06 25
3.4.2 ANSYS CFX 14.5.0 26
4 Design Method **27**
4.1 Design constraints 27
4.2 Initial parameter study and scaling 28
4.2.1 Choice of reference stage 28
4.2.2 Channel modification 29
4.2.3 Scaling – Build 4b to reference scale 29
4.2.4 Meanline stage matching of B0F 31
4.3 Initial blade design 32
4.3.1 Pitch to chord ratio 32
4.4 Final design 33

4.4.1 Optimal incidence 34
4.4.2 Airfoil design - Curvature 38
4.4.3 Airfoil - CATO 2D Navier Stokes 41
4.4.4 The final design - B6 44

5 Results 47
5.1 Boundary conditions 47
5.2 Results - Full scale 47
5.2.1 Radial distributions - B6F vs. The reference stage 48
5.2.2 Radial distributions - B6F code comparison 48
5.2.3 CFX results – B6F 52
5.3 Results - Model scale 55
5.3.1 Radial distributions – B6M code comparison 55
5.3.2 CFX results – B6M 59
5.3.3 B6M - Off-design 62
5.4 Transition modelling 67
5.5 Result summary 68

6 Conclusions 70

7 Future work 71

8 Appendix A 72

Bibliography 77

List of figures

Figure 1-1 The Brayton cycle 3
Figure 1-2 Velocity triangles by Siemens definition 8
Figure 1-3 Blade geometry definition 8
Figure 1-4 Schematic velocity distribution 12
Figure 1-5 Qualitative dependence of pitch to chord ratio 14
Figure 1-6 Various forces affecting a fluid element (figure from [1]) 15
Figure 1-7 An example of vortices caused by secondary flow (figure from [9]) 17
Figure 1-8 Influence of incidence on velocity distribution 19
Figure 2-1 The aerodynamic design process. 20
Figure 2-2 Through flow computational domain of the test turbine build 4b 22
Figure 3-1 Multall pinched tip example 25
Figure 3-2 Multall TE cusp 26
Figure 4-1 Design process 27
Figure 4-2 Channel modification 29
Figure 4-3 Channel and blade fitting 31
Figure 4-4 B6M tip recess 34
Figure 4-5 B6F - Relative flow angle at blade leading edge 35
Figure 4-6 B6F - Relative flow angle at blade trailing edge 35
Figure 4-7 B6F - Approximation of relative flow angle at leading edge 36
Figure 4-8 B6F - Approximation of relative flow angle at blade trailing edge 37
Figure 4-9 B6F - Incidence at blade leading edge 38
Figure 4-10 Comparison at mid section with B6F and the reference blade 39
Figure 4-11 Curvature distribution at tip section B6 39
Figure 4-12 Curvature distribution at mid section B6 40
Figure 4-13 Curvature distribution at hub section B6 40
Figure 4-14 Isentropic Laval number at tip section B6F 41
Figure 4-15 Isentropic Laval number at mid section B6F 41
Figure 4-16 Isentropic Laval number at hub section B6F 42
Figure 4-17 Isentropic Laval number at tip section B6M 42
Figure 4-18 Isentropic Laval number at mid section B6M 43
Figure 4-19 Isentropic Laval number at hub section B6M 43
Figure 4-20 Metal angle 45
Figure 4-21 B6M Meridional coordinates 46
Figure 4-22 B6M 46
Figure 5-1 B6F - Vane leading edge 49
Figure 5-2 B6F - Vane trailing edge 50
Figure 5-3 B6F - Blade leading edge 51
Figure 5-4 B6F - Blade trailing edge 52
Figure 5-5 B6F Vane - Mach at 25%, 50% and 75% of span 53
Figure 5-6 B6F Blade - Mach at 25%, 50% and 75% of span 54
Figure 5-7 B6F – Isovolume for Ma>1 54
Figure 5-8 B6F - Isentropic Mach number and blade loading 55
Figure 5-9 B6M - Vane leading edge 56
Figure 5-10 B6M - Vane trailing edge 57
Figure 5-11 B6M - Blade leading edge 58

Figure 5-12 B6M - Blade trailing edge 59
Figure 5-13 B6M Vane - Mach at 25%, 50% and 75% of span 60
Figure 5-14 B6M Blade - Mach at 25%, 50% and 75% of span 61
Figure 5-15 B6M – Isovolume for Ma>1 61
Figure 5-16 B6M - Isentropic Mach number and blade loading 62
Figure 5-17 B6M - Total to total efficiency against pressure ratio (Beta2) 63
Figure 5-18 B6M - Total to static efficiency against pressure ratio (Beta2) 64
Figure 5-19 B6M - Flow capacity against pressure ratio (Beta2) 64
Figure 5-20 B6M - Total to total efficiency against stage loading (Beta2) 65
Figure 5-21 B6M - Mass flow against stage loading (Beta2) 65
Figure 5-22 B6M - Reaction against stage loading (Beta2) 66
Figure 5-23 B6M -Torque against stage loading (Beta2) 66
Figure 5-24 Skin friction coefficient at mid span 68
Figure 8-1 Domain overview 73
Figure 8-2 B6M Vane mesh 73
Figure 8-3 B6M Blade mesh 73
Figure 8-4 B6F - Vane TE looking upstream, total pressure 74
Figure 8-5 B6F – Blade TE looking upstream, total pressure 74
Figure 8-6 B6M - Vane TE looking upstream, total pressure 75
Figure 8-7 B6M – Blade TE looking upstream, total pressure 75
Figure 8-8 B6M – Blade, secondary flow vortices 76
Figure 8-9 B6M – Blade streamlines 76

List of tables

Table 1 Preliminary test turbine constraints after upgrade....28
Table 2 Geometrical constraints....28
Table 3 Reference stage parameters....29
Table 4 Scaling to reference scale....30
Table 5 Meanline stage matching of B0F (MAC1)....32
Table 6 Input and output values associated with Prof. Mamaev's correlation....37
Table 7 Diffusion coefficients for B6F....44
Table 8 Geometrical parameters for the final design....45
Table 9 Boundary conditions....47
Table 10 Transition model vs. Low-Re performance prediction....68
Table 11 Total to total efficiency code comparison....69
Table 12 Stage parameters (Beta2)....69
Table 13 Section parameters (data from CATO)....69
Table 14 CFX mesh statistics....72

Nomenclature

c	[m/s]	absolute velocity
c_p	[kJ/kgK]	specific heat capacity at constant pressure
c_v	[kJ/kgK]	Specific heat capacity at constant volume
Ma	[-]	Mach number
La, λ	[-]	Laval number
n	[rpm]	rotational speed
N	[MW]	power
p	[bar]	pressure
Re	[-]	Reynolds number
T	[K]	temperature
u	[m/s]	tangential blade speed
w	[m/s]	relative velocity
h	[kJ/kg]	specific enthalpy
w	[kJ/kg]	specific work
W	[J]	work
q	[J/kg]	heat per unit mass
Q	[J]	heat
s	[kJ/kgK]	specific entropy
d	[-]	denotes an incremental change
T	[Nm]	torque
v	[m^3/kg]	specific volume
P	[bar]	pressure
η_{th}	[-]	thermodynamic efficiency
m, $\dot{m}$	[kg/s]	mass flow
R_s	[kJ/kgK]	specific gas constant
κ	[-]	ratio of specific heats
E	[J]	total energy
t	[s]	time
ZW	[-]	Zweifel coefficient
PR	[-]	pressure ratio
U	[m/s]	rotational speed
ω	[rad/s]	angular speed
r	[mm]	radius
ν_{ss}	[-]	velocity ratio
h_{ss}	[kJ/kg]	static to static enthalpy drop

D	[-]	diffusion coefficient
α	[°]	absolute flow angle
β	[°]	relative flow angle
δ	[°]	radial clearance
η	[-]	efficiency

κ	[-]	ratio of specific heats
Λ_h	[-]	degree of reaction, enthalpy based
Λ_p	[-]	degree of reaction, pressure based
λ	[-]	Laval number
μ	[Pas]	dynamic viscosity
Π	[-]	total to static pressure ratio
ρ	[kg/m^3]	density
ς	[-]	loss coefficient
ϕ	[-]	flow coefficient
ψ	[-]	stage loading coefficient
Δ	[-]	denotes change
τ	[Pa]	shear stress
TI	[%]	turbulence intensity
C_f	[-]	skin friction coefficient

is	isentropic
0	vane inlet
1	vane outlet
2	blade outlet
u	tangential
a	axial
r	radial
*	total state
$\dot{}$	denotes quantities per unit time
$_0$	denotes total state
$_{tt}$	total to total
$_{ts}$	total to static
$_{cr}$	critical state
$\vec{}$	denotes vector
$_w$	denotes wall

c	[mm]	throat width
b	[mm]	real chord
B	[mm]	axial chord
d_2	[mm]	trailing edge diameter
r_1	[mm]	leading edge radius
r_2	[mm]	trailing edge radius
t	[mm]	pitch
β_{1m}	[°]	inlet metal angle
β_{2m}	[°]	outlet metal angle
δ	[°]	uncovered turning
ω_1	[°]	leading edge wedge angle
ω_2	[°]	trailing edge wedge angle
i	[°]	incidence
AR	[-]	aspect ratio

The figures below show the used definitions regarding blade geometry and flow angles.

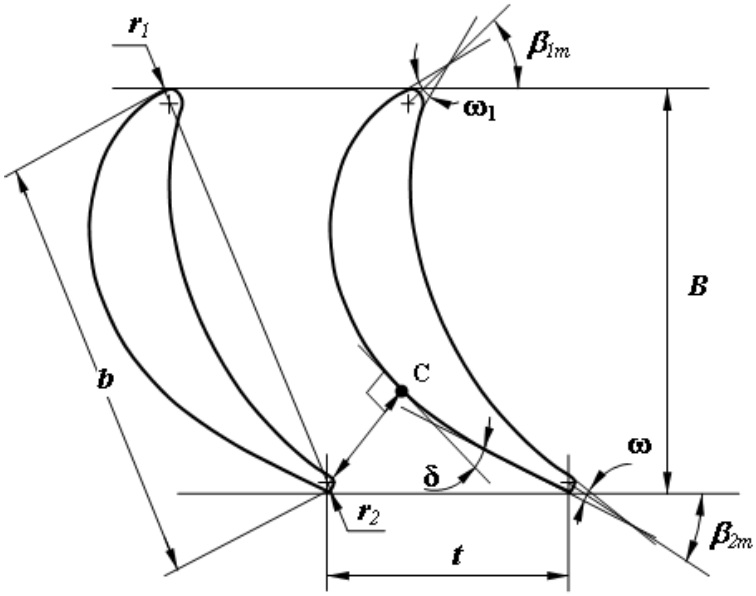

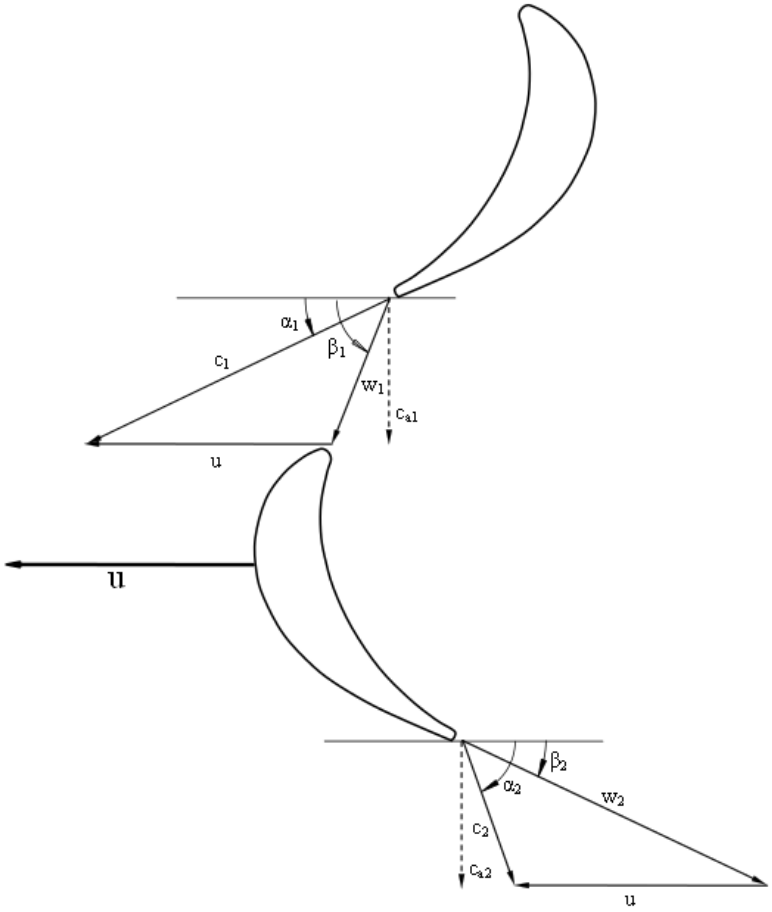

Preface

The thesis consists of two main parts over seven sections. The first part is pure theory based and the second describes the actual work and result of the thesis. A brief summary of the content follows:

- First the fundamental theory of turbomachinery is presented and the relevant parameters are defined. In section 2 the design process of a gas turbine is discussed from an aerodynamic point of view.
- Section 3 describes the different software used.
- The method of the thesis is presented in section 4. This section is to some degree representative of the work process in chronological order:
    - A full scale reference turbine stage is selected among a number of first high pressure stages from SIT gas turbines.
    - A first parameter study is performed.
    - The test turbine is scaled to reference size without cooling flows.
    - Fundamental blade parameters are determined from empirical correlations, e.g. pitch to chord, metal angles.
    - Updated values from 3D calculations results in a refined and final design. The model is scaled back to test turbine size.
- The boundary conditions and the results are presented in section 5 for the different cases:
    - Reference vs. new design
    - Full scale vs. model scale
- Finally the conclusions and the future work are discussed.

Additional results are included in appendix:

- Additional CFX discussion and results are presented in Appendix A.

Background

An air driven test rig owned by Siemens Industrial Turbomachinery but situated at KTH with typical steam turbine blading has been the subject of this thesis. The rig is originally designed for operation with up to three turbine stages but only two stages have ever been used. For the current blading three configurations are possible, build 4a with only the first stage, build 4ab with both stages in series and build 4b with only the second stage. This thesis is a part of the project TurboAero, a collaboration between Siemens, KTH and GKN, where build 4b is subject to a number of upgrades. Afterwards it will be possible to operate at conditions typical for a first stage of an industrial gas turbine excluding the temperature level.

In conjunction with the upgrades this thesis aims to design a new stage for the test turbine that is more representative of current Siemens gas turbines. It will be based on an existing stage from Siemens product portfolio in order to attain a design complying with present design rules.

The current scope of the project only enables the rotor to be switched and the existing vane will remain as a consequence of limited funding. This is one of the major limitations of the new stage since it will restrict the design to some degree. Furthermore the maximum temperature and rotational speed are constrained of structural and safety reasons.

As this thesis will become available to the public domain some results and references have been excluded maintaining sensitive material confidential. However this will not in any way affect the methodology followed or the conclusions.

1 Theory

1.1 Basic principles

1.1.1 Introduction to the gas turbine

The main contributor to the popularity of the gas turbine is without question the aviation industry. For many years the piston engine was the only possible choice of air born propulsion. During the Second World War a lot of effort was put in to developing faster aircraft which in the end led to the first commercial gas turbine engines. They were lighter and a lot more powerful compared to a piston engine of equivalent size. Nowadays using anything else than a gas turbine for aircraft propulsion is almost unthinkable. During the second half of the 20th-century gas turbines were beginning to be used more and more in stationary applications such as mechanical drive and power generation. Gas turbines can be started and ramped very fast which can be of prime importance in certain applications.
When coupled to a steam turbine and used in a combined plant the efficiency can be on par with the best of piston engines.

1.1.2 The ideal gas turbine cycle – Brayton cycle

In essence a gas turbine consists of three major parts: a compressor, a combustor and a turbine. First air is sucked in to the compressor part of the gas turbine where there is an increase in pressure. The flow of air is then mixed with fuel and ignited in the combustor. Finally the hot gas stream is expanded in the turbine and then expelled through an exhaust pipe. Even though the vast majority of gas turbines operate accordingly to the aforementioned process it is absolutely not the only way to make a gas turbine work. Several other ideas have emerged over the years including making use of another working media with external combustion etc.

A gas turbine can be considered a cyclic device hence it is often analyzed using a thermodynamic cycle. By making certain assumptions for example; steady state operation, isentropic turbine and compressor, no pressure loss, constant mass flow, perfect gas, no difference in fluid velocity across the components and so forth, simple analytical expressions of efficiency and specific work can be derived.

It is common to make use of a closed cycle approximation when making the calculations.

In reality this kind of operation is seldom used because of the difficulties associated with heat transfer from the combustion to the working fluid. With the simplifications mentioned above the cycle is said to be ideal and often called the Brayton cycle after its inventor. In Figure 1-1 below the Brayton cycle is described using a temperature entropy-diagram. Between point one and point two the compression process takes place consuming work and raising the temperature of the working media. Energy is added in the form of heat when moving from point two to three causing a large increase in temperature. Work is extracted during the expansion from point three to point four lowering the temperature. Heat is then removed lowering the temperature back to the starting value in order to complete the cycle.

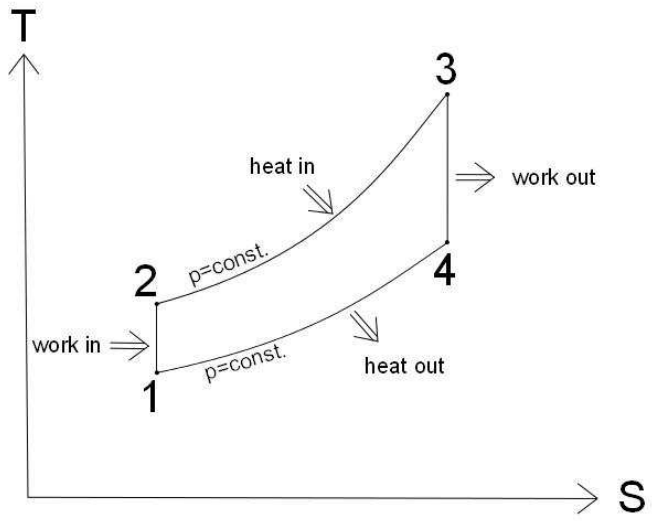

Figure 1-1 The Brayton cycle

In order to conduct an energy analysis a clear definition of what is being considered has to be determined. For this reason a so called system that defines the actual space in which the study is taking place must be constructed. Everything outside of the system boundary is called the surroundings. A system (commonly called a control volume) can be either closed or open depending on if mass is allowed to cross the boundary or not. The system can possess kinetic, potential and internal energy which constitute the total energy of a system neglecting energies associated with surface tension, electric and tension effects. Across the boundary energy can be transferred in the form of work, heat and mass flow. The first law of thermodynamics states that energy cannot be created nor destroyed only transformed between one form to another. This can be expressed mathematically: $E_{in} - E_{out} = \Delta E$ For a steady flow process the above relation becomes:

$$\dot{E}_{in} - \dot{E}_{out} = \frac{dE_{system}}{dt} = 0$$

Rearranged:

$$\dot{E}_{in} = \dot{E}_{out}$$

Mass cannot be created nor destroyed, this simple fact will state that all the mass entering a control volume must also come out during steady state operation:

$$\dot{m}_{in} - \dot{m}_{out} = \frac{dE}{dt} = 0 \Rightarrow \dot{m}_{in} = \dot{m}_{out}$$

Below the governing equations, the energy equation and the continuity equation for a steady flow process will be used in the analysis of the Brayton cycle. By treating each part of the cycle separately using a control volume approach on a per unit mass basis:

Compressor:

$$w_{in} = h_2 - h_1 \tag{1}$$

Turbine:

$$w_{out} = h_3 - h_4 \tag{2}$$

Combustor:

$$q_{in} = h_3 - h_2 \tag{3}$$

The thermodynamic efficiency is defined:

$$\eta_{th} = \frac{W_{net,out}}{Q_{in}} \tag{4}$$

With constant mass flow:

$$\eta_{th} = \frac{w_{net,out}}{q_{in}} \tag{5}$$

The net amount of work done:

$$w_{net,out} = w_{out} - w_{in} \tag{6}$$

Inserting (6) and (3) into (5):

$$\eta_{th} = \frac{h_3 - h_4 - (h_2 - h_1)}{h_3 - h_2} = \frac{h_3 - h_4 - h_2 + h_1}{h_3 - h_2} \tag{7}$$

(7) can be expressed using $h = c_p T$:

$$\eta_{th} = \frac{T_3 - T_4 - T_2 + T_1}{T_3 - T_2} = 1 - \frac{T_4 - T_1}{T_3 - T_2} \tag{8}$$

The Gibbs equation states:

$$Tds = dh - vdP \tag{9}$$

Since both the compression and expansion process are considered to be isentropic the following simplification can be done:

$$Tds = 0 \Rightarrow dh = vdP$$

By using $dh = c_p dT$ and the ideal gas law $Pv = R_s T$:

$$\frac{dP}{P} = \frac{c_p}{R_s}\frac{dT}{T} \tag{10}$$

κ and R_s can be expressed:

$$\kappa = \frac{c_p}{c_v} \tag{11}$$

$$R_s = c_p - c_v \tag{12}$$

Together (11) and (12) can express γ explicitly:

$$\frac{R_s}{c_p} = 1 - \frac{c_v}{c_p} = 1 - \frac{1}{\kappa} \Rightarrow \frac{c_p}{R_s} = \frac{1}{1 - \frac{1}{\kappa}} = \frac{\kappa}{\kappa - 1}$$

(10) rewritten:

$$\frac{dP}{P} = \frac{\kappa}{\kappa - 1}\frac{dT}{T} \tag{13}$$

(13) can be integrated between two arbitrary points:

$$\int_1^2 \frac{dP}{P} = \frac{\kappa}{\kappa - 1}\int_1^2 \frac{dT}{T} \tag{14}$$

Solving the above integral yields:

$$\frac{T_2}{T_1} = \left(\frac{P_2}{P_1}\right)^{\frac{\kappa - 1}{\kappa}} \tag{15}$$

T_2 and T_3 can be expressed:

$$T_2 = \frac{T_2}{T_1}T_1,\ T_3 = \frac{T_3}{T_4}T_4$$

Making use of (15):

$$T_2 = \left(\frac{P_2}{P_1}\right)^{\frac{\kappa-1}{\kappa}} T_1,\ T_3 = \left(\frac{P_3}{P_4}\right)^{\frac{\kappa-1}{\kappa}} T_4$$

The ideal cycle has no pressure losses so:

$$\frac{P_2}{P_1} = \frac{P_3}{P_4} = PR$$

T_2 and T_3 can be expressed as mentioned above and inserted into (8):

$$\eta_{th} = 1 - \frac{T_4 - T_1}{\left(PR^{\frac{\kappa-1}{\kappa}}\right)T_4 - \left(PR^{\frac{\kappa-1}{\kappa}}\right)T_1} = 1 - \frac{1}{PR^{\frac{\kappa-1}{\kappa}}} \tag{16}$$

From (16) it is obvious that the thermal efficiency of the Brayton cycle is only affected by the pressure ratio for a given working fluid. An expression for the specific work will yield a dependency of both pressure ratio and maximum temperature. The temperature also influences the efficiency when component losses are taken into account. However even so the efficiency is much more dependent on the pressure ratio than maximum temperature. Whenever dealing with non ideal processes the concept of isentropic efficiency is very commonly used. It is defined for an adiabatic turbine as the actual work output divided by the ideal work output which corresponds to the actual enthalpy drop divided by the isentropic enthalpy drop. Two different isentropic efficiencies exist, total to total and total to static defined below:

$$\eta_{tt} = \frac{h_{0in} - h_{0out}}{h_{0in} - h_{0out,is}} \tag{17}$$

$$\eta_{ts} = \frac{h_{0in} - h_{0out}}{h_{0in} - h_{out,is}} \tag{18}$$

The reason for defining two different isentropic efficiencies is that the outlet kinetic energy sometimes must be regarded as a loss. For example in a turbine consisting of many stages, the exit kinetic energy for all but the last stage can be used downstream. However for the last stage this is not the case as the kinetic energy possessed by the flow will be of no use outside of the turbine hence it must be considered a loss of energy.

1.1.3 The Euler work equation

All turbomachinery is based on the basic principle derived by Euler in the 18th century. From elementary mechanics the interaction between force and acceleration is well known from Newton's second law of motion, which states that the net force equals the time rate of change of momentum. There is a very similar equation

describing how torque and angular momentum is related. That is the net torque will be equal to the time rate of change of angular momentum. In a generalized turbomachine fluid enters at radius r_1 with the tangential speed c_{u1} and leaves at radius r_2 with the tangential speed c_{u2}. Under the premise of steady flow the torque in the tangential direction can be written:

$$T = \dot{m}(r_2 c_{u2} - r_1 c_{u1}) \tag{19}$$

By definition power is work per unit time that is force times speed which for a rotating device equals torque T times angular velocity ω:

$$N = T\omega = \dot{m}(r_2 c_{u2} - r_1 c_{u1})\omega = \dot{m}(r_2 \omega c_{u2} - r_1 \omega c_{u1}) = \dot{m}(U_2 c_{u2} - U_1 c_{u1}) \tag{20}$$

Since the blade speed is:

$$U = r\omega$$

Dividing (20) by the mass flow yields the specific work:

$$w = \frac{N}{\dot{m}} = (U_2 c_{u2} - U_1 c_{u1}) \tag{21}$$

(21) is the governing equation for the work output of a turbine.

1.1.4 Velocity triangles

When studying turbines so called velocity triangles are very often used in order to get an understanding of how the flow interacts with the blades. The fluid enters the stationary part of the stage, the stator, where it is usually accelerated to some degree in the absolute frame of reference. It then enters the rotating part of the turbine, the rotor. Here the flow normally experiences acceleration in the relative frame of reference. For most gas turbine stages the fluid will accelerate to some extent in both rotor and stator part but there are turbines which behave differently. For example many steam turbines can be of so called impulse design, that is all the acceleration occurs in the stator. In Figure 1-2 velocity triangles for a typical turbine stage have been drawn. Adding the blade speed and relative velocity vectorially yields the absolute velocities:

$$\vec{C} = \vec{U} + \vec{W}$$

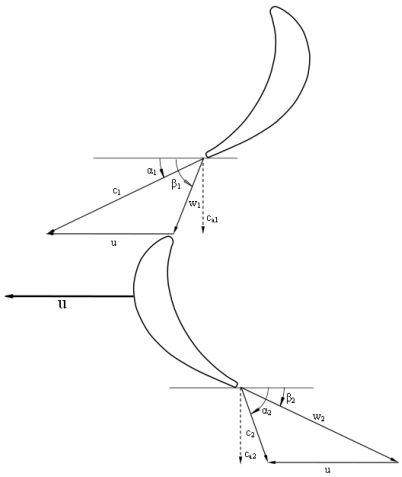

Figure 1-2 Velocity triangles by Siemens definition

The angles corresponding to velocity vectors are measured from the tangential plane which is common in Russian and German literature. In the figure above the axial velocity is constant through the stage as seen from the velocity triangles having equal height. This is a reasonable approximation since in reality the axial velocity generally varies very little through the stage in comparison to the other velocity components. The approximation greatly simplifies the mathematical derivations of expressions relating the shape of the triangles to different key parameters defining the stage.

1.1.5 Blade geometry

In this section some of the common parameters used to describe blades geometrically will be presented. In Figure 1-3 below an arbitrary blade with definitions can be seen:

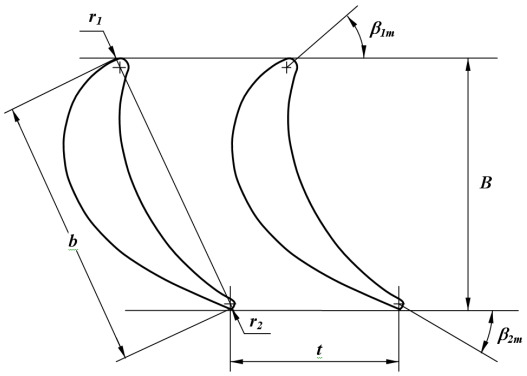

Figure 1-3 Blade geometry definition

The difference between metal and flow angle at inlet is called incidence and at outlet deviation:

$$i = \beta_{1m} - \beta_1$$
$$\varsigma = \beta_{2m} - \beta_2$$

1.1.6 Key parameters

In order to define a gas turbine stage the following set of parameters are often used:

Stage loading is a quantity often used in gas turbine practice and defined as the total enthalpy drop divided by the square of blade speed:

$$\psi = \frac{\Delta h_0}{U^2} \tag{22}$$

Velocity ratio can be seen as the inverse of stage loading and it is often used when studying steam turbines. Defined as the blade speed divided by the square root of two times the isentropic static to static enthalpy drop:

$$\nu_{ss} = \frac{U}{\sqrt{2\Delta h_{ss}}} \tag{23}$$

Flow coefficient is defined as the axial component of the absolute speed divided by the blade speed:

$$\phi = \frac{c_a}{U} \tag{24}$$

Flow capacity is defined as the mass flow times the square root of total temperature divided by the total pressure:

$$Flow\ Capacity = \frac{\dot{m}\sqrt{T_0}}{p_0} \tag{25}$$

Stage reaction enthalpy based:

$$\Lambda_h = \frac{\Delta h_{rotor}}{\Delta h_{stage}} \tag{26}$$

Stage reaction pressure based:

$$\Lambda_h = \frac{\Delta p_{rotor}}{\Delta p_{stage}} \tag{27}$$

For an isentropic process (26) and (27) are equal. This can be derived using Gibbs equation (9) with $Tds = 0$ yielding $dh = vdp$. Using the result in (26) and assuming constant specific volume (and hence constant density):

$$\Lambda_h = \frac{dh_{rotor}}{dh_{stage}} = \frac{vdp_{rotor}}{vdp_{stage}} = \frac{dp_{rotor}}{dp_{stage}} = \frac{\Delta p_{rotor}}{\Delta p_{stage}} = \Lambda_p \tag{28}$$

Both definitions of stage reaction are used in the literature and differ typically a couple of percent but they give the same type of information.

Two dimensionless quantities are very often used when studying the velocity near the surface of a blade. The first one is the Laval number defined as the local velocity divided by the so called Laval velocity:

$$\lambda = \frac{c}{c_{cr}} \tag{29}$$

Using the steady flow energy equation for an arbitrary adiabatic channel between static and stagnation states yields:

$$h_0 = h + \frac{c^2}{2} \tag{30}$$

For a perfect gas with constant c_p equation (30) can be rewritten:

$$T_0 = T + \frac{c^2}{2c_p} \tag{31}$$

The velocity can be expressed:

$$c = \sqrt{2c_p(T_0 - T)} = \sqrt{\frac{2\kappa R_s}{\kappa - 1}(T_0 - T)} \tag{32}$$

A critical speed is defined when the Mach number is unity:

$$c_{cr} = \sqrt{\kappa R_s T_{cr}} \tag{33}$$

This critical speed can also be expressed using (32) and equated to (33):

$$c_{cr} = \sqrt{\frac{2\kappa R_s}{\kappa - 1}(T_0 - T_{cr})} = \sqrt{\kappa R_s T_{cr}} \tag{34}$$

Simplifying the above expression yields:

$$\frac{T_{cr}}{T_0} = \frac{2}{1 + \kappa} \tag{35}$$

Solving for T_{cr} and inserting into (34):

$$c_{cr} = \sqrt{\frac{2\kappa R_s T_0}{1+\kappa}} \tag{36}$$

The ratio of the local speed and the critical speed yields the Laval number, also known as the characteristic Mach number. For a more thorough explanation see Anderson [12].

The second dimensionless quantity often used is the Mach number defined as the local velocity divided by the speed of sound:

$$Ma = \frac{c}{a} = \frac{c}{\sqrt{\kappa R_s T}} \tag{37}$$

Equation (15) can be rewritten between static and stagnation conditions:

$$\frac{T_0}{T} = \left(\frac{p_0}{p}\right)^{\frac{\kappa-1}{\kappa}} \tag{38}$$

Making use of equation (31) and (37) the left hand side of equation (38) can be expressed:

$$\frac{T_0}{T} = 1 + \frac{\kappa-1}{2} Ma^2 \tag{39}$$

By inserting the right hand side of equation (39) into equation (38) an expression for the so called isentropic Mach number can be derived:

$$Ma_{is} = \sqrt{\left(\left(\frac{p_0}{p}\right)^{\frac{\kappa-1}{\kappa}} - 1\right)\frac{2}{\kappa-1}} \tag{40}$$

Equation (40) expresses a Mach number often used when studying velocity distributions along a blade surface. The isentropic Laval number is also often quoted in the same context. It is defined neglecting the influence of friction or viscosity and heat transfer present in the boundary layer i.e. at conditions present for an isentropic process.

1.1.7 Degree of reaction

The degree of reaction describes how the expansion is divided by the stator and rotor blade. A low degree of reaction corresponds to a larger part of the acceleration taking place in the stator than in the rotor. Consequently a high degree of reaction results in the reverse situation. Looking at a simplified stage as the one illustrated in Figure 1-2, mathematical expressions linking degree of reaction and angles can be derived. A common choice is the 50 percent reaction design implying symmetrical velocity

triangles, as in Figure 1-2. The exact choice of reaction is not that critical when considering the efficiency of the stage. Many different philosophies regarding the choice exist and designs with degree of reaction far removed from 50 percent can have high efficiency.

The reaction varies along the span because of varying static pressure and static temperature. As outlined in section 1.2, whenever the flow has a whirl component there must be a pressure gradient for the condition of radial equilibrium to be fulfilled. Looking at a general stage this will mean that the static pressure increases with radius. Corresponding to this change is the velocity distribution that will vary in the opposite way. When designing a stage it is important to check how the degree of reaction varies with radius in order to achieve good efficiency since a too low value in the hub or too high value in the tip tend to be detrimental.

1.1.8 Velocity distribution and curvature

An important part of evaluating the aerodynamic performance of a blade is to study the velocity distribution along the surface. As flow is deflected by the blade an equal but opposite force is exerted on the blade. This force means a net imbalance of pressure that is different pressures on either side of the blade hence the names pressure and suction side. When making an aerodynamic assessment the suction side is of special interest because it is normally more sensitive from an aerodynamic point of view than the pressure side. The gas flowing along the suction side will generally be accelerated to a high speed creating a low pressure zone. However, the flow at the suction and pressure side must join at the trailing edge of the blade fulfilling the Kutta-condition [12]. This means that the flow on the suction side will experience some diffusion which if taken too far can lead to separation. A schematic velocity distribution is displayed in Figure 1-4 showing the velocity plotted versus a surface coordinate for both suction and pressure side.

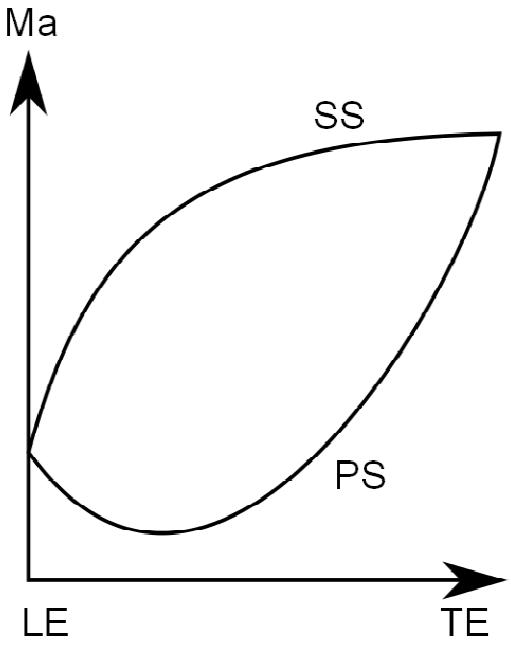

Figure 1-4 Schematic velocity distribution

In order to check for excessive deceleration so called diffusion factors are introduced. From the literature values can be found providing a safe limit for the maximum diffusion allowed. The following diffusion factor is defined as proposed by Prof. Mamaev [10]:

$$D = \frac{\lambda_{\max}}{\lambda_2} - 1 \tag{41}$$

Where $\lambda_{\max}$ is the maximum isentropic Laval number on the suction side and λ_2 is the average isentropic Laval number downstream of trailing edge. The design should comply with $D \le D_{opt}$ [10]. Depending on the value of λ_2 different values of D_{opt} will be used.

The area enclosed by the lines in Figure 1-4 can be thought of as a measure of blade loading. Generally the pressure distribution is almost the complete inverse of the velocity distribution and this integrated along both surfaces will yield the blade loading. Depending on the distribution of loading the blade can be said to be front, mid or aft loaded. The choice of loading is often not explicitly given but depends very much on the design philosophy followed.

In general it is suggested that the velocity should increase smoothly along the surface right up to the point of diffusion giving a continuous acceleration. This provides stability to the flow and avoids unnecessary separations.

When the flow becomes transonic or supersonic shocks can appear leading to increased losses. Since there is no real advantage of having supersonic flow it is often avoided if possible.

A common geometrical parameter used in blade profile design along with velocity distribution is the curvature. It is calculated as a function of the first and second derivative of the polynomials used for describing the profile mathematically, and it should be continuous for the whole profile. The curvature should decrease monotonically towards the trailing edge providing the possibility of having controlled diffusion with minimized risk of separation.

1.1.9 Zweifel

A very common parameter used in turbine design is the Zweifel blade loading coefficient. It is used in order to get a value of the pitch/axial chord ratio which yields minimum losses. Once this coefficient is determined, one can calculate the pitch and hence the blade number if the axial chord is known. If certain assumptions are made for example constant density, constant axial velocity and so on, the coefficient can according to Moustapha et al. [2] be expressed as in equation (42) and equation (43). Note the nomenclature used below. The flow angles are defined using axial definition, s and c_a denote the pitch and axial chord respectively.

For the stator using axial definition:

$$ZW = 2\left(\frac{s}{c_a}\right)\left(\tan(\alpha_1) + \tan(\alpha_1)\right)\cos^2(\alpha_2) \tag{42}$$

For the blade using axial definition:

$$ZW = 2\left(\frac{s}{c_a}\right)(\tan(\beta_2)+\tan(\beta_3))\cos^2(\beta_3) \tag{43}$$

A qualitative reasoning for finding the pitch/axial chord ratio that will yield minimum losses can be as follows. Increasing the pitch/axial chord ratio for a given radius and axial chord means fewer blades that are spaced further apart. A consequence of this is less area being wetted by the fluid and hence lower frictional loss. On the other hand for a given stage work output each blade will have to contribute with a larger quota of work. This corresponds to a higher blade loading which will have greater diffusion losses. A schematic figure of how the pitch/axial chord ratio affects the frictional and diffusion losses can be seen in Figure 1-5. From this it is understood that there is a certain pitch/axial chord ratio which will give minimum losses.

A Zweifel coefficient of 0.75-0.85 used to be quoted as optimal according to Moustapha et al [2]. However nowadays it is not uncommon with coefficients beyond unity. The main contributors to permitting such high values are advanced tools in blade design. Even though blade designers today make use of sophisticated fluid dynamics software during development rather than certain values of the Zweifel coefficient, it is still used to get a rough estimate of what to expect.

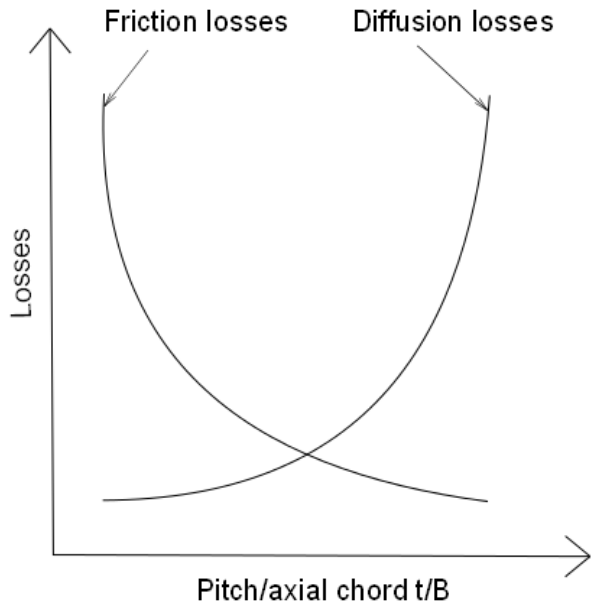

Figure 1-5 Qualitative dependence of pitch to chord ratio

1.2 Vortex theory

The velocity triangle described in the section above will change with radius mainly because of two reasons. The blade speed will increase with increasing radius and the static pressure which will generally not be uniform along the blade. This variation of

pressure will most certainly affect the velocity varying in a similar manner. The reason for this will be explained below along with a design philosophy that can be used to construct the velocity triangles at any arbitrary radius.

A fluid element will generally have velocity components in all three directions radial, axial and tangential. Often the radial velocity is very small compared to the other two especially stages of high hub to tip ratio. A force balance can be derived taking in to account all the forces associated with a fluid element, see Figure 1-6 [1]

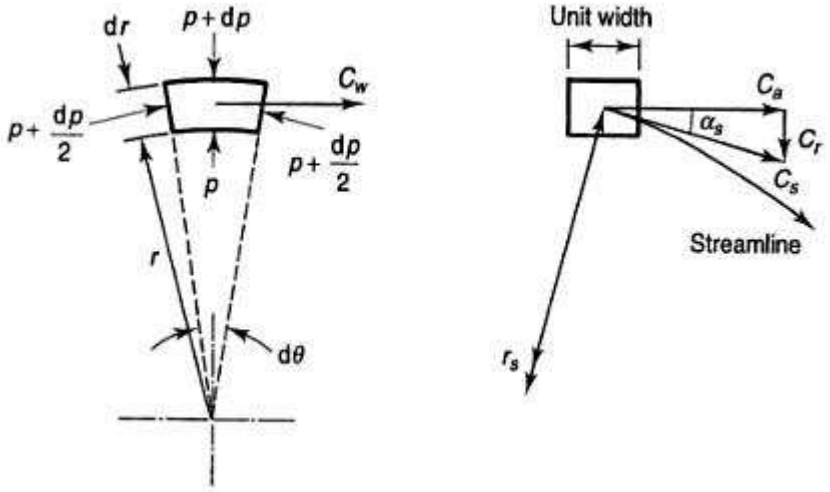

Figure 1-6 Various forces affecting a fluid element (figure from [1])

In the radial direction the fluid element experiences centripetal forces resulting from the tangential velocity, the curvature of the streamline as well as the radial component of force needed to accelerate along the streamline. The resulting pressure force in the radial direction is derived from the figure above. By equating the resulting inertial and pressure force using the nomenclature given by Figure 1-6 one arrives at:

$$\frac{1}{\rho}\frac{dp}{dr} = \frac{c_w^2}{r} + \frac{c_s^2}{r_s}\sin\alpha_s + \frac{dc_s}{dt}\sin\alpha_s \tag{44}$$

Often the terms including r_s and α_s can be neglected since the streamline radius is large and the streamline angle is small due to c_r being considerably smaller than the axial and tangential velocity components resulting in the famous Euler n-equation:

$$\frac{1}{\rho}\frac{dp}{dr} = \frac{c_w^2}{r} \tag{45}$$

Basically the equation above states that whenever the fluid is being deflected and a whirl component is induced a pressure gradient in the radial direction is needed to balance the inertial forces. This equation explains why the static pressure increases from root to tip in a turbine.

Equation (45) will now be used to analytically derive an expression linking the tangential velocity to the radius which will define the velocity triangles at any

arbitrary radius. From the definition of stagnation enthalpy, assuming no radial velocity and by considering incremental changes of stagnation enthalpy with radius:

$$\frac{dh_0}{dr} = \frac{dh}{dr} + c_a \frac{dc_a}{dr} + c_w \frac{dc_w}{dr} \tag{46}$$

From the Gibbs equation the static enthalpy for an incremental change with radius can be derived and substituted above. Neglecting second order terms and making use of the Euler n-equation:

$$\frac{dh_0}{dr} = T \frac{ds}{dr} + c_a \frac{dc_a}{dr} + c_w \frac{dc_w}{dr} + \frac{c_w^2}{r} \tag{47}$$

Under the assumption of no entropy gradient, no variation of stagnation enthalpy with radius and constant axial velocity the equation above reduces to:

$$c_w r = const. \tag{48}$$

Equation (48) is known as the free vortex equation.

1.3 Secondary flows

When the flow turns in the blade passage a pressure gradient must be present according to Euler's n-equation. The fluid in the boundary layer experiences it just like the main flow. However the fluid velocity is lower because of the velocity gradient present in the boundary layer as a consequence of the viscosity. This will imply sharper turning of the flow in this region which can be realized by looking at Euler's equation. For an approximately equal pressure gradient as experienced by the main flow but with a lower velocity, the radius becomes smaller hence the flow will deviate from the general path to some degree. These so called secondary flows will form vortices disturbing the main flow. Even though the flow in a turbine is very complex it is still possible to visualize the vortices at least to some extent. In Figure 1-7 below a schematic illustration is shown.

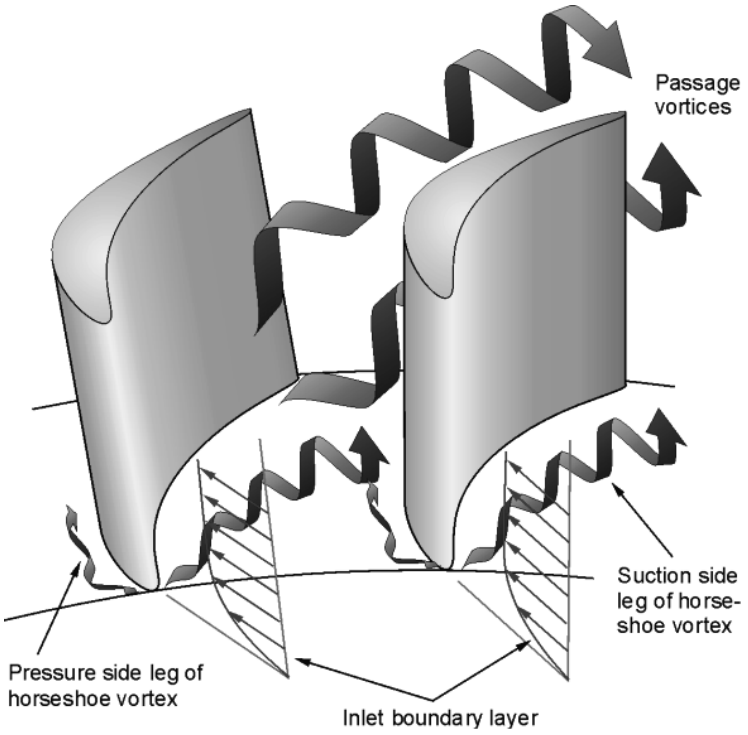

Figure 1-7 An example of vortices caused by secondary flow (figure from [2])

The boundary layer flow at the leading edge of the blade will split and form what is called a horseshoe vortex because of its shape. Downstream passage vortices start to roll up near the blade surface. Generally secondary flows are mainly dependent of aspect ratio and the flow turning. The main flow will be less affected by secondary flows considering blades of high aspect ratio compared to blades of low aspect ratio. This is a consequence of secondary flows being an end wall phenomenon influencing a relatively large part of the passage in the latter case. More flow turning means larger pressure gradient in the blade passage resulting in a greater potential for secondary flow formation.

1.4 Losses

According to Moustapha et. al. [2] there exist many types of loss generating mechanisms in a turbine which can be difficult to differentiate since they often interact in a very complex manner. However three major contributions to the overall loss can be identified:

- **Profile loss -** which can be understood as skin friction on the blade**:** it is dependent on the wetted area, surface roughness, Reynolds number and Mach number.
- **Annulus loss –** end wall friction.
- **Secondary losses -** a consequence of the vortices being a source of momentum and energy loss caused by the secondary flows. As described in section 1.3 they are mainly dependent on the flow turning and aspect ratio.

In the rotor part of a stage an additional major loss is present, tip loss. It is the result of fluid leaking past the rotor blade contributing with little or no work. The reason for this is the tip clearance needed as a result of manufacturing tolerances and operational constraints. The blade will elongate under the centrifugal and thermal load present. Depending on the temperature and material used, blade and casing might differ in thermal growth. Two main leakage paths exist depending on if the blade is shrouded or not. When designed with a shroud, a “roof” is present at the tip making it possible to lock the rotor blades together. This makes it impossible for flow leaking from pressure to suction at the blade tip. Instead the main leakage path is over the shroud from leading to trailing edge. Compared to an un-shrouded blade the tip clearance loss can be considerably lower, however mass has been added at the worst possible location since the stress from centrifugal load will be great at the blade root. For an un-shrouded blade the tip leakage flow from pressure to suction side will form a vortex that together with the secondary flow vortices can create complex flow patterns. Locally at the tip the flow leaking from pressure to suction side will cause underturning. The main flow will in this region experience negative deviation. Considering shrouded blades there will be fewer tendencies for the behavior described above.

One important parameter influencing the losses is the incidence which has great consequences for the blade design. Both profile and secondary losses change with incidence to some extent. The optimal value of incidence minimizing the losses at design point is often called design incidence. This is not achieved at zero degree incidence since the pressure field resulting from the blades being aerodynamically loaded extends somewhat outwards from the leading edge. At off design conditions the blades will experience an incidence angle somewhat different than at design conditions. The velocity distribution will be greatly influenced by incidence causing velocity peaks near the leading edge. Subsequent diffusion can lead to separation if taken too far leading to an increase in losses. Usually negative incidence is less detrimental for the aerodynamic performance compared to positive incidence. The reason for this can be explained considering the velocity distribution for the two cases, see Figure 1-8. At positive incidence the stagnation point will move some distance along the pressure side. This will require the flow to turn considerably before reaching the suction side resulting in a high velocity spike near the leading edge. The flow will experience substantial diffusion which could lead to separation. At negative incidence the flow will reach a high velocity on the pressure side instead. The turning done by the flow and therefore the blade loading is less than for positive incidence becoming less susceptible of separation and associated losses.

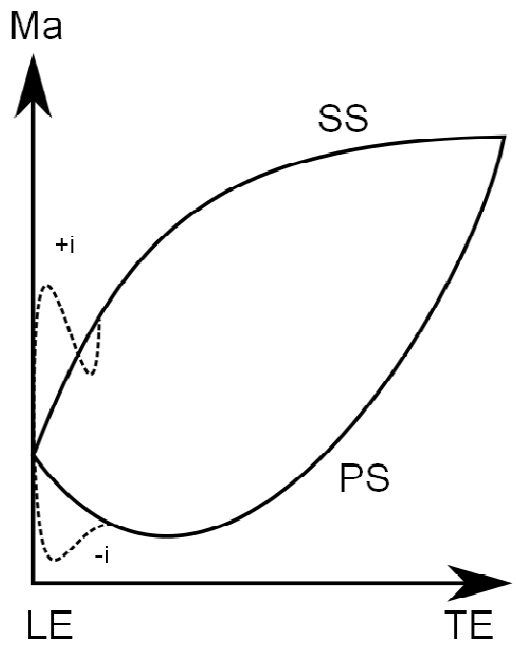

Figure 1-8 Influence of incidence on velocity distribution

2 The design process

The design process of a gas turbine is an iterative process between different phases of complexity where the result from one phase is the input to the following. The design method and work procedure described in this chapter is mainly based on the methodology presented by Moustapha et. al.[2] but is also well represented by the actual procedure used in the industry. Since the task of this thesis was to achieve a scaled design of an existing rotor blade, the design process explained here has not been strictly followed but modified to fit the purpose. Still, the main ideas and goals of each design step are valid and acts as good guidelines of what parameters to modify at each step. In general some basic conditions are initially known, or at least are said to be known, in form of specifications. These conditions naturally depend on the application of the turbine. Different applications require certain specifications that have to be fulfilled. Required output for power generation or thrust propulsion for aeronautic use combined with requirements on machine weight, shaft rotational speed and inlet conditions generally forms the initial starting point for the design. Figure 2-1 shows the basic design process from an aerodynamic design perspective. The different steps will be discussed in the same order as in the work process in the diagram.

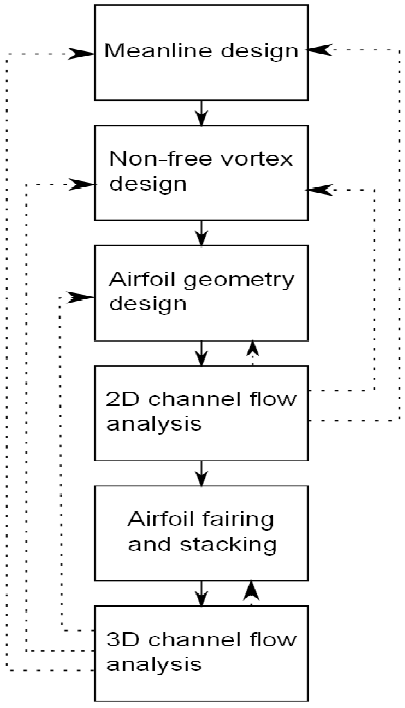

Figure 2-1 The aerodynamic design process.

2.1 1D Mean line design

It is customary to start the design with a meanline 1D design of the turbine. As a one dimensional analysis, no variation in the radial or the tangential direction will be captured and the flow will only be calculated along a streamline at, or close to, the mean radius. However far from representative of the real flow it is sufficient enough as a first approximation. In this phase of the design many of the parameters discussed in section 1 come to play as preliminary guidelines and every manufacturer has its own restrictions regarding the acceptable range of every parameter. For an example, the choice of stage reaction decides the velocity triangles at the leading and trailing edges and is therefore one of the more crucial parameters to decide initially. Again there are many philosophies regarding the choice of optimal stage reaction and no explicit answer exists. The overall purpose of the meanline design is to determine the basic parameters of the turbine at mid radius. Together with empirical or semi-empirical loss models a first estimation of the performance of the turbine stage can be made already at this early stage.

2.2 2D Through flow design

The next step is to consider the radial variations together with the axial variations. This is done in a two dimensional through flow design. Even though no three-dimensional effects can be captured, the main flow behaviour is provided. The goal in the through flow design is to estimate, and optimize, the radial distribution of work in the turbine. This is done by calculating the flow along a number of streamlines at different radii, see Figure 2-2. The radial distribution of the flow is governed by the radial equilibrium equation, see section 1.2, which together with the variation in blade speed governs the velocity triangles at a given radius. One of the earliest design philosophies in turbomachinery was to design with constant specific work across the span. If also the loss and axial velocity distribution is constant over the span the free vortex equation (Equation (48) in section 1.2) can be derived, which for a long time was the praxis of turbine design. The drawback of this method is that the variation of the blade inlet angle may differ greatly from hub to tip which will expose the blade to high mechanical stresses, and nowadays it is more common to apply a non-free vortex design (non constant work distribution across the span). Either way the radial equilibrium must still be fulfilled. Since many of the design parameters are still not decided assumptions have to be made about the flow blockage due to the blades themselves. Further simplifications and assumptions are introduced with respect to boundary layer thickness and losses before the radial equilibrium equation can be solved. The effects of viscosity may be neglected or included in the calculations. A viscous solver, as the name implies, takes viscous effects into account and will give a more physical result at the expense of being more time consuming and the accuracy of the result will still be a coarse approximation of the real flow. An inviscid solver is more dependent of assumptions and correlations but with well calibrated loss models and reasonable assumptions a good result could still be provided. The first result from the through flow calculation has to be validated and most certainly remade later in the design process when further and more accurate information is known from three dimensional flow analysis.
.

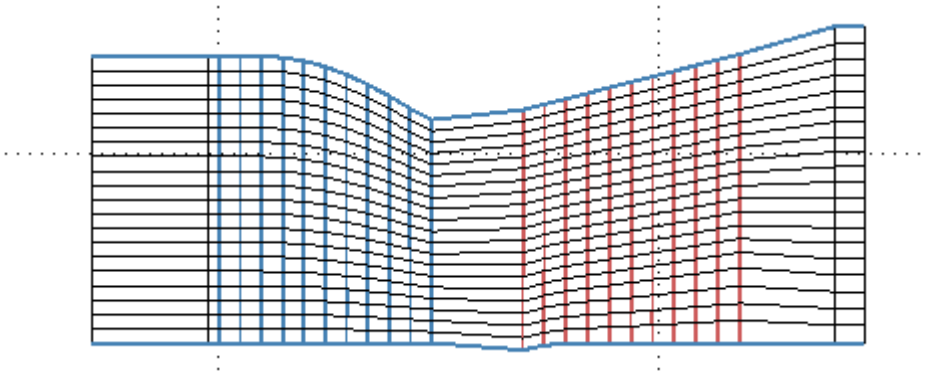

Figure 2-2 Through flow computational domain of the test turbine build 4b

2.3 2D Airfoil design

With the flow conditions given at a number of sections by the through flow design the airfoils for each section can be designed. The number of required sections will depend on the complexity of the blade, where simple blade geometries require fewer sections. At this step the metal angles of the blades will be decided with regard to incidence for the inlet angle and deviation for the outlet angle, see section 1.4. The goal with the aerodynamic design of the airfoils is to minimize the aerodynamic related losses but still fulfill structural and manufacturing limitations and, if necessary, requirements regarding internal cooling flows. Nowadays the actual geometry of the airfoil surface is commonly created by computer programs where the curvature is described by a number of Bezier polynomials. The curvature is defined as a function of the first and second derivate of the coordinates and must be designed without any discontinuities. During the design, the Mach number distribution along the airfoil surface is calculated and the geometry should be optimized to give the desired distribution. Governing parameters could be absolute values, e.g. subsonic Mach numbers, or other parameters as the diffusion coefficient (section 1.1.8). Many airfoil design programs also have functions for loss correlations implemented which directly give the designer further hints about the performance of the airfoil.

When the airfoils at every section have been determined they are stacked and the full three dimensional geometry of the blade is created. There are many ways to stack the sections depending on the design philosophy. To ensure that the centrifugal force on a rotating blade does not introduce any bending moments it is desirable to stack the sections with their centre of mass along a radial line. However, from an aerodynamic point of view it is often desirable to lean or bow the blade to minimize the effects of secondary flow losses and tip leakage. Hence the final design is a compromise between performance and structural limitations.

2.4 3 D Flow analysis – CFD

The final design or control step is a fully three dimensional flow analysis of the proposed design. This is done by CFD (computational fluid dynamics) where the complete Navier Stokes equations are solved to some extent depending on the method. A full 3D simulation of a turbine stage can take from a couple of hours up to weeks or even months to solve depending on the method and the requirements of

accuracy of the solution. The purpose of the CFD analysis is to validate the performance prediction from the through flow analysis or to enlighten unknown flow behavior that has not been accounted for. Based on the CFD result the blade design may have to be reconsidered, in which case the designer has to change the airfoil design or even revisit the through flow or meanline design. It is clear that a good initial design saves a lot of time and the more work and thought spent at the earlier steps, the more likely it is that the designer does not have to redo the whole procedure. Finally it should be said that the results from a CFD calculation are not more accurate than the boundary conditions, which in many cases are not fully known. Even apart from this there are bound to be approximations, both in the model of the blade geometry and in the CFD code with regard to turbulence modeling, numerical discretization etc. and the actual performance of the blade will differ from the calculated result.

3 Software

Throughout the thesis several different codes have been used. A brief description of each program is presented here.

3.1 1D Meanline – MAC1

The meanline calculations were performed with the code MAC1 which is an in-house program developed by Siemens. The code utilizes empirical correlations to calculate and estimate the performance of the turbine. MAC1 was only used in the initial design and no results from MAC1 will be presented in the results section.

3.2 2D Through flow – Beta2

Beta2 is an in-house through flow code developed by Siemens. The correlations used to estimate the losses are based on the same empirical data as in MAC1. In the current version of Beta2 there is an option to activate a simple transition model. All the Beta2-cases were run with this model activated using standard values. This setting gives transition to turbulent boundary layer upstream the point on the suction side where the maximum velocity occurs.

3.3 Airfoil design – CATO

In order to create the rotor blade, sections at different radii were specified and stacked in the in-house software CATO. The geometry for each section is described using so called Bezier polynomials, very often encountered in vector graphics when dealing with smooth curves. It is possible to analyze the sections aerodynamically in CATO using a range of numerical solvers. The computations are relatively fast providing a sound basis for quick evaluation of different designs.

3.4 3D analysis

For the 3D flow analysis two different programs have been used; Multall which is a program based on a code developed by John Denton at Cambridge and the commercial CFD software ANSYS CFX. The programs differ greatly with regards to complexity and serve totally different purposes in the design process. Multall is a relative simple program fine tuned for turbomachinery applications and relies more on robustness and simplicity than the ability to capture every detail in the flow. These properties make it easy to create a working model and allow Multall to be used as a design tool at an early stage in the design process. CFX however, being a commercial software, offers more with regards to complexity and flexibility. It is more suited at a later stage in the design process since a good model is very time consuming to create and to solve. Due to the difference in time cost CFX models were only created for what is to be considered as the final design of the test turbine stage. Multall, however, was present much earlier in the design process and used to iterate between 2D and 3D calculations until a final design was achieved.

One of the main purposes of the CFX model was to investigate to what extent the boundary layers are laminar at model scale, and no reliable method to model

transition is implemented in Multall. This is of great concern since the Reynolds number at model scale is uncharacteristically low in comparison to typical values of a first stage in a full scale gas turbine. In the Multall code fully turbulent boundary layers are assumed while two cases were tried for the CFX models; one with fully turbulent boundary layers (referred to as Low-Re) and another with a semi-empirical transition model (γ-θ model) activated. The details of the γ-θ transition model which is implemented in CFX falls outside the scope of this thesis but more details can be found in the CFX theory guide [6] and Langtry's and Menter's report [11]. The settings for each case will be presented here in short and a more detailed description is given in Appendix A.

3.4.1 Multall06

Multall06 is a steady-state code and only one cascade passage was modeled.
The turbulence model used in Multall is the Baldwin-Lomax model which is a zero equation model used together with wall functions. The Baldwin Lomax model is well suited for attached high speed flows and is known to be robust and reliable for turbomachinery applications [5]. The boundary layers are assumed to be fully turbulent since no verified transition criterion is implemented in the code. Tip clearance is modeled with a pinched tip method where the blade progressively thins out across a number of cells near the casing. This method enables simple and quick meshing but may give unrealistic flow physics with high Mach numbers at the tip if care is not taken. An example of how the pinched tip method was used can be seen in Figure 3-1. The trailing edges are modeled with a so called "cusp" to force the flow to separate at the trailing edge. Without cusp, the flow stays attached and is accelerated around the curvature of the trailing edge, again causing unrealistic physics and high Mach numbers. Figure 3-2 shows the cusped trailing edge of one of the modeled blades.

Figure 3-1 Multall pinched tip example

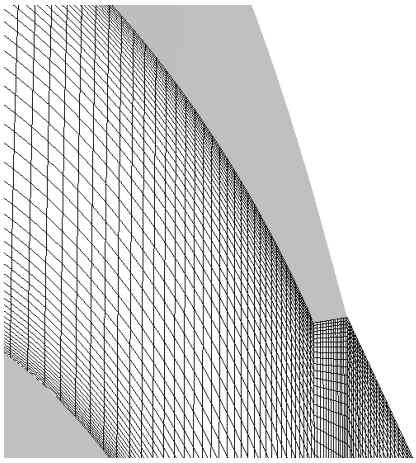

Figure 3-2 Multall TE cusp

3.4.2 ANSYS CFX 14.5.0

The mesh for CFX was created by the meshing software TurboGrid which is especially developed for meshing of turbomachinery parts. Since one of the purposes of creating a CFX model to begin with was to investigate the effects of turbulent transition, the mesh had to be fine enough to resolve the boundary layers. TurboGrid is limited to hexahedral mesh (structured mesh) which makes it unavoidable to have very large element aspect ratios and element expansion rates if sufficient y^+ values are to be achieved. This particularly becomes a problem at the tip clearance where the velocity gradients are very large and the mesh quality is inevitable poor. To overcome initial instabilities at the tip clearance region every case was run with a local “timescale” during the initial iterations. Later on the timescale was increased and switched to the same for the whole domain to ensure convergence. For the cases at full scale this method was not enough and the mesh refinement at the tip clearance had to be sacrificed to reach a solution. Further details are presented in Appendix A. The SST k-ω model with standard values was chosen to model the turbulence. The model is widely used for turbomachinery flow simulations and also compatible with the γ-θ transition model. CFX allows for transient solution where the whole stage can be modeled. However, such approach is very demanding computational wise and it was sufficient to model just one passage and to assume steady state.

4 Design Method

The method of this thesis has in many ways followed the steps of the design process described in section 2 though with some important deviations. As the task was to develop a blade for an existing turbine stage and with the aim to mimic a full scale turbine, many conditions were already decided in beforehand. With the geometry of the KTH test turbine given, the most fundamental geometrical parameters of the gas channel were fixed. Since the existing vane will remain the flow and geometrical characteristics of the stage will be limited. For example, the trailing edge thickness of the vane is not representative of a cooled gas turbine stage and these restrictions have to be considered during the blade design.

It is important to point out that the presented design process in this report is only intended so serve the purpose of describing the main methodology used to reach the final design proposal. As the project went on new constraints were set and earlier known specifications had to be reconsidered. Consequently the actual design process was all but straightforward with several blade versions which were updated and optimized as new information become known. After every major change in blade geometry all the design criteria had to be reconsidered and controlled once again, e.g. optimal pitch to chord, number of blades etc. It serves no purpose to, in detail, describe all the minor adjustments made during the work but instead the main design steps are described together with the major changes that occurred during the design which ultimately resulted into the final design. A condensed version of the actual procedure is seen in Figure 4-1. The following sections will describe the different design phases in further detail.

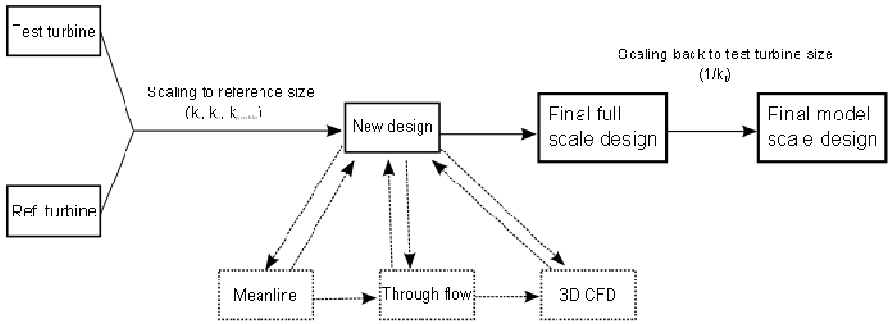

Figure 4-1 Design process

4.1 Design constraints

During the design several limitations of the KTH test turbine had to be considered, not only strict geometric parameters to ensure that the new blade will fit the channel but also regarding structural and safety constraints. The final specifications of the test turbine after the planned upgrade are to yet to be decided at the time of writing but preliminary target specifications are presented in Table 1.

Parameter	Maximum value	Limiting factor
Pressure ratio [-]	2	Outlet temperature
Inlet temperature [K]	333	Safety regulation
Outlet static temperature [K]	283	Dew point at outlet pressure
Mass flow [kg/s]	4.7	Compressor rating
Shaft speed [rpm]	13000	Structural

Table 1 Preliminary test turbine constraints after upgrade

Earlier calculations done at Siemens suggest that neither the mass flow nor the shaft speed will exceed their maximum allowed values for any relevant test case for the test turbine [7]. The pressure ratio however is greatly limited by the inlet temperature constraint. Since the outlet temperature is to be held above the dew point the inlet temperature will increase if the pressure ratio is to be increased. A higher pressure ratio is desirable if the stage is to be redesigned to better represent a gas turbine stage and because of this the test turbine casing may have to be insulated to allow a further increase in inlet temperature.
Pure geometrical constraints are the channel height, the axial distance between the vane and blade to allow for probe traversing and the axial width of the blade disc, see Table 2. During the design of the new blade further consideration had to be made regarding the minimal length of the chord of the new blade. This since the limitations of the manufacturing were not fully known at the time of the design.

Parameter	Value
Tip clearance [mm]	0.3
Max axial blade width [mm]	~ 25
Axial gap between vane TE and blade LE at mid span [mm]	10

Table 2 Geometrical constraints

4.2 Initial parameter study and scaling

4.2.1 Choice of reference stage

A number of Siemens gas turbines were studied in a meanline and geometric analysis. Several parameters were considered as; stage loading, vane flow angles (important since the existing vane will be left as it is), degree of reaction, r_{tip}/r_{hub} *etc.* One of the turbine stages was chosen and will hereafter be referred to as the reference turbine. The considered flow parameters of the reference are seen in Table 3 and these values acted as “target parameters” during the initial design.

	Reference stage
Π [-]	2.155
ψ [-]	1.385
$\Lambda_{p,mid}$ [-]	0.412
Φ [-]	0.412
Ma_{2rel} [-]	0.818

Table 3 Reference stage parameters

4.2.2 Channel modification

The first change to the current model of the test turbine build (build 4b) was to set the blade shroud hade angle to zero as seen in Figure 4-2. This in accordance with how the gas channel commonly is designed for the first rotor blade due to tip clearance limitations with respect to axial displacement during transients.

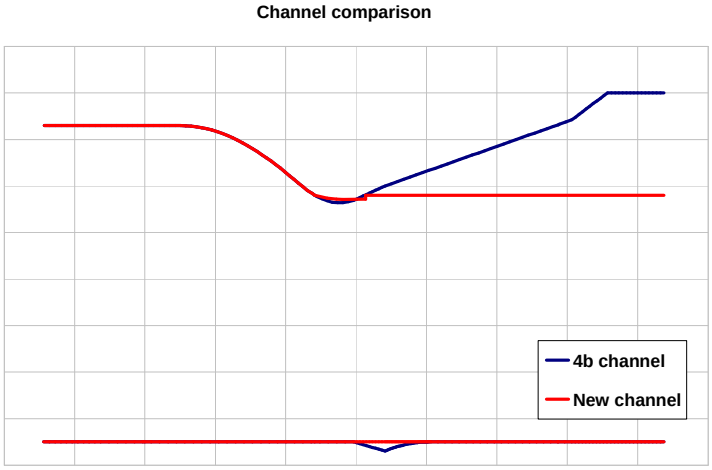

Figure 4-2 Channel modification

Compared to the original 4b, the change to the new channel decreased the outlet area which, for given inlet conditions, increase the acceleration over the rotor blade and therefore causes an increase in reaction. Since the existing build has a low degree of reaction typical for steam turbines, this is a change in the desired direction.

4.2.3 Scaling – Build 4b to reference scale

With a suitable turbine set as reference the next step was to evaluate the most appropriate way to perform the actual geometrical scaling. The radial coordinates were scaled with a radial factor k_r:

$$k_r = \left[\frac{r_{hub,ref}}{r_{hub,4b}} \right]_{vaneoutlet}$$

This will result in a very short axial chord when the blade is scaled back to test turbine dimensions because of the aspect ratio difference. As a consequence of the uncertainties regarding manufacturing of blades that small, it was desirable to increase the axial width of the blade. With this in mind the axial chord of the new design was set to the maximum allowed in the test turbine. This approach will result in a blade with much larger axial chord and smaller aspect ratio than the reference blade. Even though undesirable this deviation from the reference was said to be necessary.

The new blade will be referred to as BxF/BxM where B - blade, x – number indicating the design version, M/F stand for model and full scale design respectively. The first design version introduced here is B0F where no modification but pure scaling was performed to the original blade geometry.

Since the aspect ratio of the reference blade could not be kept in the B0F design, the airfoil geometry had also to be scaled in order to conserve the relative profile geometry. The profile factor was defined as:

$$k_{profile} = \frac{k_r \cdot B_{hub,4b}}{B_{hub,ref}}$$

The relative conicity of the reference blade was to be maintained which was achieved by calculating the axial chord at the tip section by the factor k_c:

$$k_c = \frac{B_{tip,ref}}{B_{hub,ref}}$$

In Table 4 a geometrical summary of the first design B0F can be seen. Figure 4-3 shows the channel and blade fitting to the reference scale. As a first assumption the axial distance between the vane and the blade at mid span is kept the same as in the reference. The decrease in hub radius at the trailing edge for the reference casing shown in Figure 4-3 is neglected in further calculations and the hub radius is said to be constant.

	ref blade 1	**B0F**
$\mathbf{r_{hub}}$	$r_{hub,ref}$	$k_r \cdot r_{hub,4b}$
$\mathbf{r_{tip}}$	$r_{tip,ref}$	$k_r \cdot r_{tip,4b}$
$\mathbf{B_{hub}}$	$B_{hub,ref}$	$k_r \cdot B_{hub,4b}$
$\mathbf{B_{tip}}$	$B_{tip,ref}$	$k_c \cdot B_{hub,BxF}$
LE diameter (mid)	$d_{1,ref}$	$k_{profile} \cdot d_{1,ref}$
TE diameter (mid)	$d_{2,ref}$	$k_{profile} \cdot d_{2,ref}$

Table 4 Scaling to reference scale

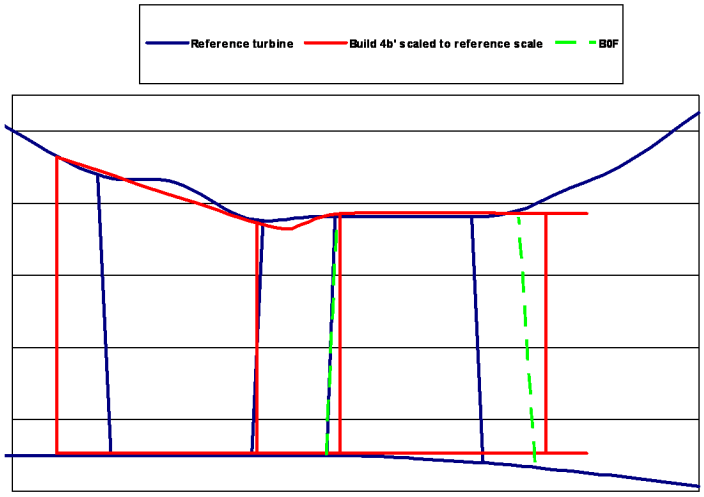

Figure 4-3 Channel and blade fitting

4.2.4 Meanline stage matching of B0F

The next step was to determine the pitch to chord ratio which in turn will decide the number of blades. Many correlations exist for calculation of optimal pitch to chord ratio, e.g. the Zweifel coefficient discussed in section 1.1.9, and SIT has their own versions used in this thesis. To provide the relevant parameters for the correlations a meanline stage matching of B0F was performed. The calculation was done with the same number of blades and at the same rotational speed as the reference stage. The axial chord at mid span was at this stage approximated as a mean of the hub and tip values and the real chord was calculated by conserving the *B/b*-ratio of the reference. Special concerns had to be considered regarding the cooling flows of the reference stage. Since it is too complicated to recreate such flows in the test turbine stage B0F was modeled without any cooling injections. In order to preserve the characteristics of the reference turbine the inlet temperature and the blade throat area had to be adjusted properly due to lack of cooling. It was decided that an appropriate approach was to adjust the inlet temperature for B0F so that the same relative total temperature at the blade inlet was achieved. Ideally it was desirable to achieve matching degree of pressure based reaction and at the same time have matching blade outlet Mach number, $Ma_{2,rel}$, to get a good agreement of stage characteristics. This however was not possible within the limits of the design constraints and it was decided to prioritize the matching of the outlet Mach number. To compensate for the smaller mass flow through the B0F blade passage the throat area had to be decreased if the same blade outlet Mach number was to be achieved.
This was done by manual modification of the throat area in the meanline code input file until the same relative Mach number at the blade outlet was reached. The result from the meanline stage matching is presented in Table 5. Although without cooling B0F experiences very similar flow conditions compared to the reference stage.

	Reference stage	B0F
Π [-]	2.155	2.154
ψ [-]	1.385	1.363
$\Lambda_{p,mid}$ [-]	0.412	0.404
Φ [-]	0.412	0.431
α_1 [°]	14.52	14.72
β_1 [°]	63.00	55.17
α_2 [°]	71.23	71.15
β_2 [°]	19.91	20.60
Ma_{1abs} [-]	0.787	0.793
Ma_{1rel} [-]	0.206	0.237
Ma_{2rel} [-]	0.818	0.817
La_{2rel} [-]	0.836	0.835
Re_{1abs} [-]	29.75e5	29.14e5
Re_{2rel} [-]	15.90e5	21.20e5

Table 5 Meanline stage matching of B0F (MAC1)

4.3 Initial blade design

4.3.1 Pitch to chord ratio

In order to determine the optimal pitch to chord ratio, $\bar{t}_{0nm}$, with regard to flow angles, Laval number and trailing edge thickness Prof. Mamaev's guidelines [4] were used. The correlation is a function of three coefficients, $\bar{t}_{0nm_O}$ is the optimal pitch chord for a reference exit Laval number, K_{KP} is a correction for a reference trailing edge diameter and $\Delta\bar{t}_{0nm}$ is a correction for exit velocity:

$$\bar{t}_{0nm} = f(\bar{t}_{0nm_O}, K_{KP}, \Delta\bar{t}_{0nm})$$

The first coefficient on the right hand side is dependent on the inlet and outlet flow angle, the second one on trailing edge diameter and the third one on exit Laval number. The coefficients are determined by reading values of graphs using input flow parameters from previous MAC1 results together with the trailing edge diameter defined above in Table 4. As soon as the pitch chord ratio is determined the number of blades can be found for a given chord and radius. The only geometric parameter known at this stage is the axial chord at the hub. In order to retain the characteristics of the reference it was determined that B0F should have the same conicity factor k_c. With k_c the axial chord at tip and mid can be calculated. The value at mid section is simply an average of the hub and the tip section. The ratio of real chord to axial chord at mid has been conserved just like the conicity factor:

$$k_r = \left[\frac{b}{B}\right]_{mid,ref} = \left[\frac{b}{B}\right]_{mid,B0}$$

Both k_c and k_r have been calculated from a CAD-model of the reference stage. By using the ratio above the chord at mid section for B0F can be determined and it was used together with the axial chord at mid in the MAC1 calculations. The corresponding radius at mid is the average value of hub and tip section from input to the 1D calculation.

With known values of radius, chord and pitch chord ratio the number of blades can be calculated:

$$Number\ of\ blades\ = \frac{2\pi R_{mid}}{\left[\frac{t}{b}\right]_{opt} b_{mid}} \cong 45$$

The data used as input to calculate the pitch chord ratio was generated with the same number of blades as the reference since the program required this parameter in order to run. After optimizing, the number of blades is now 45 and new data will be generated to check the values of different flow parameters corresponding to 45 blades. Fortunately the number of blades does not influence the flow angles or the exit relative Laval number to a very large extent. Subsequent calculations with updated input values yield the same result and the blade number have been fixed throughout the rest of the design process.

In the used airfoil profiling software CATO the real chord cannot be set. The reason for this is the way the geometrical parameters are defined in the software, the real chord is calculated as an output geometrical parameter among others. Hence the pitch to chord ratio of the final design will differ to some degree compared to the optimal value.

4.4 Final design

All blade optimization was performed at the reference scale. However it should once again be clarified that the full scale design is a fictive turbine. Once the blade and the stage is as good as it can be at reference scale the geometry is directly scaled back to test turbine dimensions. The same factor, k_r, as before is now used for the downscaling of the entire geometry.

It was stated early in the work that the new turbine should be designed with a so called tip recess, which means that there is a small overlap between the blade tip and the upstream casing. The purpose of this design is to intentionally cause a separation of the flow at the recess, hence minimizing the tip leakage flow. The details regarding the actual geometry of the casing in the region between the vane trailing edge and blade leading edge were initially not fully determined. Later on in the work process it was realized that the current design would not fit if the existing casing contour where to be kept. In order to still design with a tip recess without violating the casing curvature far too much, a compromise was made. The casing was changed to some degree and the blade tip radius decreased enabling a tip recess according to SIT guidelines. A close up of the proposed casing design is shown in Figure 4-4.

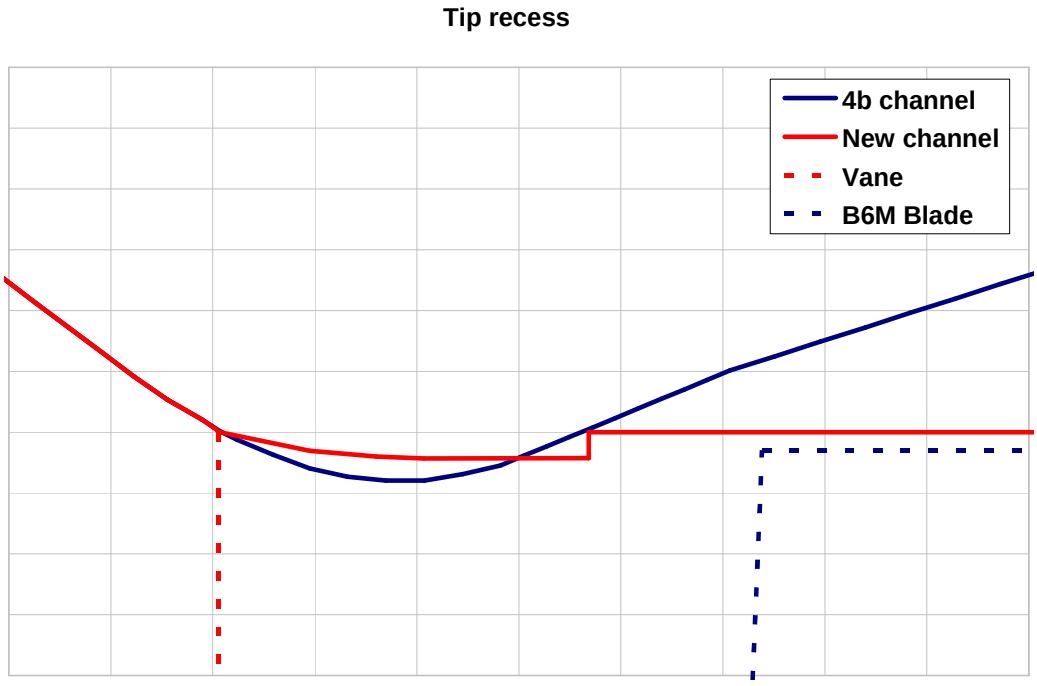

Figure 4-4 B6M tip recess

The decrease of the casing radius at the blade naturally decreases the blade throat area, accelerating the flow more than intended. An increase in acceleration in the rotor increases the degree of reaction and the outlet Mach number. To compensate for this effect the throat area had to be increased until the target Mach number once again could be achieved with the new casing design. This was done by rotation of the blade, causing an increase in blade outlet metal angle. The blade geometry with adjustments to the new channel is from now on referred to as B6F/B6M for full and model scale respectively. Earlier versions have only acted as necessary design steps and it serves no purpose to show results from any of these. The design methodology regarding inlet metal angle and curvature for the B6 geometry is presented in the following sections 4.4.1 and 4.4.2.

4.4.1 Optimal incidence

As described in section 1.4 there is a certain value of incidence that corresponds to minimum losses associated with this parameter. When designing the blade inlet metal angles Prof. Mamaev's correlations for finding optimum incidence has been used at hub, mid and tip. After optimizing with regard to incidence the three sections have been stacked in order to create the blade.

The starting point for determining the incidence has been radial distributions of flow angle at the blade leading and trailing edge from the through flow code Beta2. Based upon the 2D results the first 3D model was created. The 3D calculation predicted different flow angles, resulting in a different optimal blade twist. Based on the 3D computation the blade inlet metal angle was updated resulting in a refined blade version.

Below some of the results from Beta2 and Multall (3D-code) can be seen for B6F in Figure 4-5 and Figure 4-6. The values of relative flow angles at hub, mid and tip were used as input to Prof. Mamaev's correlations.

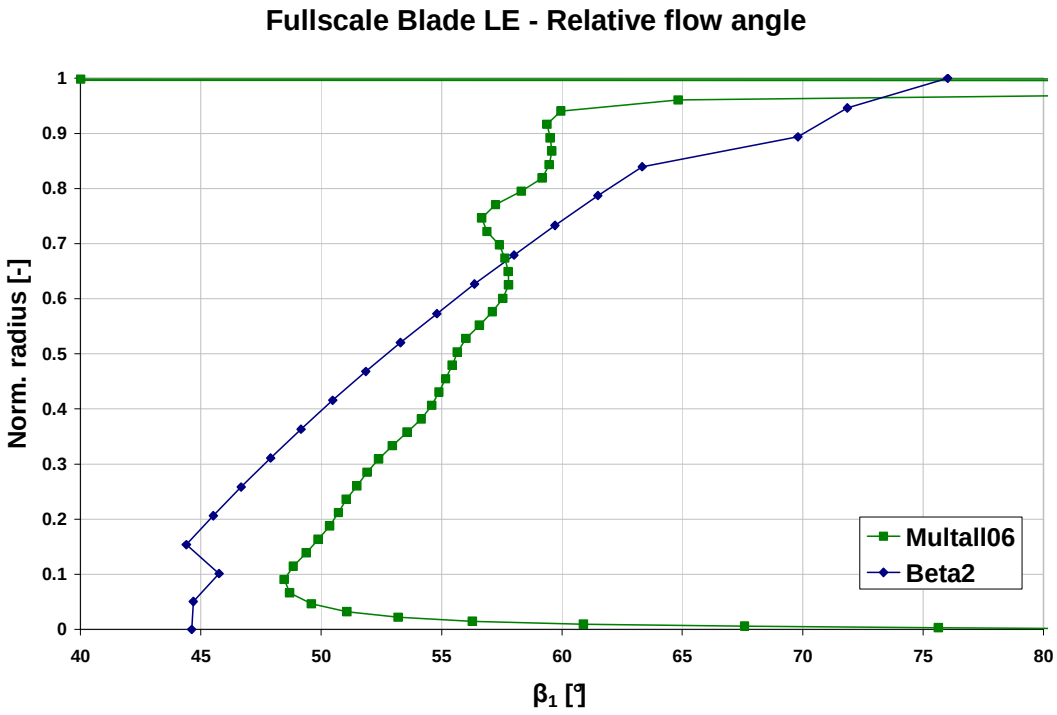

Figure 4-5 B6F - Relative flow angle at blade leading edge

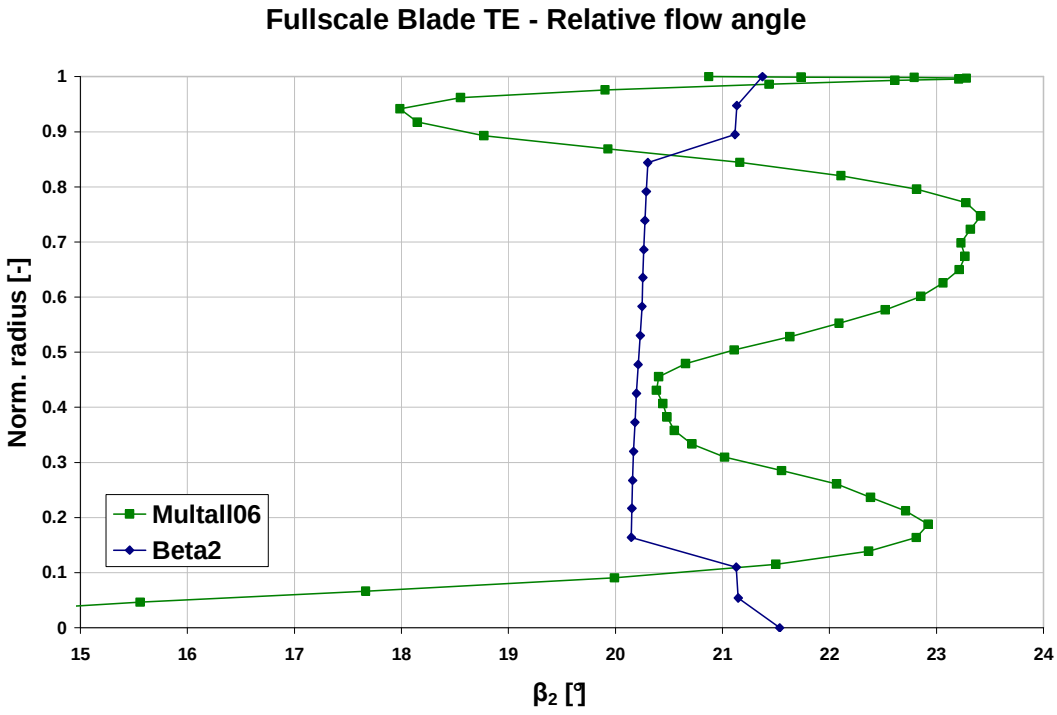

Figure 4-6 B6F - Relative flow angle at blade trailing edge

In order to obtain the inlet relative flow angles at hub and tip from the Multall06 results in Figure 4-5 a line is inserted from an extrapolation between two points at approximately 10 and 90 percent of normalized radius. The reason for this is the behavior at the extremes. At the region towards the blade hub and tip many complex flow patterns affect the angles considerably as can be seen in Figure 4-5. It would have been unreasonable to design exactly to these since they do not represent the flow in general at hub and tip. This can be seen when comparing to the Beta2 results. The extrapolated line is seen in Figure 4-7. In the same figure the angle at mid can be found simply by reading of the x-axis corresponding to a normalized radius of 50 percent.

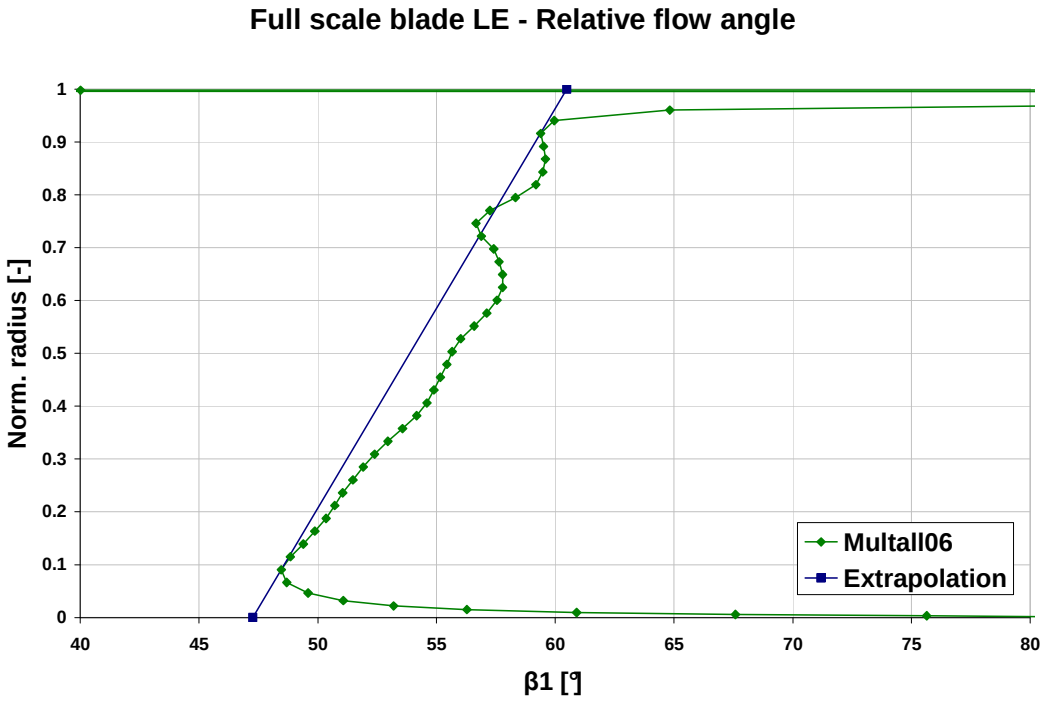

Figure 4-7 B6F - Approximation of relative flow angle at leading edge

By looking at the Multall06 results in Figure 4-8 the outlet relative flow angle varies considerably over the blade span. This is an effect of secondary flow vortices. The amplitude of the variation though is relatively small, just a few degrees, excluding the values near the hub. In the graph used for determining the blade inlet metal angle the influence of β_2 is very small especially in the region being considered. Along with the fact that the precision in reading of a graph is not greater than a couple of degrees, β_2 was kept constant at 20˚ as an approximation. A vertical line is superimposed in Figure 4-8 showing that this value is not that far off at 10, 50 and 90 percent of normalized radius.

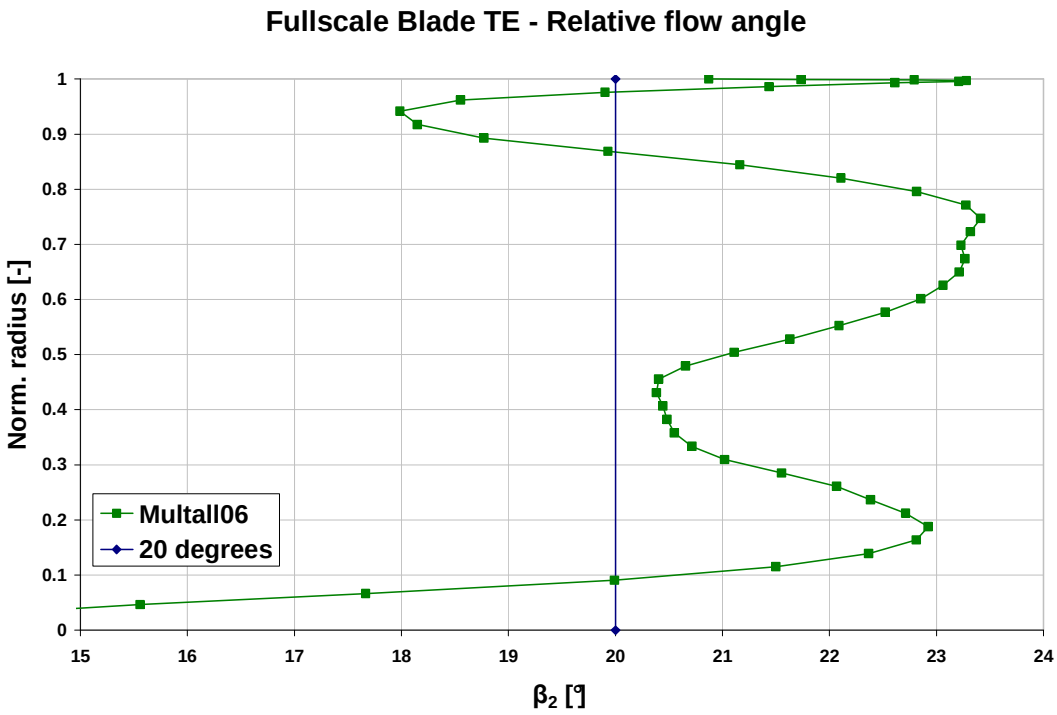

Figure 4-8 B6F - Approximation of relative flow angle at blade trailing edge

Considering the Beta2 results in Figure 4-7 and Figure 4-8 the flow angles have been obtained just by reading of the x-axis at 0, 50 and 100 percent of normalized radius. In the table below, the angles used as input to Prof. Mamaev's correlation from the figures above and the resulting metal angles for B6F can be seen based on both Beta2 and Multall06 results.

B6F			
	Hub	**Mid**	**Tip**
β_1 [°] Beta2	45	53	76
β_2 [°] Beta2	22	20	21
β_{1m} [°] Beta2	51	59	77
β_1 [°] Multall06	47	56	61
β_2 [°] Multall06	20	20	20
β_{1m} [°] Multall06	56	62	66

Table 6 Input and output values associated with Prof. Mamaev's correlation

Figure 4-9 below shows a plot of the resulting incidence after optimizing accordingly to the Multall06 results in Table 6.

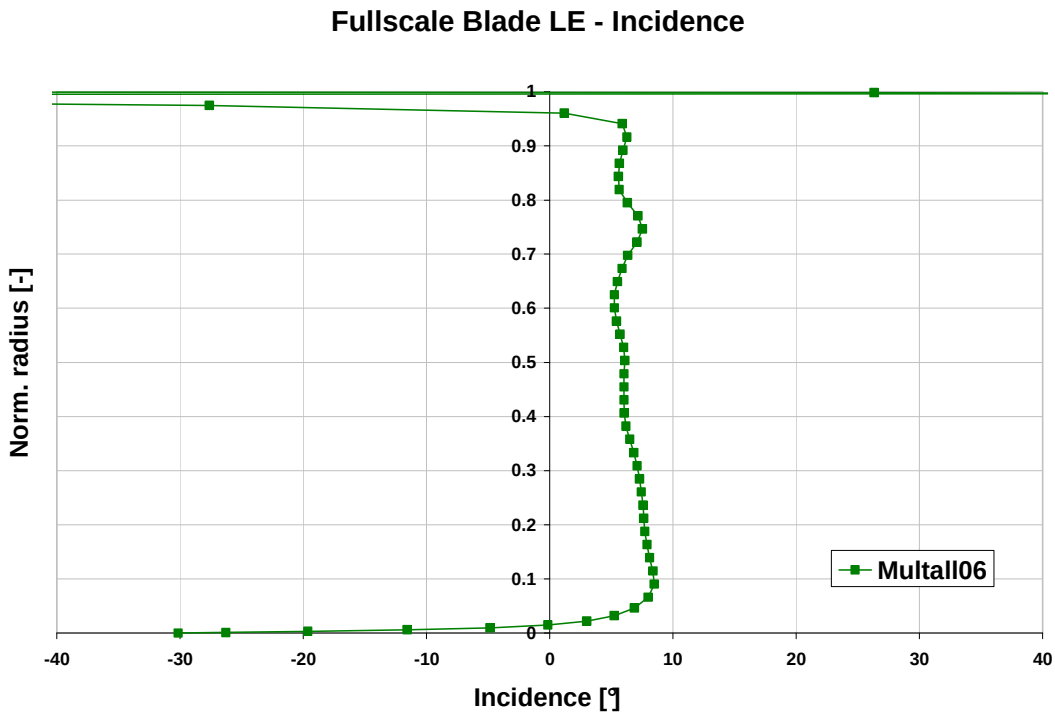

Figure 4-9 B6F - Incidence at blade leading edge

4.4.2 Airfoil design - Curvature

The sections at hub, mid and tip defining the blade should comply with the rule of monotonically decreasing suction side curvature according to Siemens guidelines. In the airfoil software CATO the influence of different geometrical parameters on curvature can be evaluated. The curvature was first studied in the later parts of the design process. The reason for this is that the basis for the whole design, the reference stage complies with the constraint described above and the shape has not been greatly modified, see Figure 4-10 below. This should imply that the design is probably already reasonable in terms of curvature distribution. As this turned out to be the case only very small adjustments were made in order to satisfy the criterion of monotonically decreasing curvature on the suction side. Since the pressure side is less sensitive to disturbances only the suction side has been adjusted.

The curvature has been plotted as a function of a normalized axial coordinate for hub, mid and tip section belonging to the final design version, B6F. Here just referred to as B6 since the curvature is the same both at full scale, B6F, and model scale, B6M.

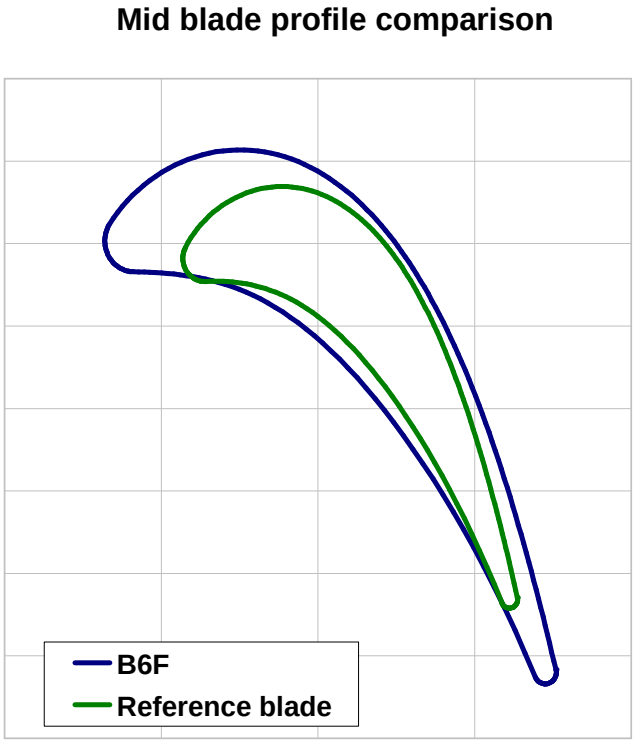

Figure 4-10 Comparison at mid section with B6F and the reference blade

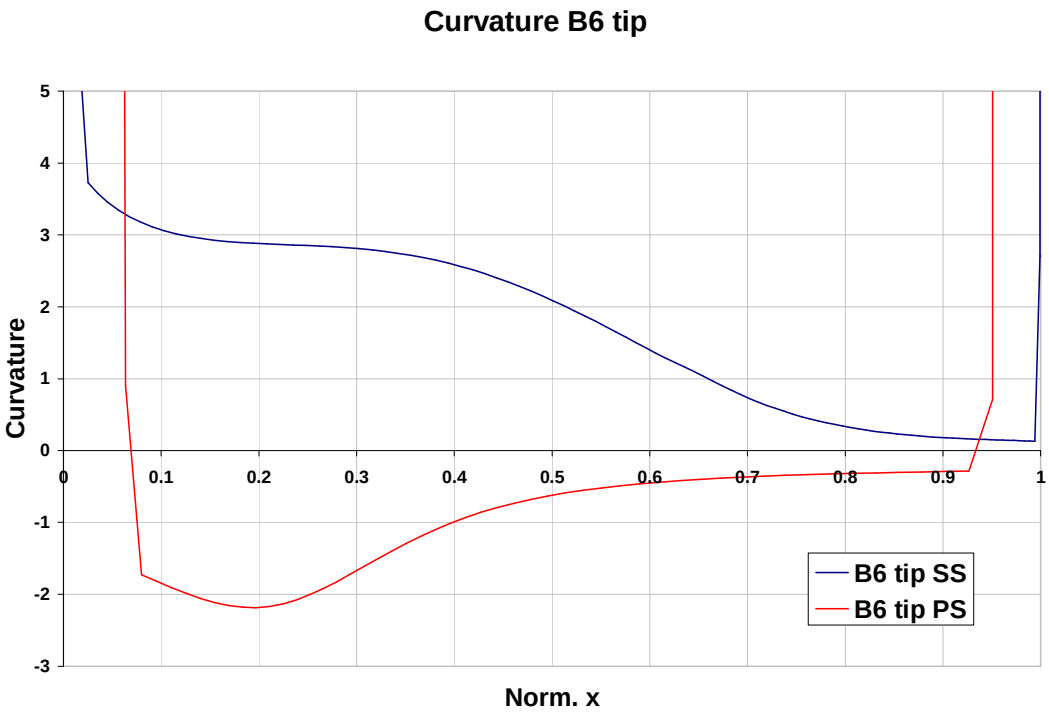

Figure 4-11 Curvature distribution at tip section B6

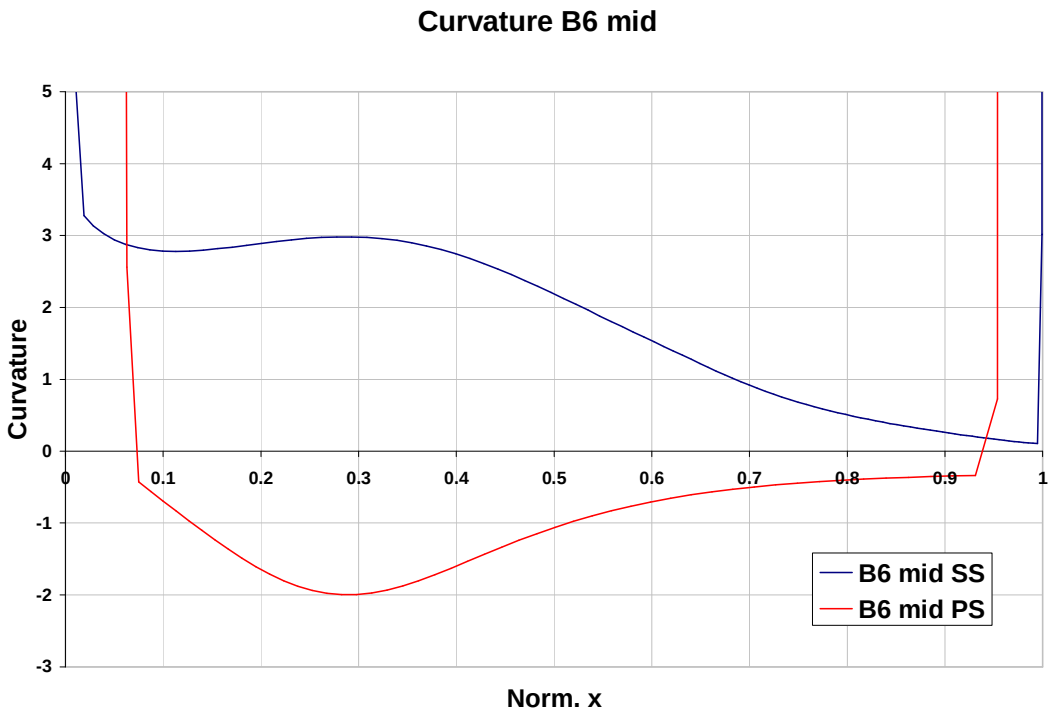

Figure 4-12 Curvature distribution at mid section B6

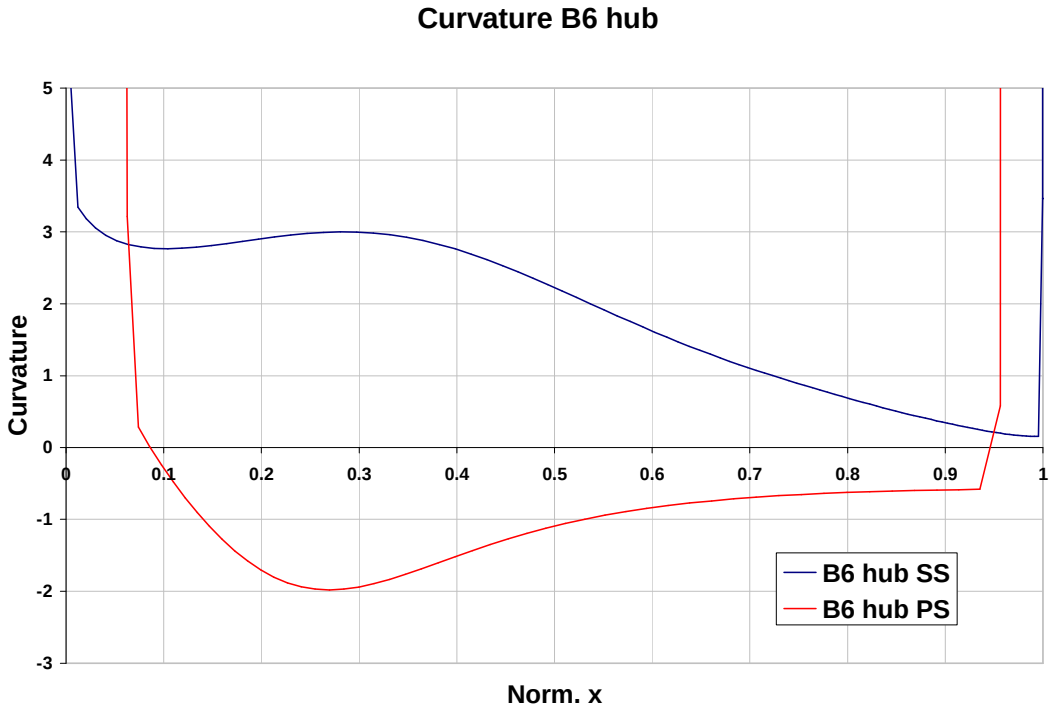

Figure 4-13 Curvature distribution at hub section B6

4.4.3 Airfoil - CATO 2D Navier Stokes

The last step considering the airfoil was to study the velocity distribution at hub, mid and tip section. Since the starting point of the design was a reference stage used in a real gas turbine along with its flow conditions the velocity distribution should be relatively similar. Below the isentropic Laval number as a function of a surface coordinate can be seen for B6F and B6M at hub, mid and tip section for the blade.

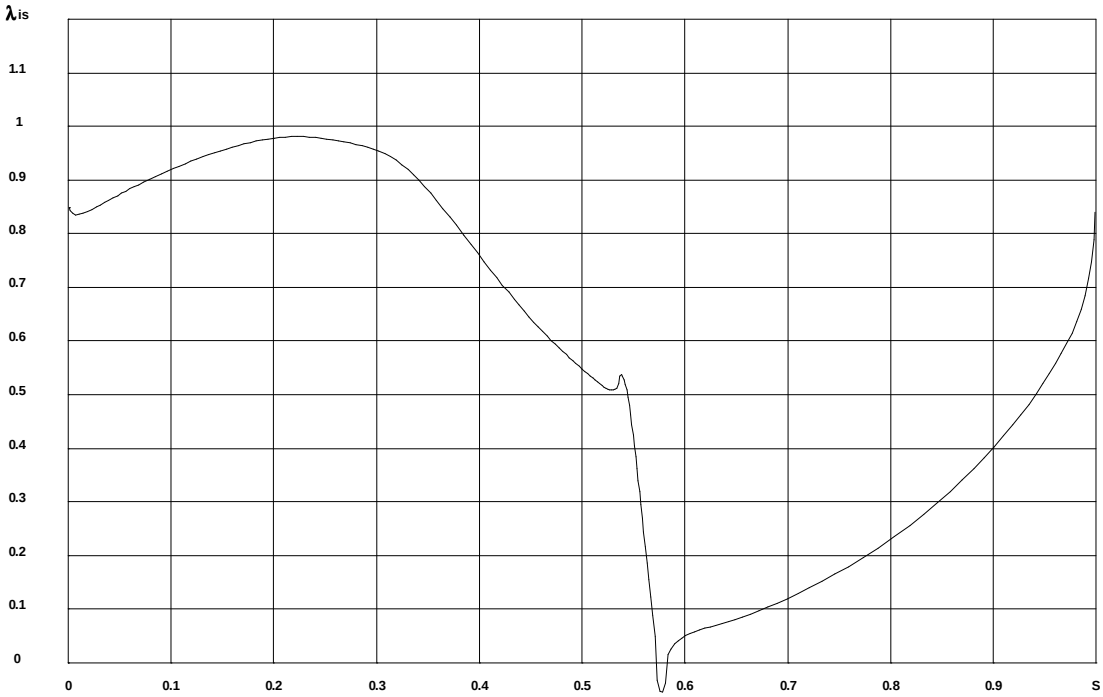

Figure 4-14 Isentropic Laval number at tip section B6F

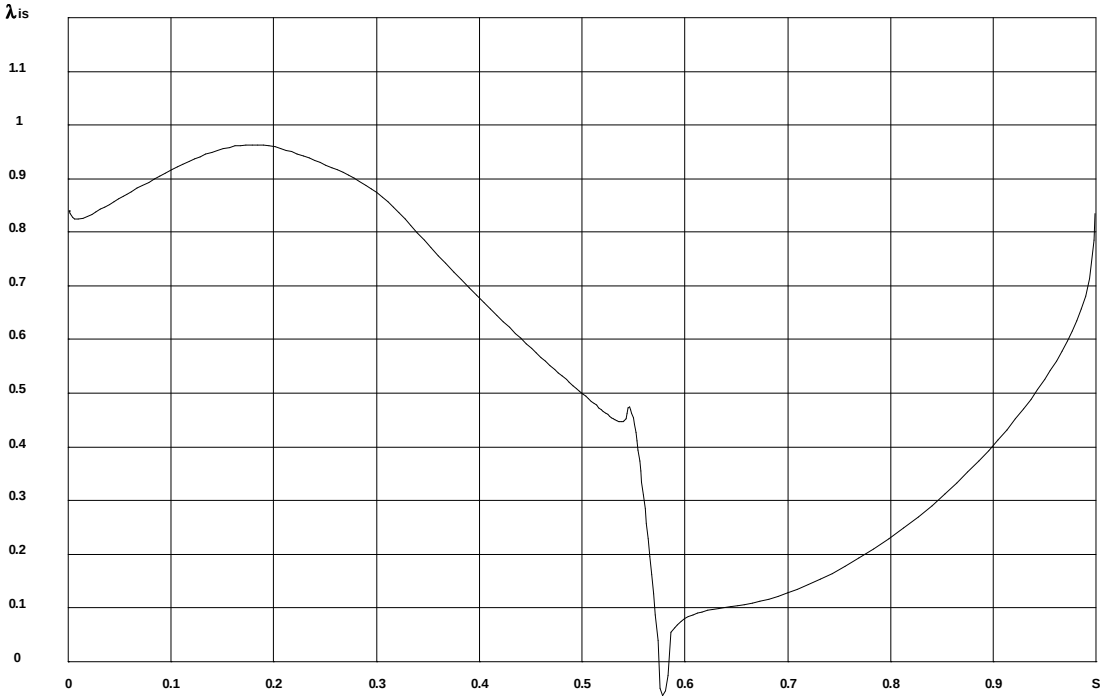

Figure 4-15 Isentropic Laval number at mid section B6F

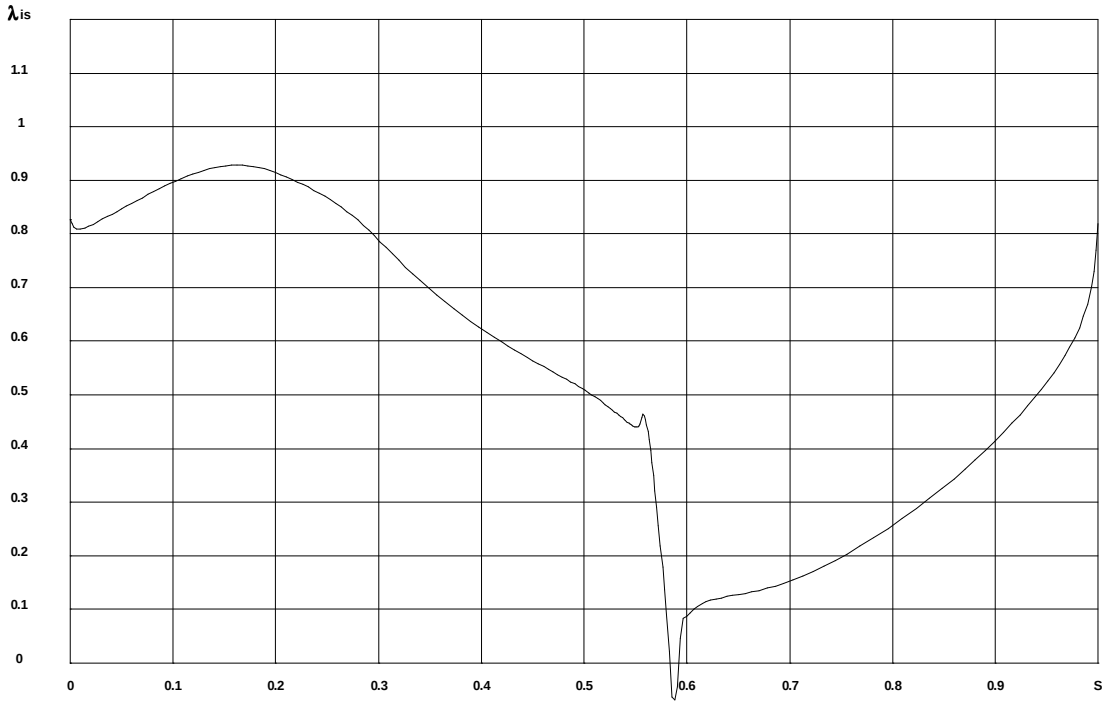

Figure 4-16 Isentropic Laval number at hub section B6F

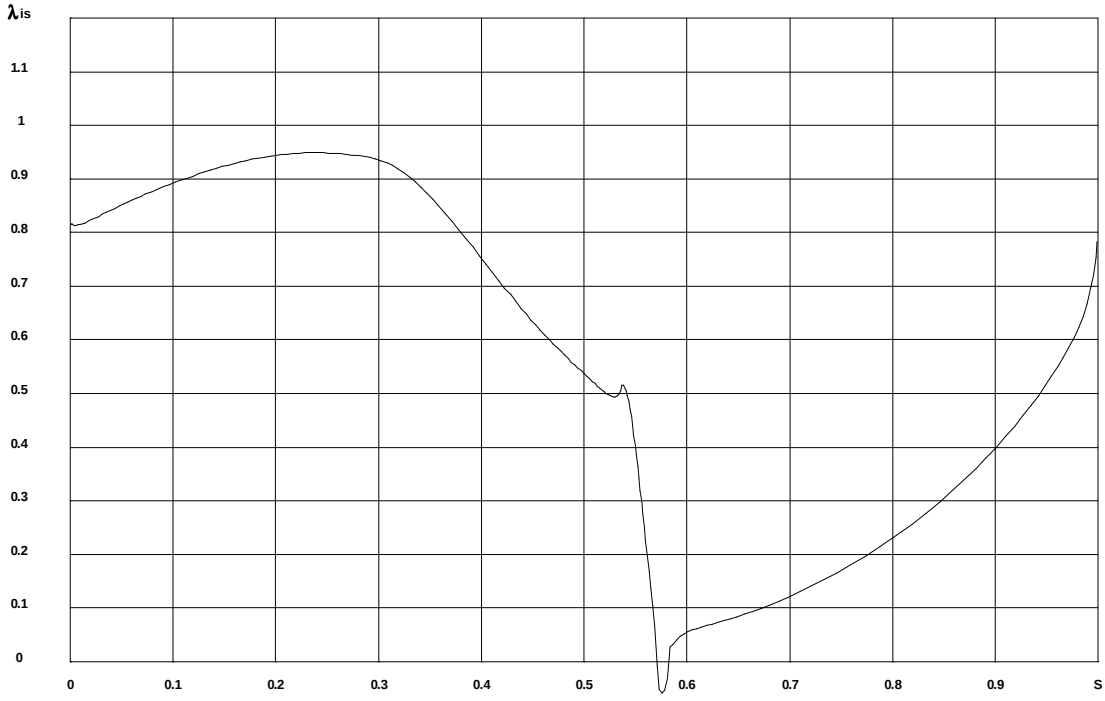

Figure 4-17 Isentropic Laval number at tip section B6M

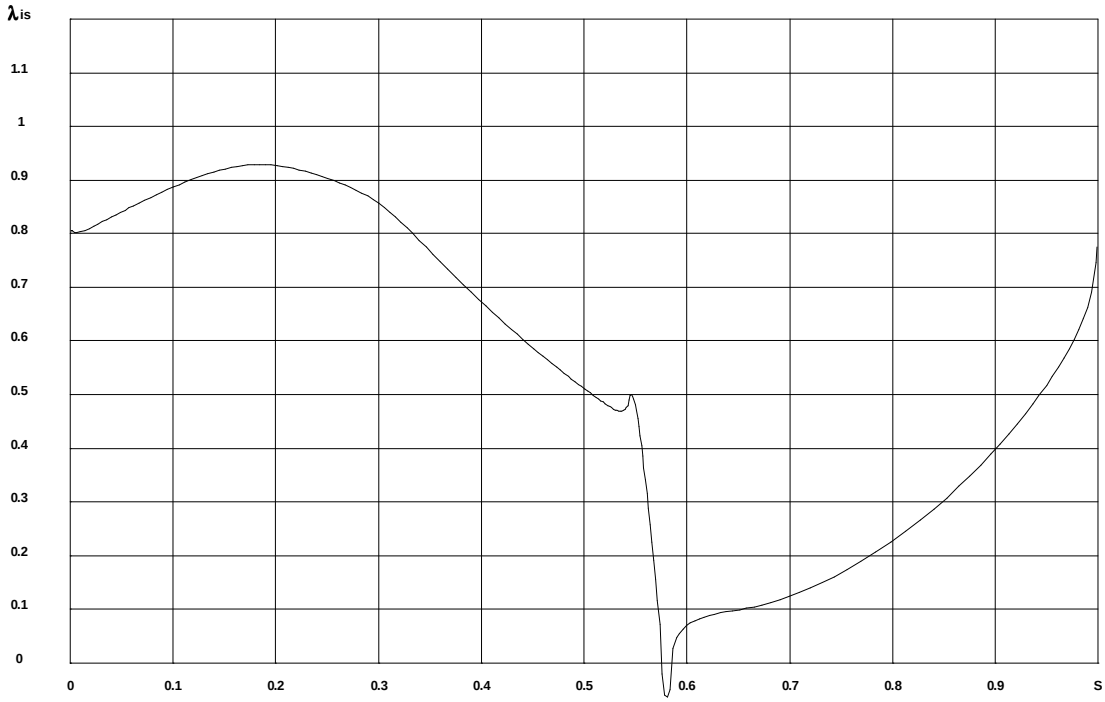

Figure 4-18 Isentropic Laval number at mid section B6M

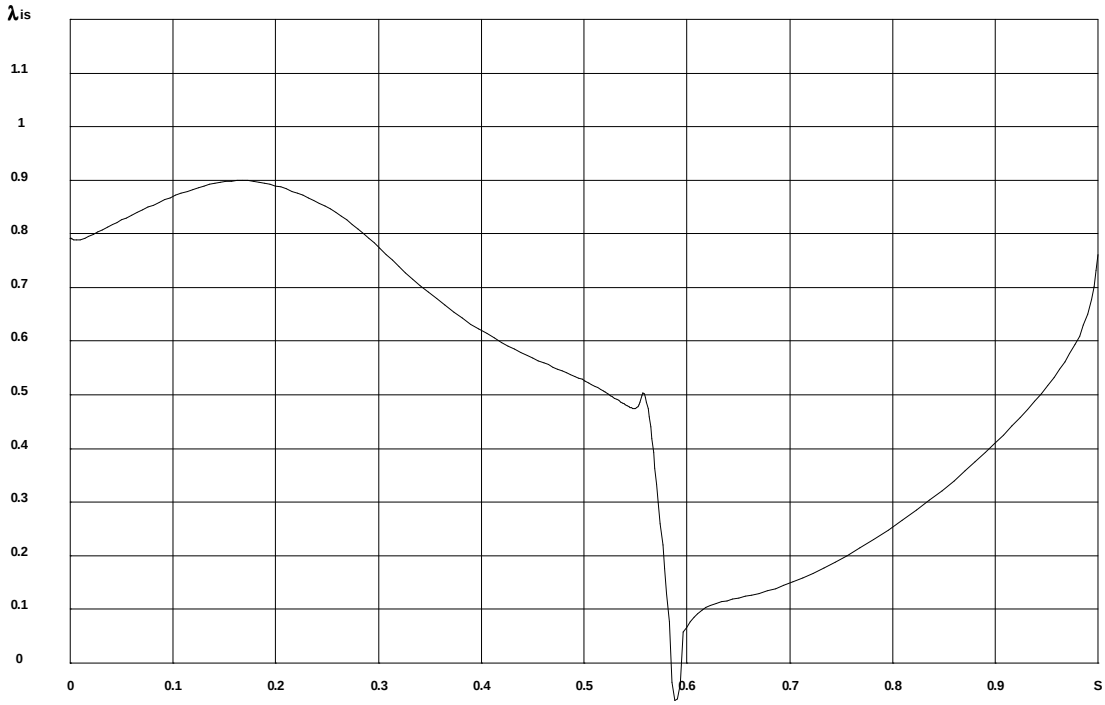

Figure 4-19 Isentropic Laval number at hub section B6M

From the figures above a small velocity “spike” can be seen just to the left of the stagnation point. This is mainly a consequence of the transition between the circular leading edge and the subsequent curvature of the suction side not being entirely continuous. The reason for this is due to a shortcoming of the profile generator used at time of the design of the reference stage. It has been kept to be as similar to the

reference stage as possible. The spike could possibly be removed in the new profile software CATO.

The diffusion coefficient has been calculated from the velocity distributions above for hub, mid and tip section belonging to B6F. Mamaev's criterion, $D \leq D_{opt}$, is fulfilled at every section, see Table 7 below:

	D	D_{opt}
Tip	0.157	0.21
Mid	0.159	0.22
Hub	0.152	0.23

Table 7 Diffusion coefficients for B6F

4.4.4 The final design - B6

The specification of the hot geometry of B6, both in full and model scale are presented here and can be seen summarized in Table 8. Especially noteworthy is the aspect ratio and the number of blades of the proposed design which are lower than typical gas turbine values. The reason for is, as mentioned earlier, a deliberate choice because of possible manufacturing limitations. This low aspect ratio together with the relative low number of blades is a direct consequence of the decision to extend the axial chord.

Another important result is the relative trailing edge thickness, d_2/b, which is much smaller for 4b compared to B6. The difference originates from the fact that the reference blade has a trailing edge slot, enabling cooling air to be ejected, which limits the minimum trailing edge diameter. Since the airfoil profile of the reference is directly scaled to B6 the relative trailing edge thickness will follow. This is a deliberate decision and the relative trailing edge thickness of 4b is not characteristic of a cooled gas turbine blade.

Blade parameter	B6F	B6M	4b
r_{hub} [mm]	430.44	177.50	177.50
r_{tip} [mm]	493.97	203.70	204.80 (entry)
b_{hub} [mm]	75.65	31.20	26.11
b_{mid} [mm]	76.46	31.53	26.14
b_{tip} [mm]	77.46	31.94	26.14
B_{hub} [mm]	61.13	25.21	24.59
B_{mid} [mm]	57.72	23.8	24.59
B_{tip} [mm]	54.48	22.47	24.59
Blade height$_{entry}$ [mm]	63.53	26.20	28.29
t_{mid} [mm]	64.54	26.61	20.65
$AR_{mid,axial}$ [-]	1.10	1.10	1.15
$AR_{mid,real}$ [-]	0.83	0.83	1.08
$(r_{tip}/r_{hub})_{entry}$ [-]	1.15	1.15	1.16
d_2 [mm]	2.80	1.15	0.27
d_2/b_{mid} [%]	3.66	3.65	1.03
# of blades	45	45	58
$(t/b)_{mid}$ [-]	0.84	0.84	0.79
tip clearance [mm]	0.73	0.30	0.20

Table 8 Geometrical parameters for the final design

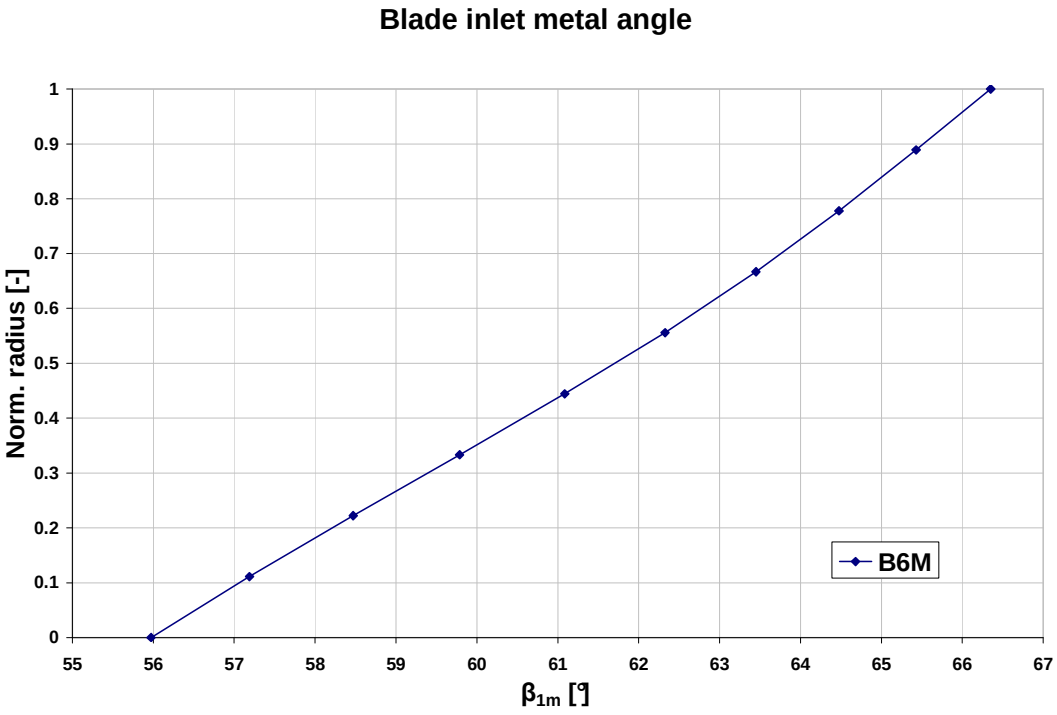

Figure 4-20 Metal angle

Figure 4-20 shows the blade inlet metal angle for B6M. The metal angle for B6 is designed with regards to optimal incidence at full scale as described in section 4.4.1. Since B6 is designed without any cooling flows the metal angle is almost linearly distributed. The corner coordinates for B6M is shown in Figure 4-21.

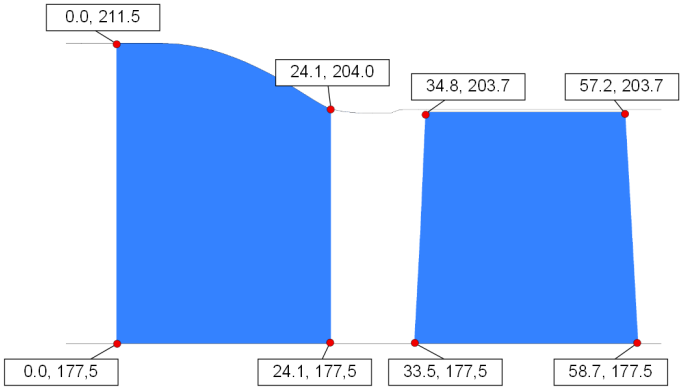

Figure 4-21 B6M Meridional coordinates

A 3D view of the new turbine design, generated in ANSYS CFX, is shown in Figure 4-22.

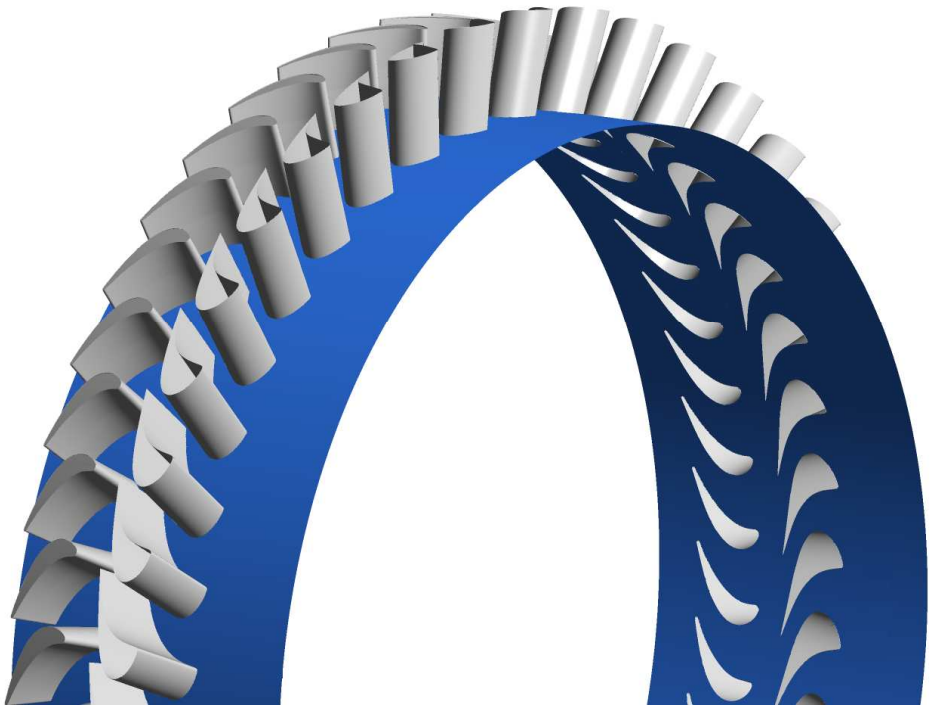

Figure 4-22 B6M

5 Results

5.1 Boundary conditions

Since the total to static pressure ratio of the reference stage was to be achieved, the total pressure was set at the inlet and the static pressure at the outlet. The goal was to match the radial distribution of total pressure to measured data from the test turbine as inlet condition. However, because of stability issues in CFX, with backflow at the inlet, the total pressure was approximated as constant across the span. This was applied as a boundary condition for all the programs so that the results could be compared. The effects on the result caused by this approximation are believed to be minimal.

The total inlet temperature was modeled as constant with radius for both model and full scale. At model scale this is in good agreement with the actual profile provided by the test turbine compressor however the set value of 345 K is slightly above the target value in Table 1. This was not considered a problem since the test turbine casing probably will be insulated to allow for a higher inlet temperature.

In Multall there is no option but to model the fluid as a perfect gas while CFX offers the ability to have fluid properties which depends on pressure and temperature. Even though it would have been desirable to define a real gas for the full and model scale cases in CFX the fluid was modeled as a perfect gas due to time shortage. Experience from other simulations at Siemens suggests that the effects of the perfect gas approximation should be acceptable, especially at model scale where the test turbine operates at very moderate temperatures. The heat capacity for each case was provided by results from the through flow code (Beta2) and the rotational speed was adjusted to give the same stage loading as the reference stage in Beta2. Steady state and just a single passage were assumed in all of the calculations. The boundary conditions used in both the 3D analysis and the through flow analysis for B6F/B6M are summarized in Table 9.

	Full scale	**Model scale**
$\mathbf{p^*_0}$ [bar] (constant dist.)	21.879	2.167
$\mathbf{T^*_0}$ [K] (constant dist.)	1540	345
$\mathbf{p_2}$ [bar] (constant ave.)	10.229	1.013
Π [-]	2.139	2.139
$\mathbf{TI_0}$ [%]	6	6
n [rpm]	9140	10270

Table 9 Boundary conditions

5.2 Results - Full scale

The results for the full scale cases are from calculations with the boundary condition in Table 9 for B6F. The CFX results are from the case with the transition model activated.

5.2.1 Radial distributions - B6F vs. The reference stage

A comparison between B6F and the reference stage was done both in Beta2 and Multall06. Because of confidential reasons, no values or figures are presented of this study. In general the result was in good agreement between the turbines and the key characteristics are maintained. Relatively large local deviations did occur though because of the lack of cooling in B6F.

5.2.2 Radial distributions - B6F code comparison

Figure 5-1 to Figure 5-4 show the radial distribution of the total pressure, static pressure, total temperature, Mach number and tangential flow angle for the vane and blade leading and trialing edge respectively as predicted by Beta2, Multall06 and CFX. As can be seen the predictions differ between the codes. The general trend is that CFX predicts lower static pressure and higher Mach number than Multall06 and Beta2 except at the blade trailing edge where the opposite is true. Therefore the predicted degree of reaction is lower in CFX compared to Beta2 and Multall06. Both Multall06 and CFX are able to capture the effects of secondary flows to some degree which are seen by strong radial variation in pressure and velocity at the blade trailing edge. CFX predicts a smoother flow near the blade tip compared to Multall06, explained by the more accurate tip modeling in CFX. Regarding the tangential flow angle at the blade leading edge CFX and Multall06 predict very similar values which confirm the decision to design the blade inlet metal angel according to Multall06 results. Overall the main predicted behavior is similar between the codes even comparing Beta2 and CFX. However, there are differences especially regarding Mach number and pressure. These deviations may be explained by the difference in how the flow physics are captured, e.g. 2D vs. 3D, mesh density, etc., and, for Multall06 and CFX, how the three-dimensional flow is averaged across the span. It is also important to note that the positions of the planes in Multall06 and CFX from which the data is extracted differs somewhat between the programs which also may be a factor affecting the result.

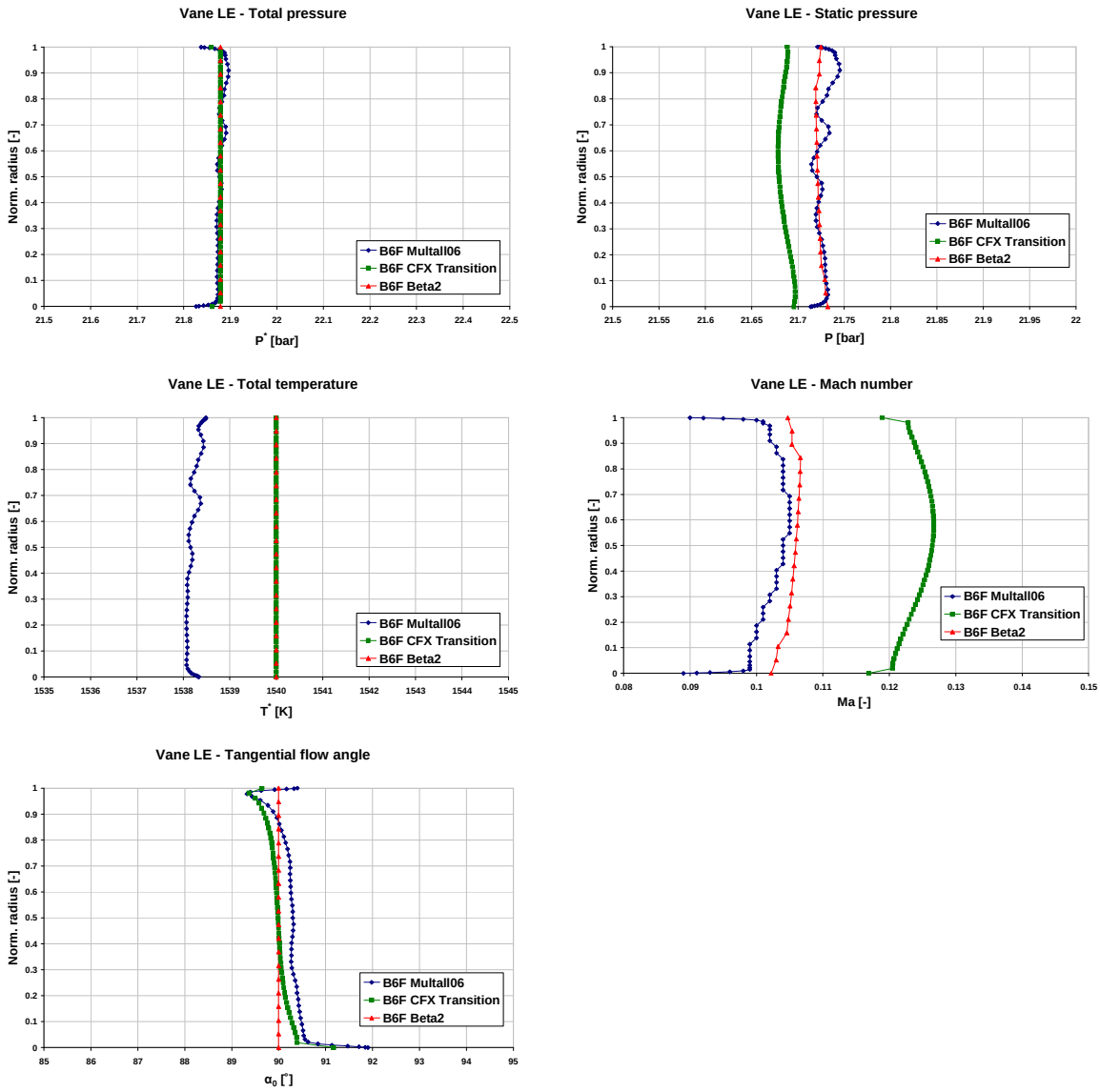

Figure 5-1 B6F - Vane leading edge

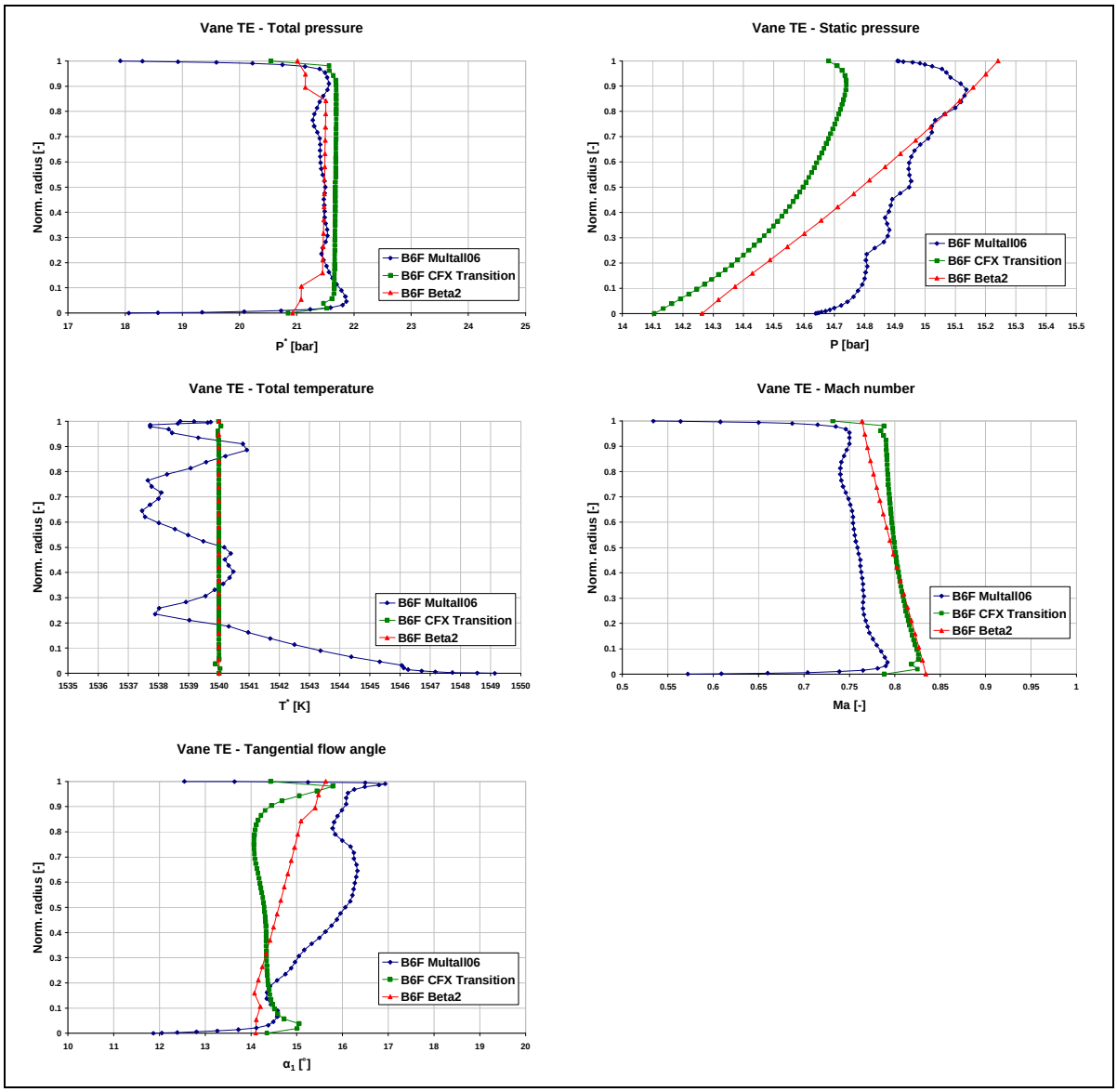

Figure 5-2 B6F - Vane trailing edge

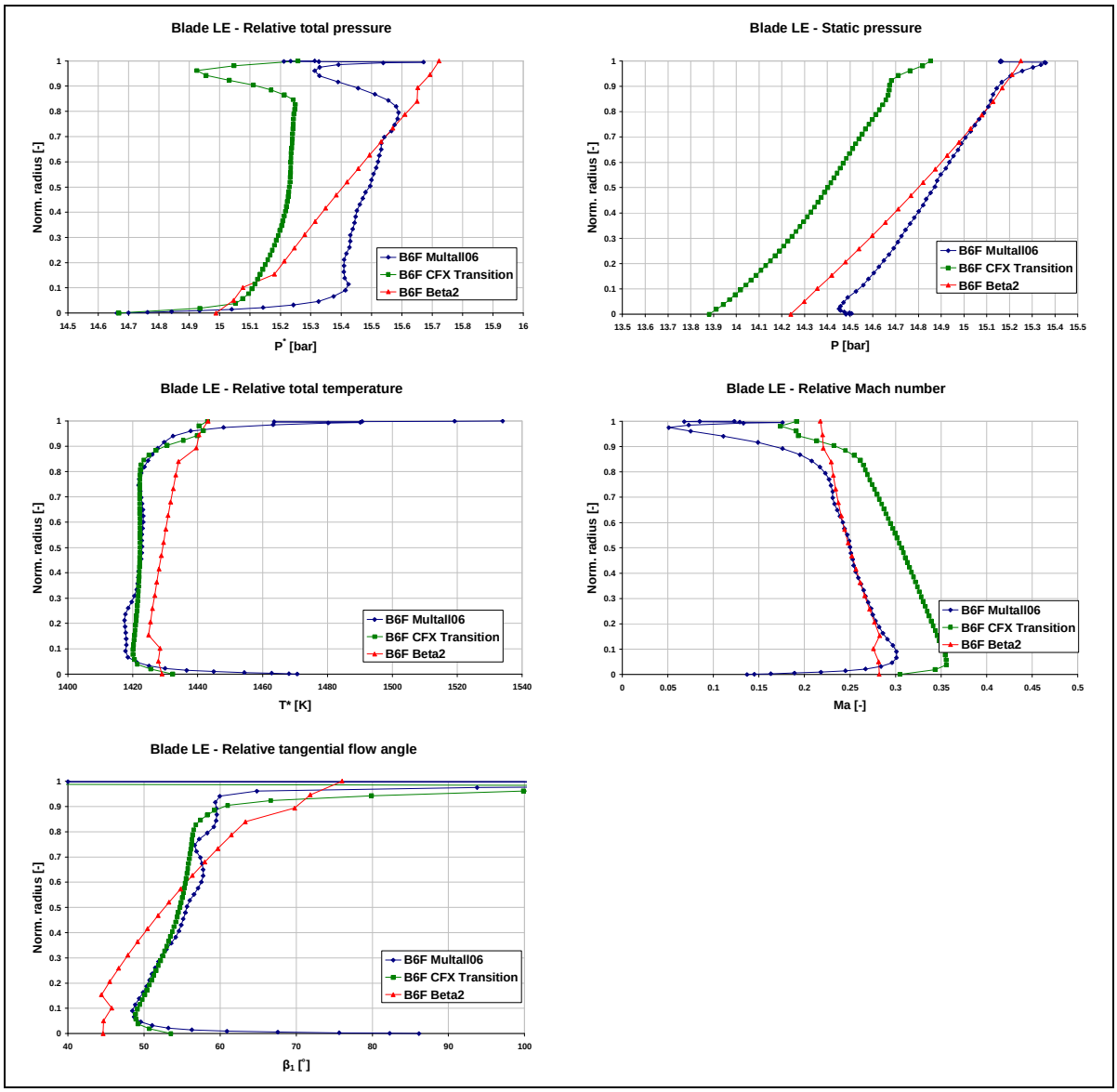

Figure 5-3 B6F - Blade leading edge

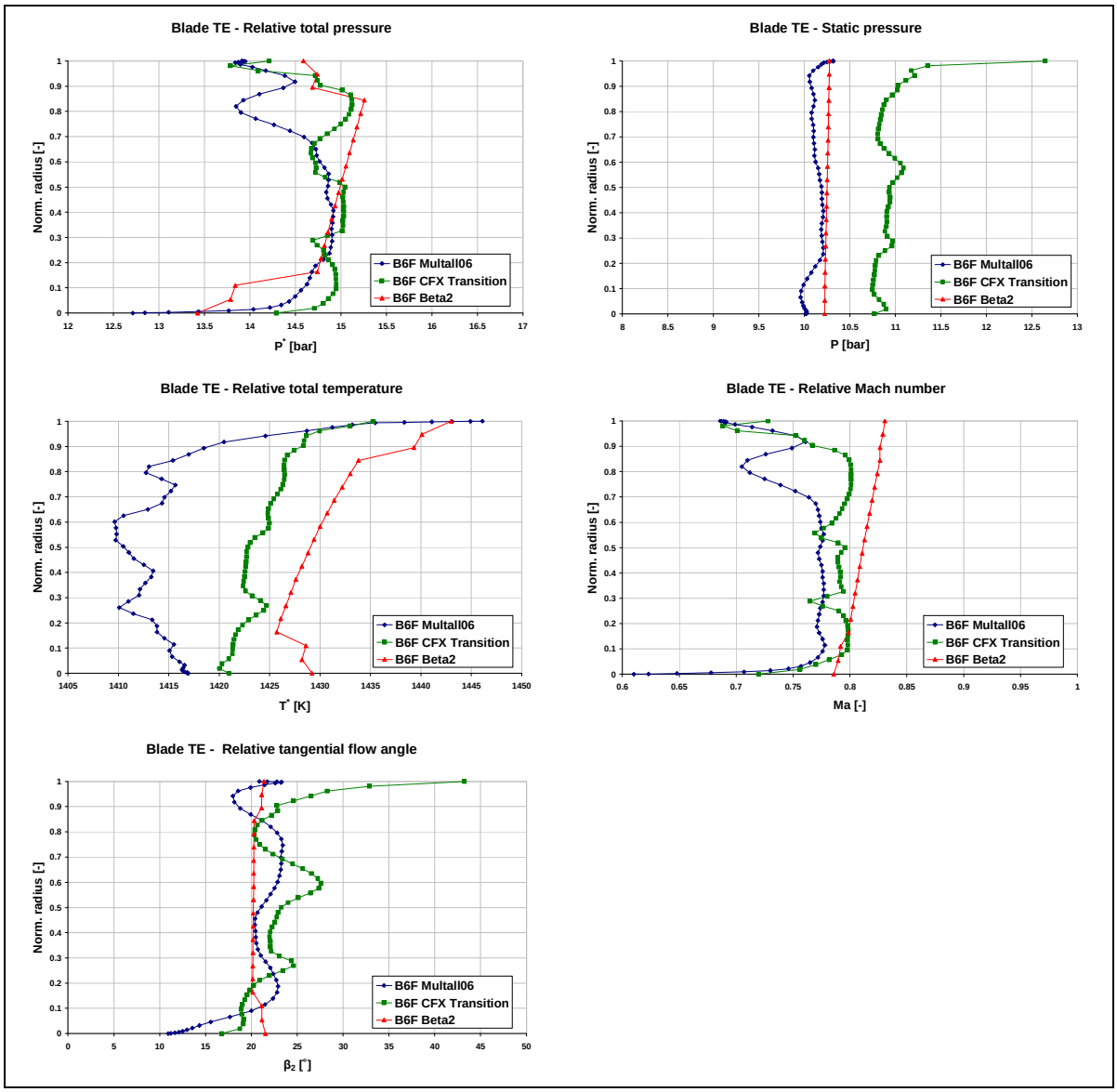

Figure 5-4 B6F - Blade trailing edge

5.2.3 CFX results – B6F

Figure 5-5 and Figure 5-6 show Mach contours as predicted by CFX at a radius of 25%, 50% and 75% of the span for the vane and blade respectively. Higher Mach numbers are reached at the blade but the values are below 0.95 even at the blade throat. The vane is designed for an inlet swirl angle which can be seen by the location of the stagnation point in Figure 5-5. This is also the cause of the Mach number peak near the leading edge in Figure 5-8. As can be seen from the contour plots and from Figure 5-7 the flow is subsonic in the whole domain except at a smaller region at the tip. This is to be expected since the pressure difference between the pressure and suction side forces the flow across the tip, causing acceleration to supersonic flow. The isentropic Mach number and blade loading for the vane and the blade at 25%, 50% and 75% of the span is seen in Figure 5-8. The isentropic Mach

number is plotted against normalized surface position, with starting point at the trailing edge and moving upstream the suction side with increasing *s*. The blade loading is plotted against the axial fraction. A comparison with the isentropic Laval number distributions shown in Figure 4-14 to Figure 4-19 indicates on the same trend regarding the isentropic Mach number. The peak in Mach number close to the blade stagnation point is explained, as mentioned in section 4.4.3, by the transition between the cylindrical leading edge and the suction side curvature. A similar peak occurs for the vane near the stagnation point, a consequence of the original 4b design. The 4b vane was designed for 20˚ interstage swirl in contrast to 0˚ when used in a first stage as in this case.

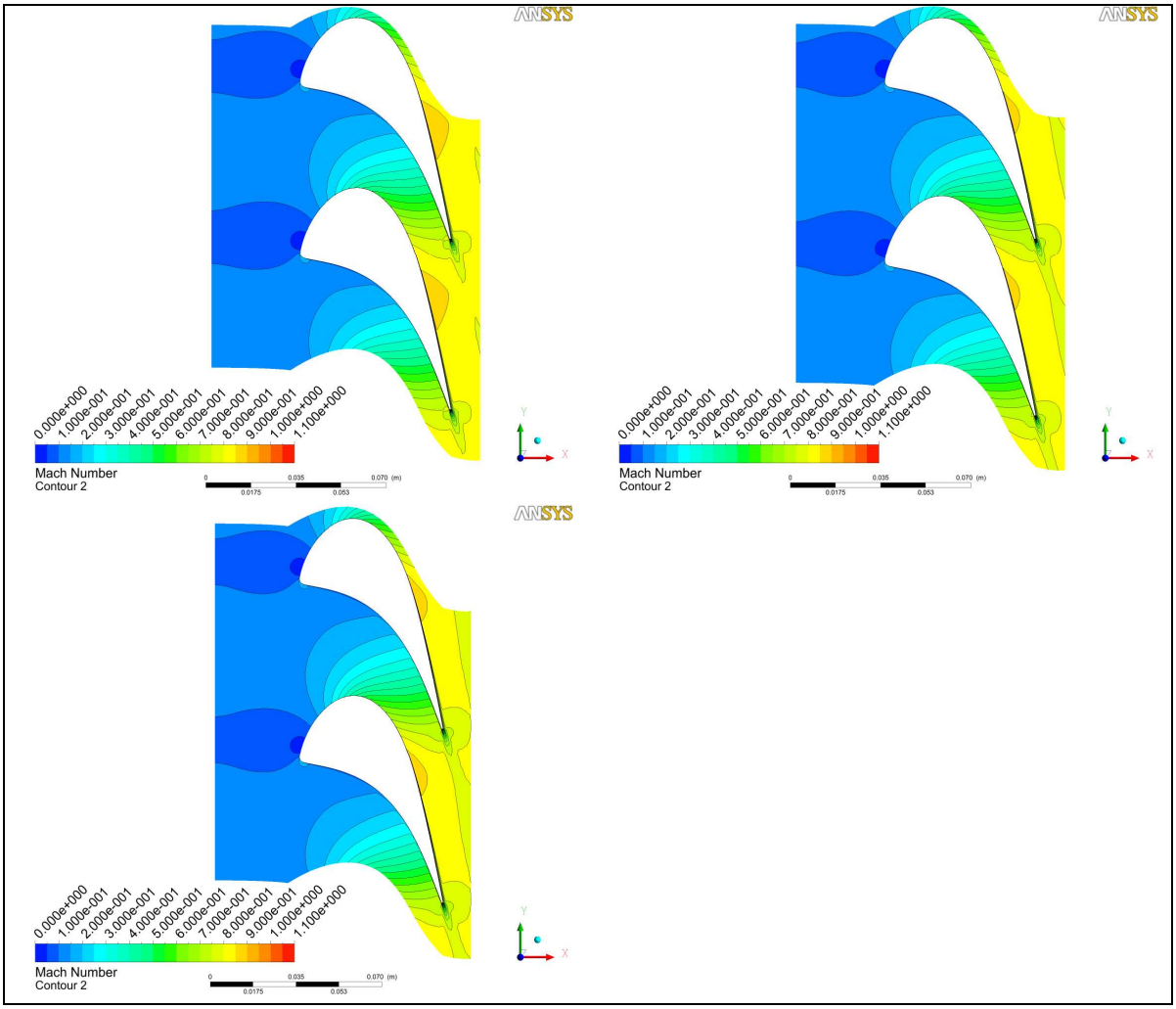

Figure 5-5 B6F Vane - Mach at 25%, 50% and 75% of span

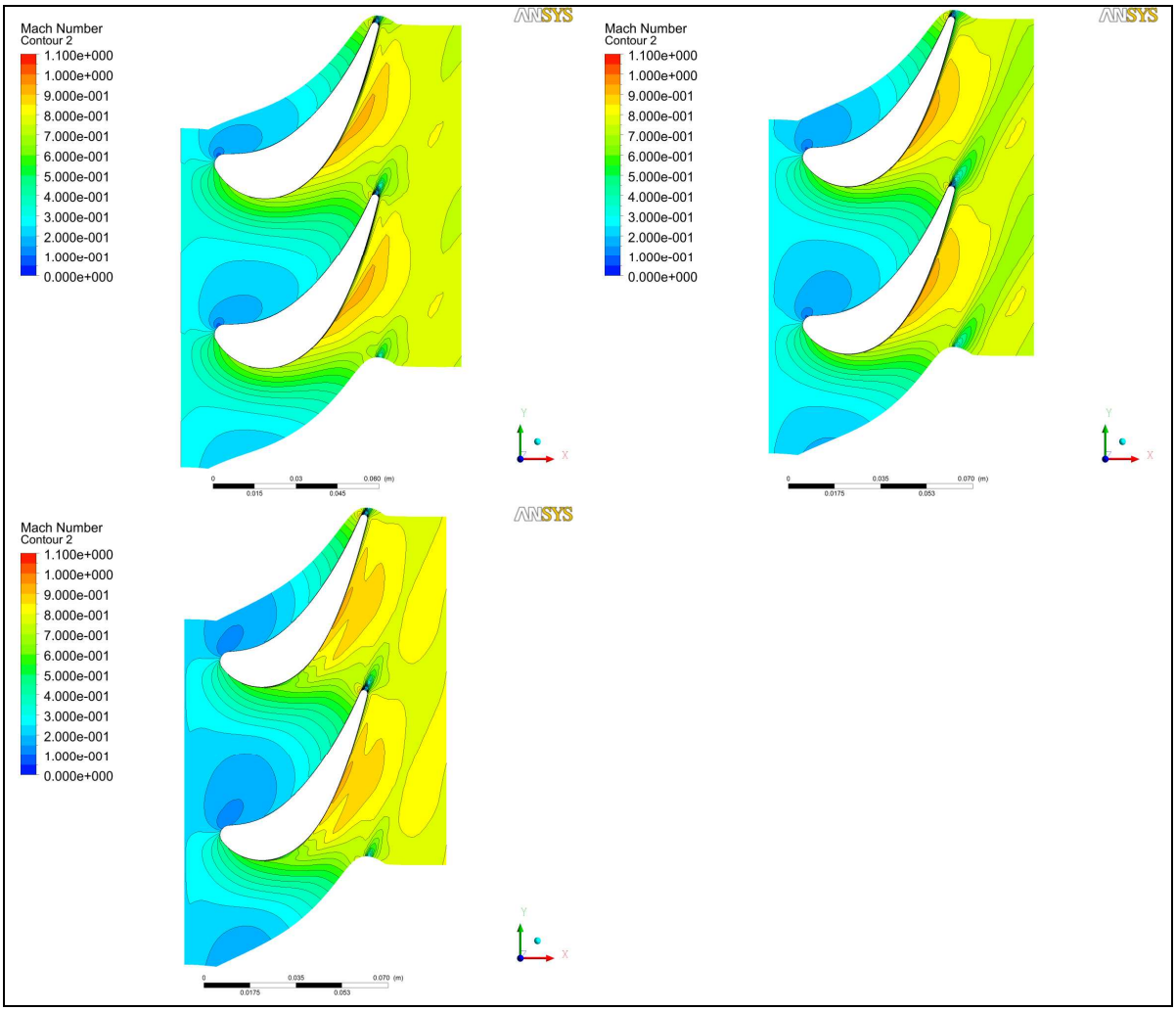

Figure 5-6 B6F Blade - Mach at 25%, 50% and 75% of span

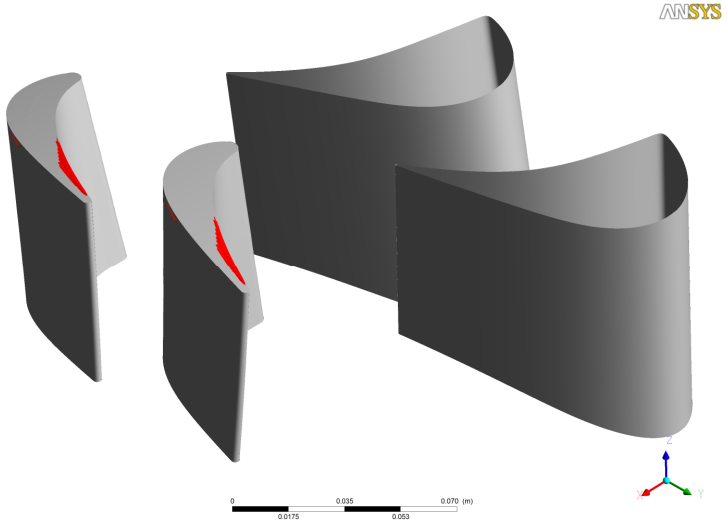

Figure 5-7 B6F – Isovolume for Ma>1

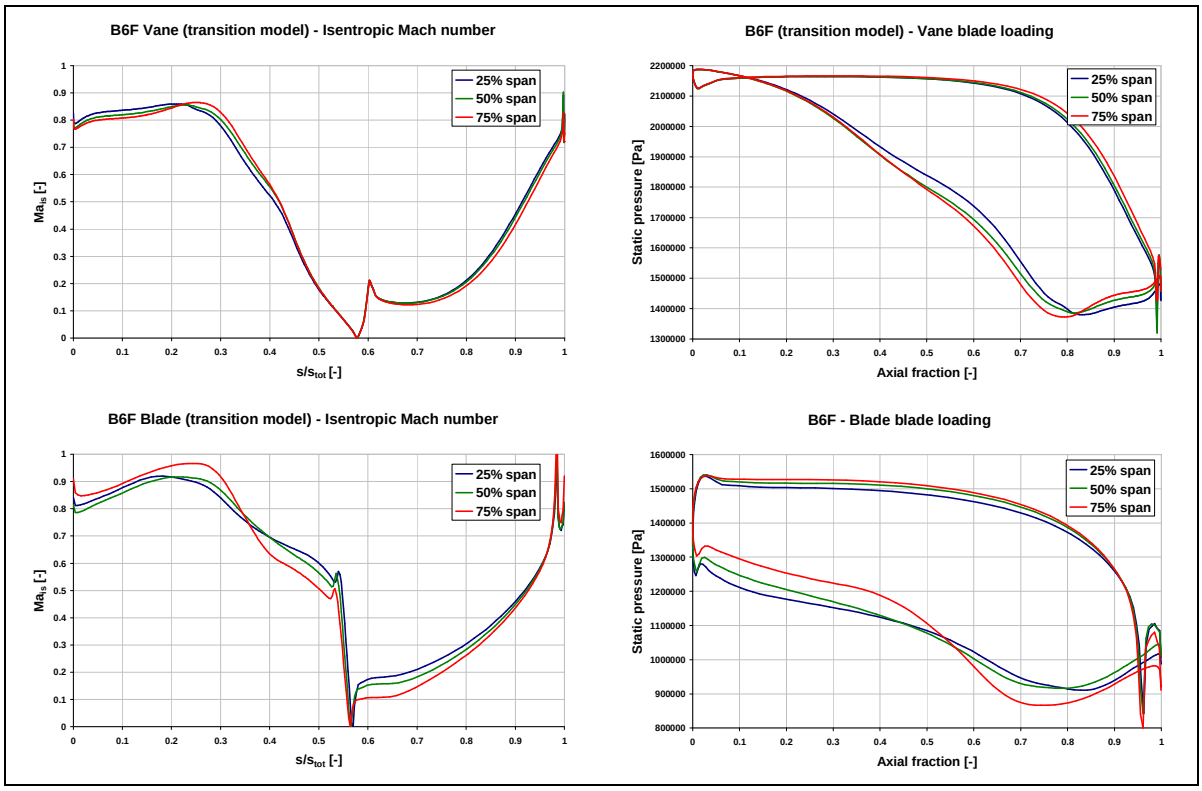

Figure 5-8 B6F - Isentropic Mach number and blade loading

5.3 Results - Model scale

The cases at model scale are run with the boundary conditions shown in Table 9. The CFX results are from the case with the transition model activated.

5.3.1 Radial distributions – B6M code comparison

In Figure 5-9 to Figure 5-12 are radial distributions for B6M presented. The code comparison regarding the radial distributions shows the same trends as in the full scale case. Again, CFX predicts lower static pressures and higher Mach numbers except at the blade trailing edge compared to Beta2 and Multall. The agreement between Multall and CFX regarding the tangential flow angle at the blade leading edge is conserved to the model scale. This indicates that the metal angle is appropriately designed also at model scale.

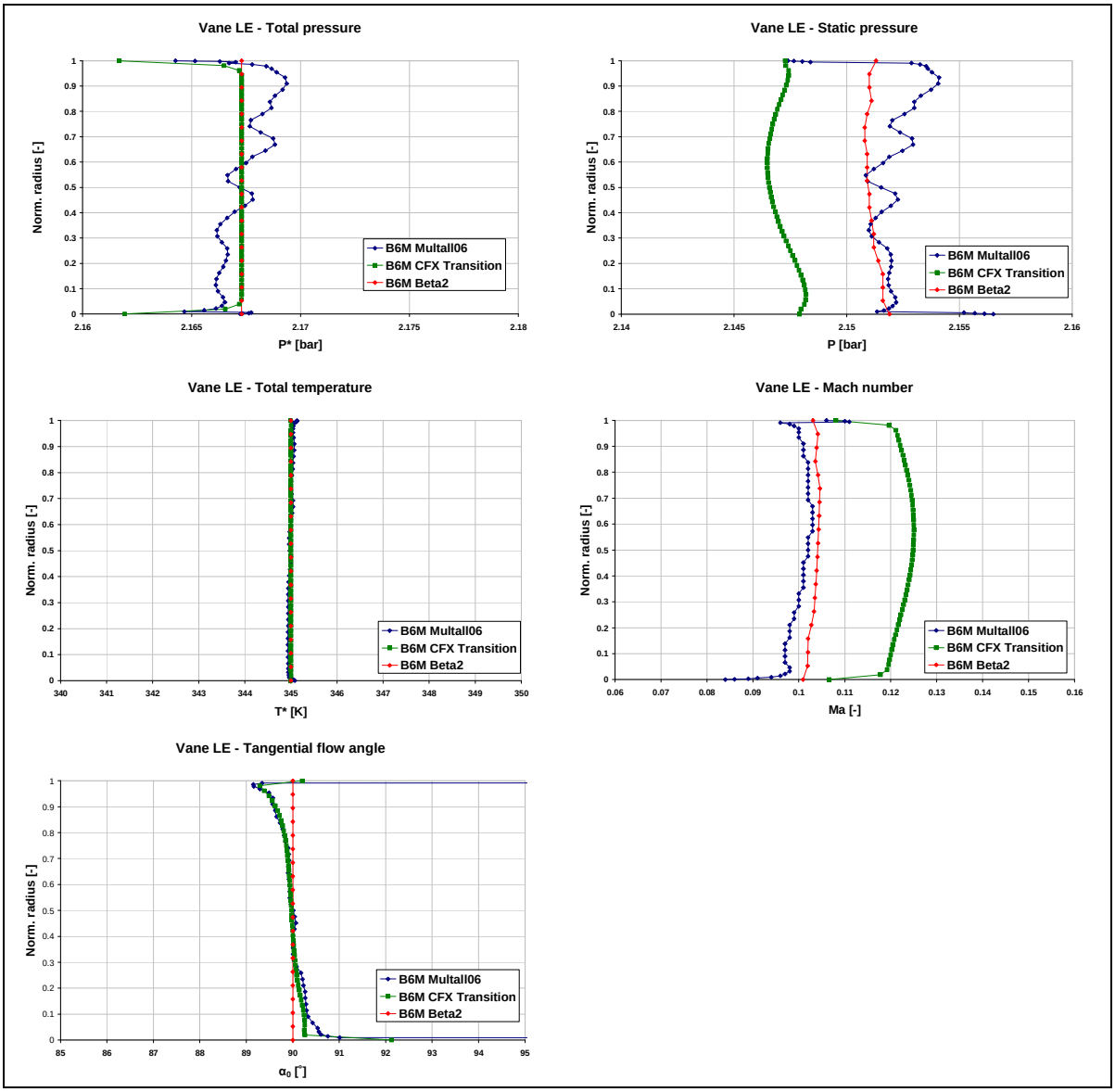

Figure 5-9 B6M - Vane leading edge

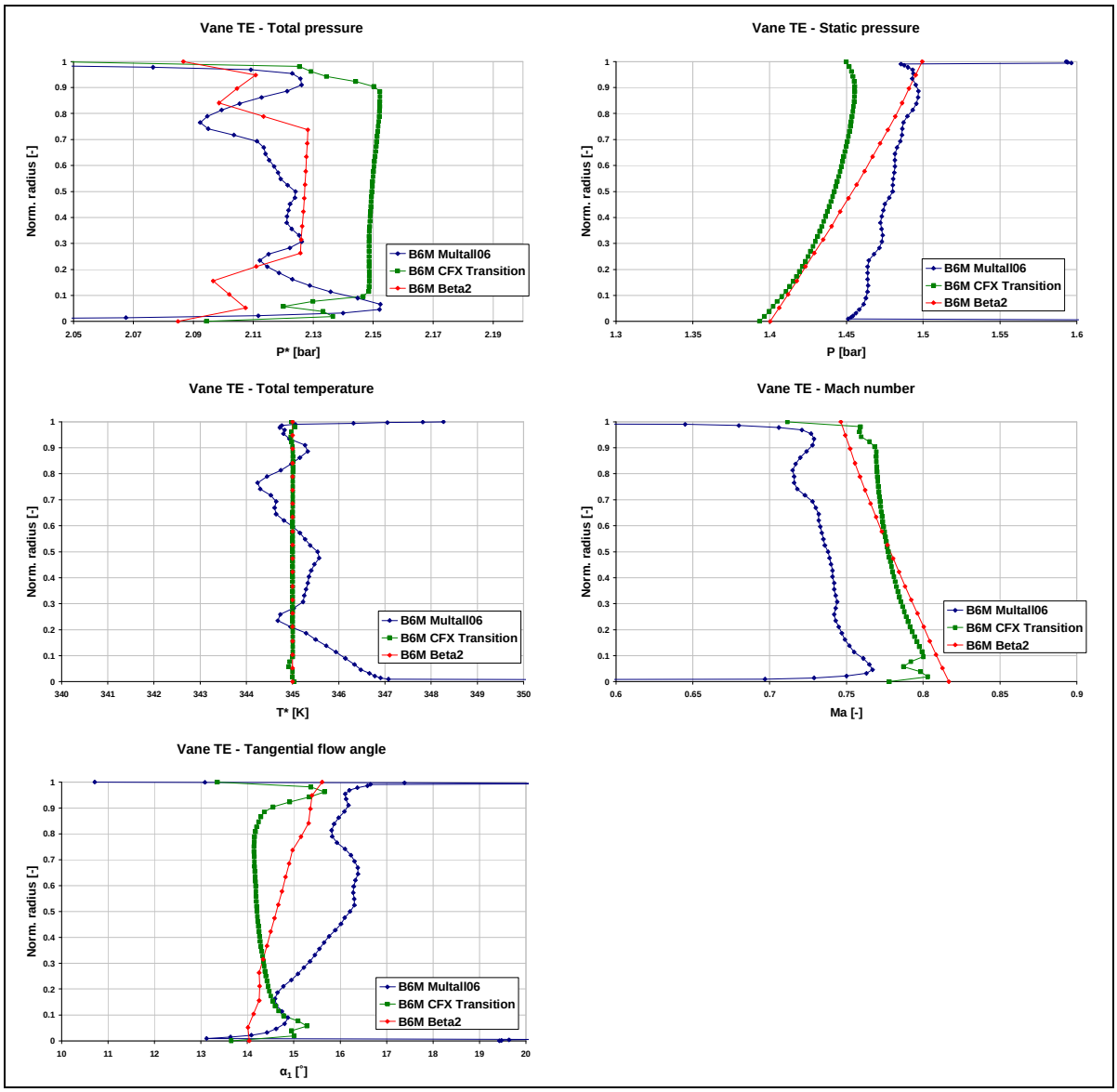

Figure 5-10 B6M - Vane trailing edge

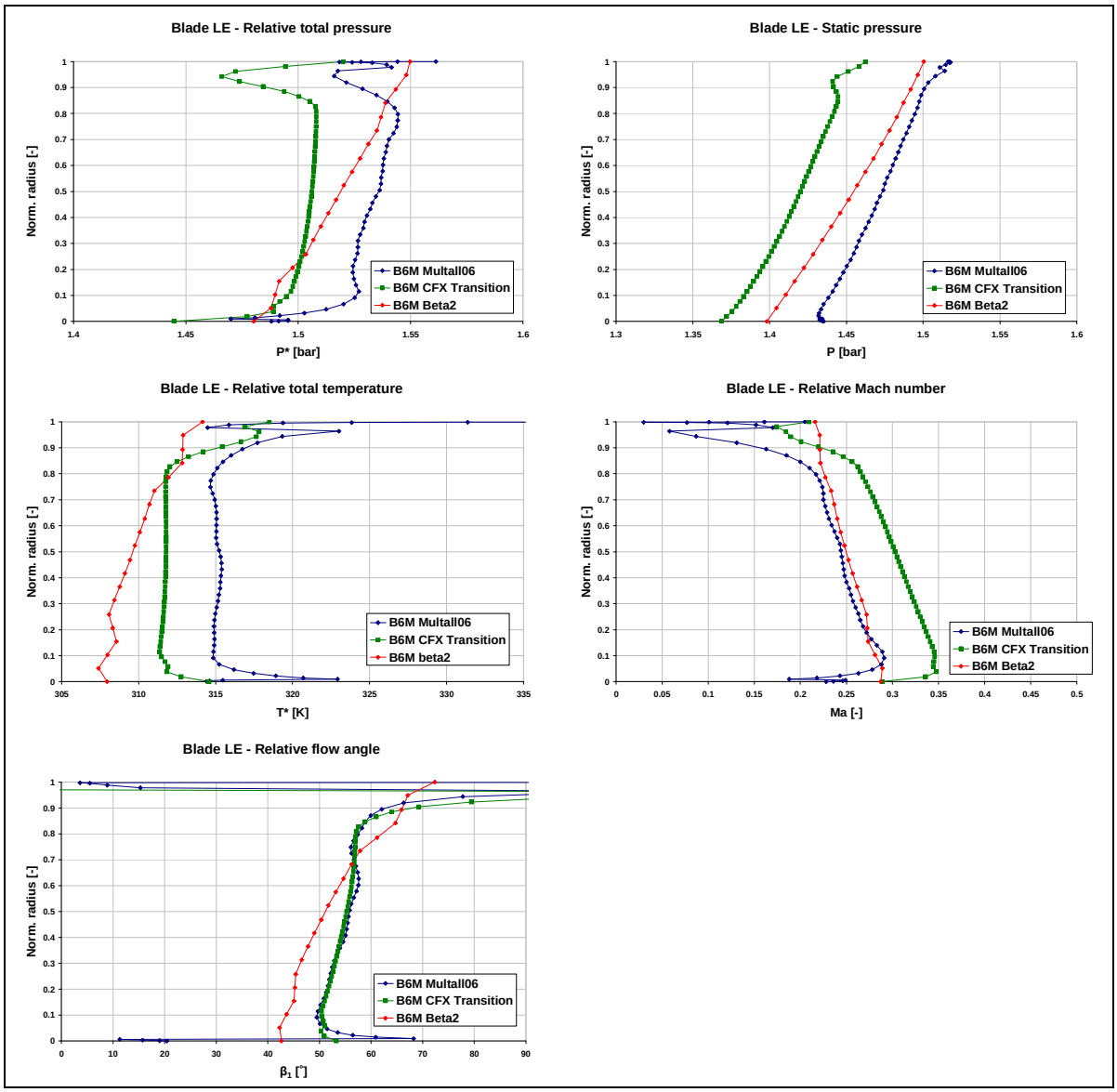

Figure 5-11 B6M - Blade leading edge

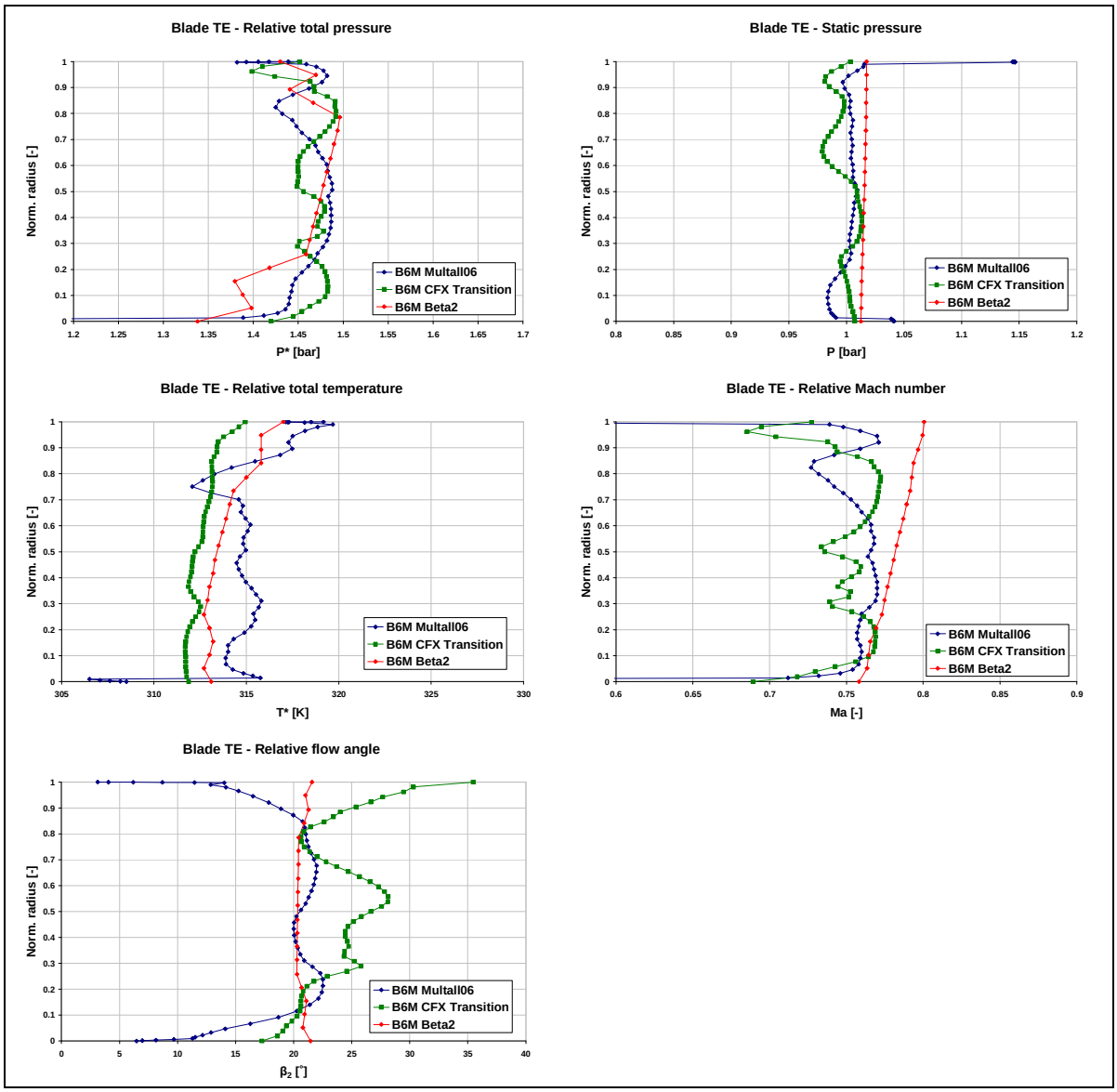

Figure 5-12 B6M - Blade trailing edge

5.3.2 CFX results – B6M

Figure 5-13 and Figure 5-14 show Mach number contour plots for the vane and the blade respectively. Compared to the full scale case in Figure 5-5 and Figure 5-6 the Mach number is in general lower at model scale. As can been seen in Figure 5-15 the tip leakage flow is supersonic to a lesser degree compared to the full scale case. This could be explained by the lower Mach number in general but also by the fact that the mesh was far more refined in the model scale cases (see section 3.4.2 and Appendix A). The more refined mesh should allow for better representation of the actual flow physics. Figure 5-16 shows the isentropic Mach number and blade loading compared to the full scale case. There are very small deviations, indicating that the design philosophy used at full scale is well translated to model scale.

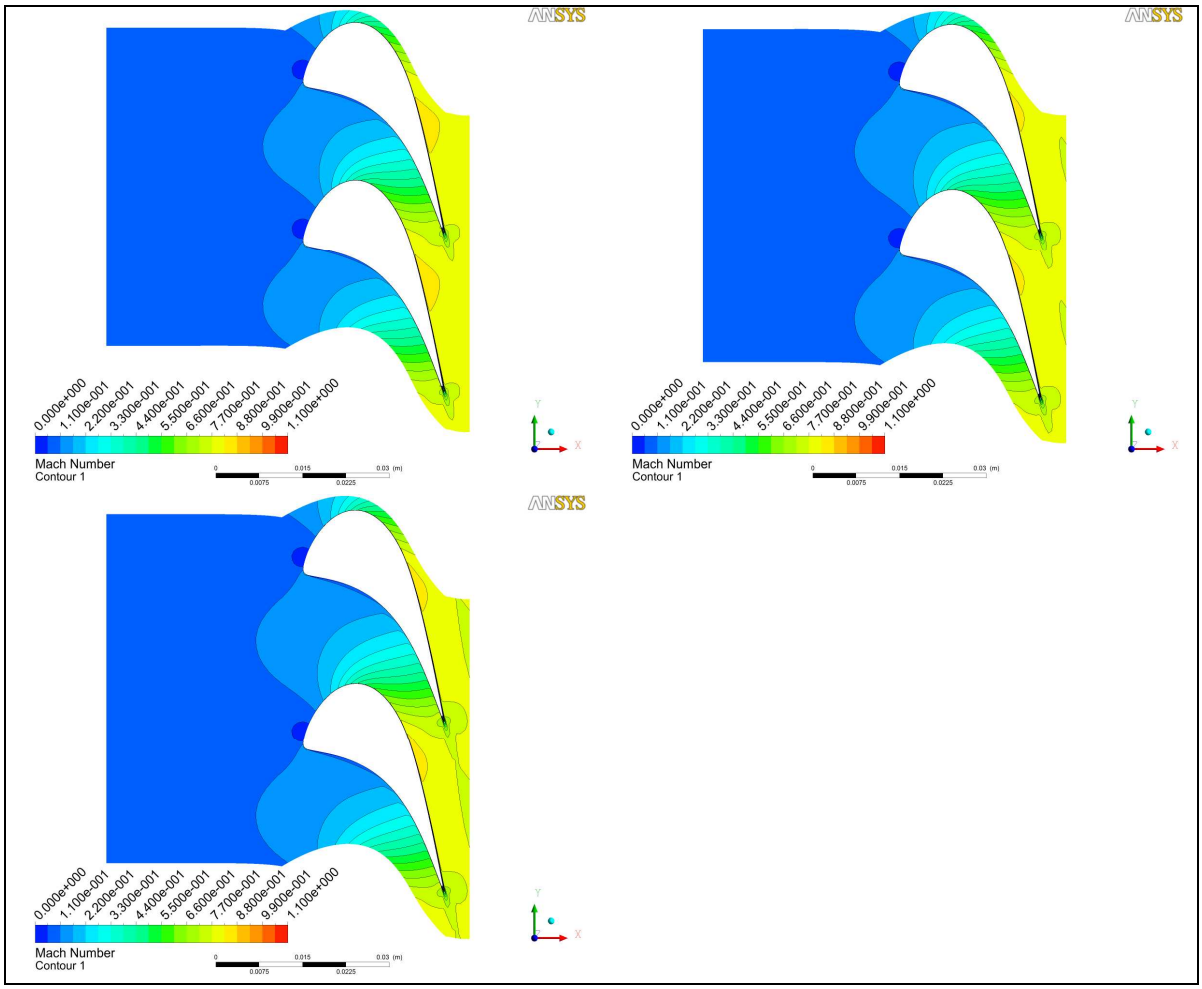

Figure 5-13 B6M Vane - Mach at 25%, 50% and 75% of span

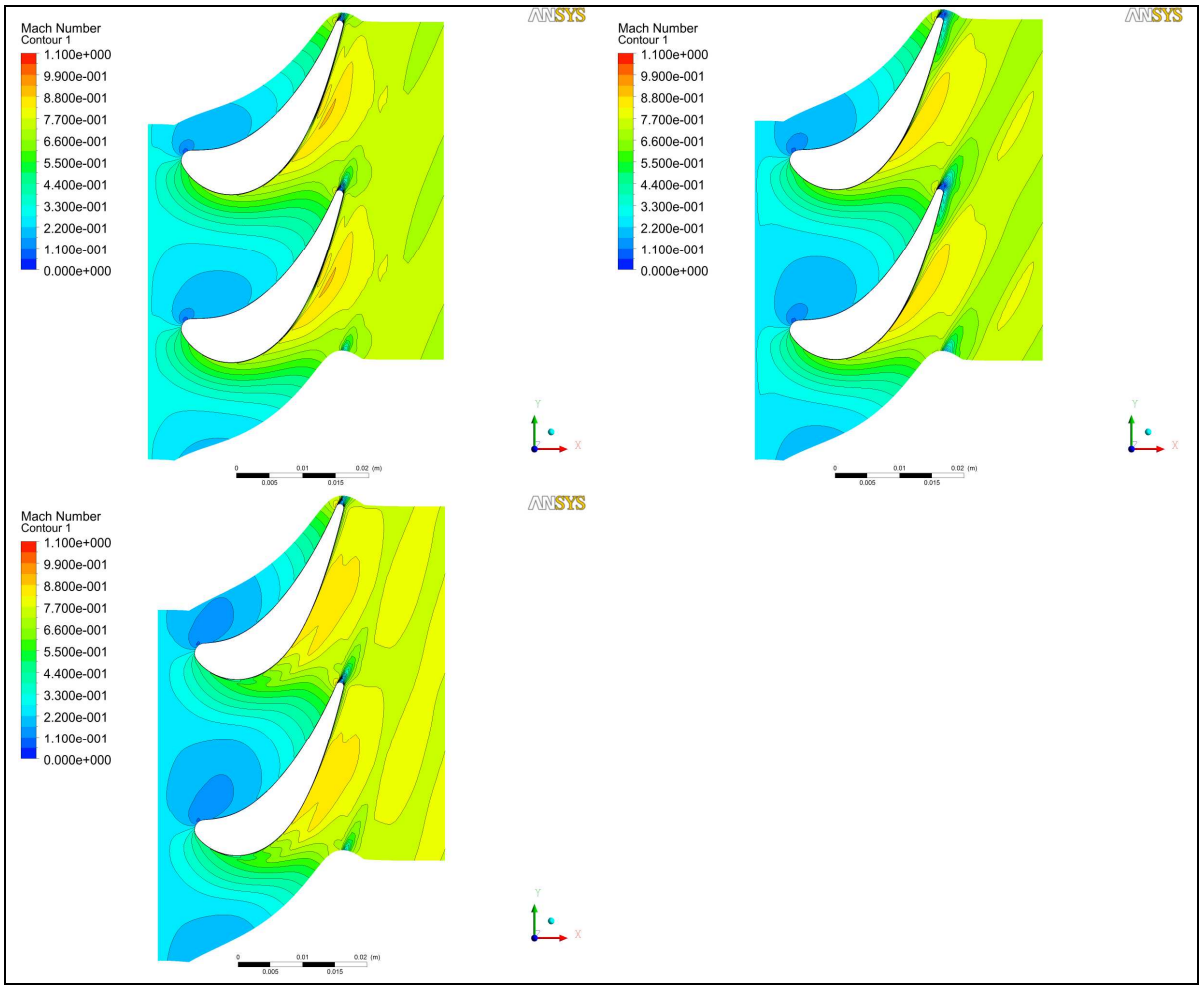

Figure 5-14 B6M Blade - Mach at 25%, 50% and 75% of span

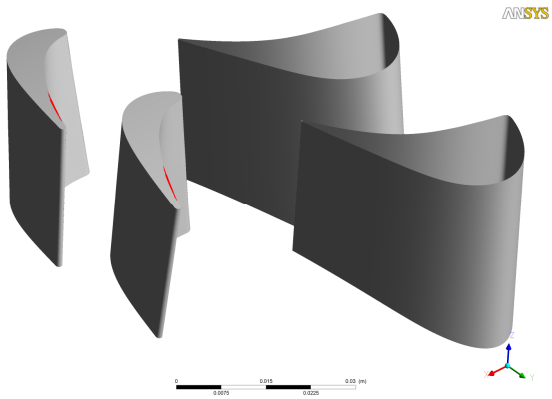

Figure 5-15 B6M – Isovolume for Ma>1

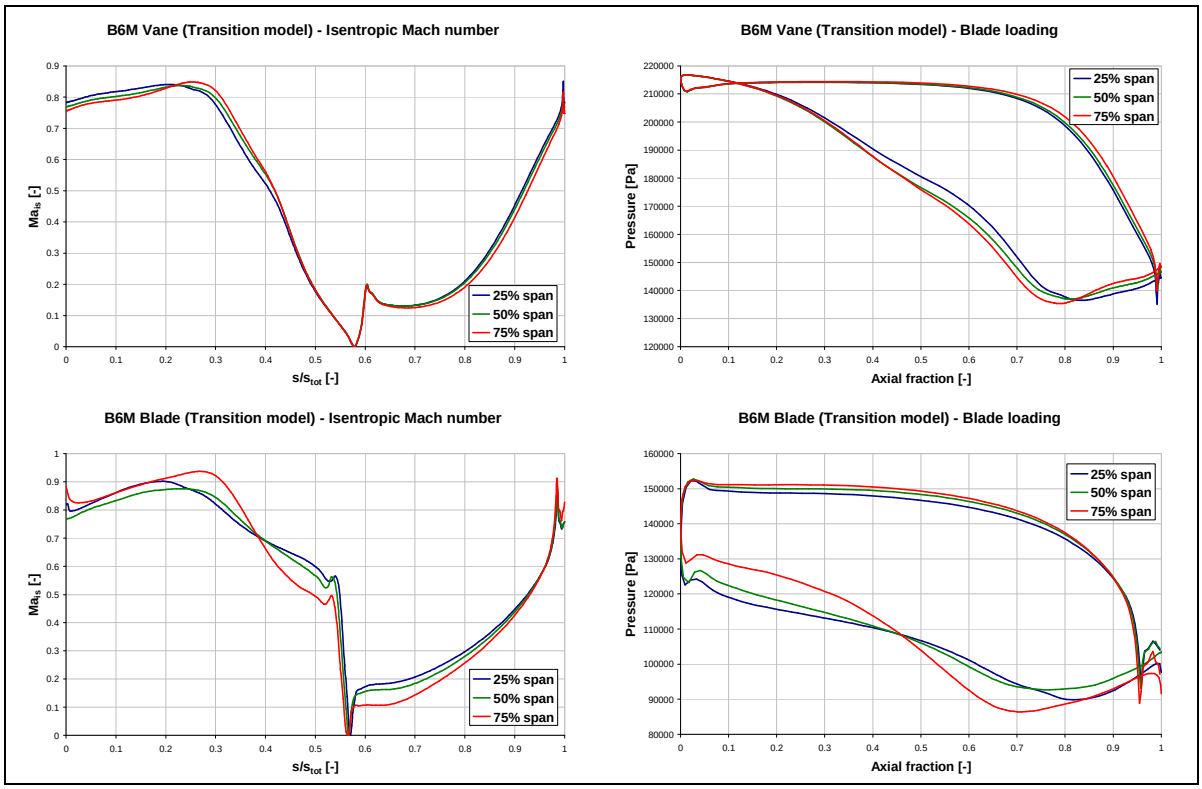

Figure 5-16 B6M - Isentropic Mach number and blade loading

5.3.3 B6M - Off-design

Design conditions are only achieved at a certain pressure ratio and rotational speed but the test turbine will run far from design during experiments. It is therefore interesting to explore how the turbine will behave at off design. The results from sweeps done in Beta2 with pressure ratios and values of stage loading corresponding to probable operating points can be seen below. Figure 5-17 to Figure 5-19 are plotted against total to static pressure ratio for 80%, 100% and 120% $N/\sqrt{T^*}$, where 100% is given by the value at design load (Π=2.139, ψ=1.37).

In Figure 5-17 the point of optimal efficiency moves to higher pressure ratios when increasing the speed parameter. At some point the curves flatten and become less sensitive, a consequence of turbine blades being relatively unaffected of arising incidence losses. This is a typical behavior encountered when studying turbines operating at off design, see Moustapha [2]. Figure 5-18 shows similar trends.

The flow capacity is not very susceptible to changes in the speed parameter, pressure ratio being the dominant driving force as seen in Figure 5-19. When the curve starts to become entirely horizontal the turbine has choked meaning the mass flow becoming independent of pressure ratio as soon as sonic conditions are reached in the blade throat.

Figure 5-20 and Figure 5-21 show approximately the same trends described above, though Figure 5-20 clearly indicates that the maximum efficiency is at a lower load than design load. This characteristic is deduced to the lack of cooling air which moves the maximum efficiency to a lower loading. Optimally the stage should be designed to have its maximum efficiency at the design load, this was however not possible with the vane geometry fixed.

The trend of an increase in degree of reaction with pressure ratio for a fix value of stage loading is shown in Figure 5-22. As the back pressure is fixed, increasing the pressure ratio will lead to a greater static pressure drop across the rotor compared to the stator and the degree of reaction will rise. It is seen that for low pressure ratios and high stage loading there is a sudden increase in reaction. For these cases the positive incidence is very large (>35˚) and it seems that the Beta2 code has problem to achieve physical results. Further studies in Beta2 in this region indicate numerical instability and the reliability cannot be verified.

Torque is increasing considerably with pressure ratio, stage loading having a significant, but still smaller, impact as seen in Figure 5-23. The pressure ratio dependency could be explained by the increase in mass flow together with the increased isentropic enthalpy drop over the stage. This is just a simplified way of explaining the trend in the figure to some extent.

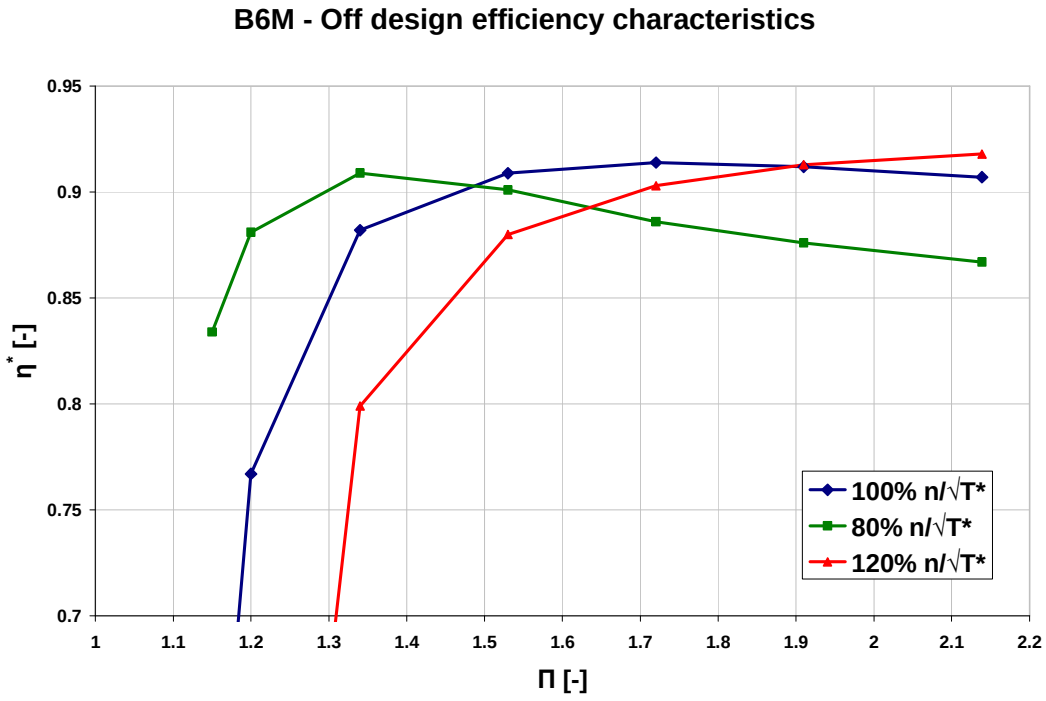

Figure 5-17 B6M - Total to total efficiency against pressure ratio (Beta2)

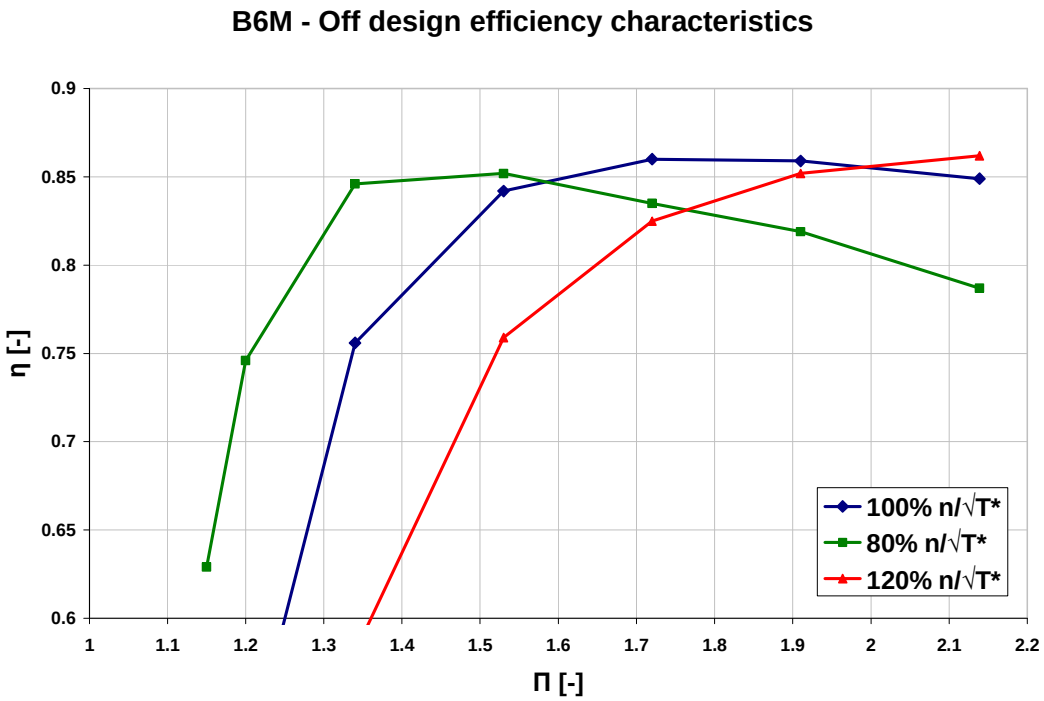

Figure 5-18 B6M - Total to static efficiency against pressure ratio (Beta2)

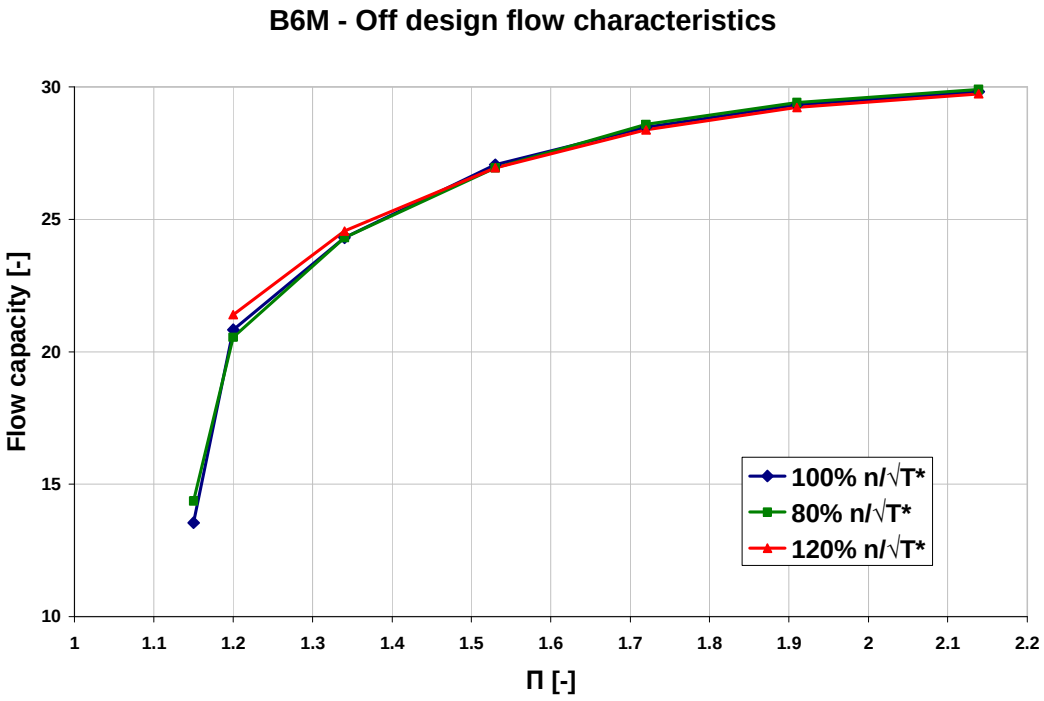

Figure 5-19 B6M - Flow capacity against pressure ratio (Beta2)

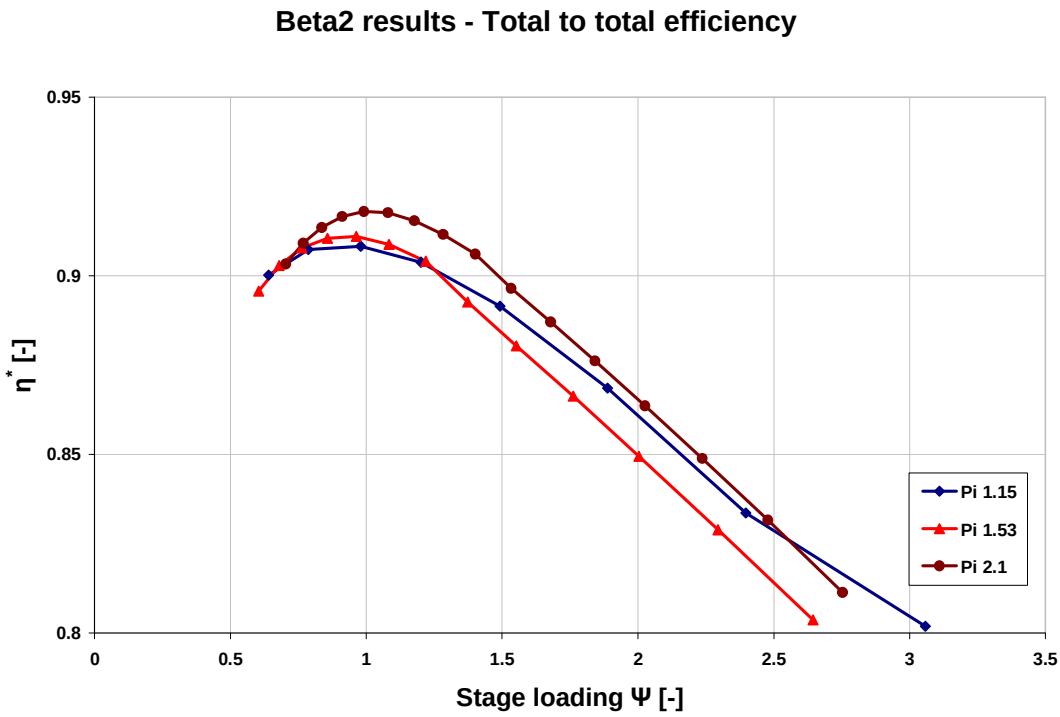

Figure 5-20 B6M - Total to total efficiency against stage loading (Beta2)

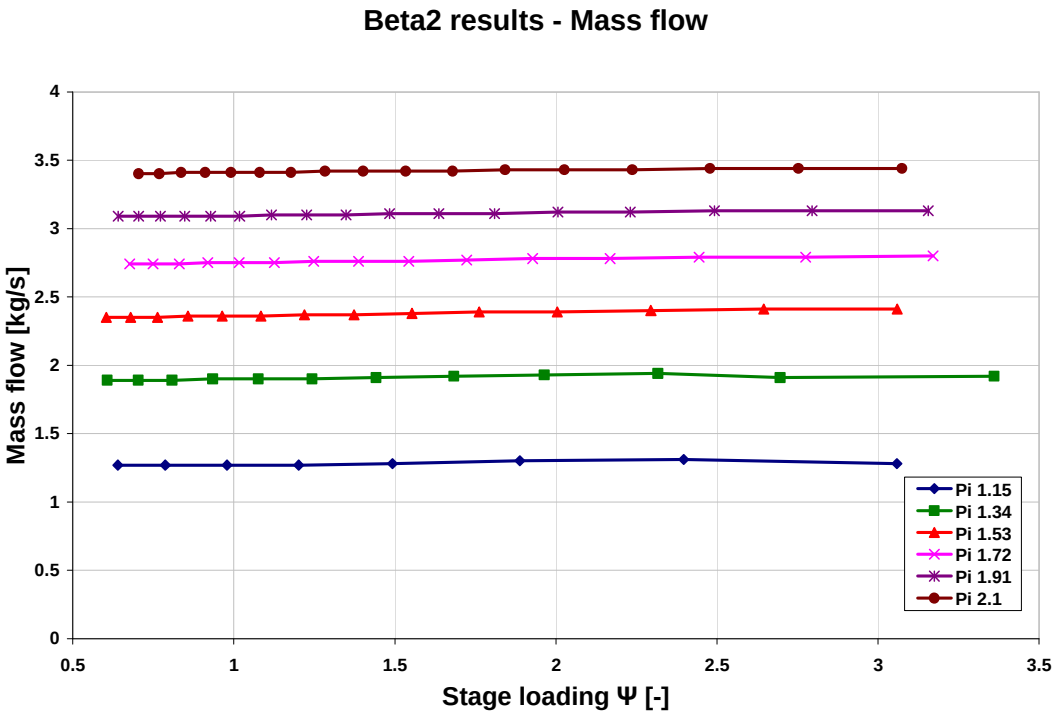

Figure 5-21 B6M - Mass flow against stage loading (Beta2)

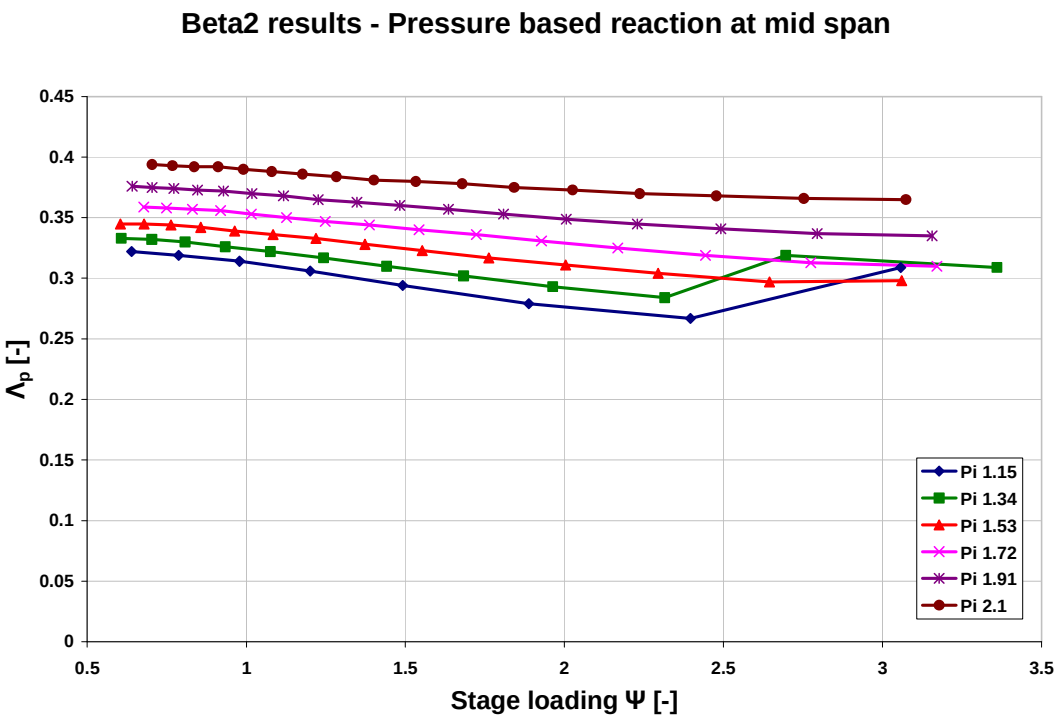

Figure 5-22 B6M - Reaction against stage loading (Beta2)

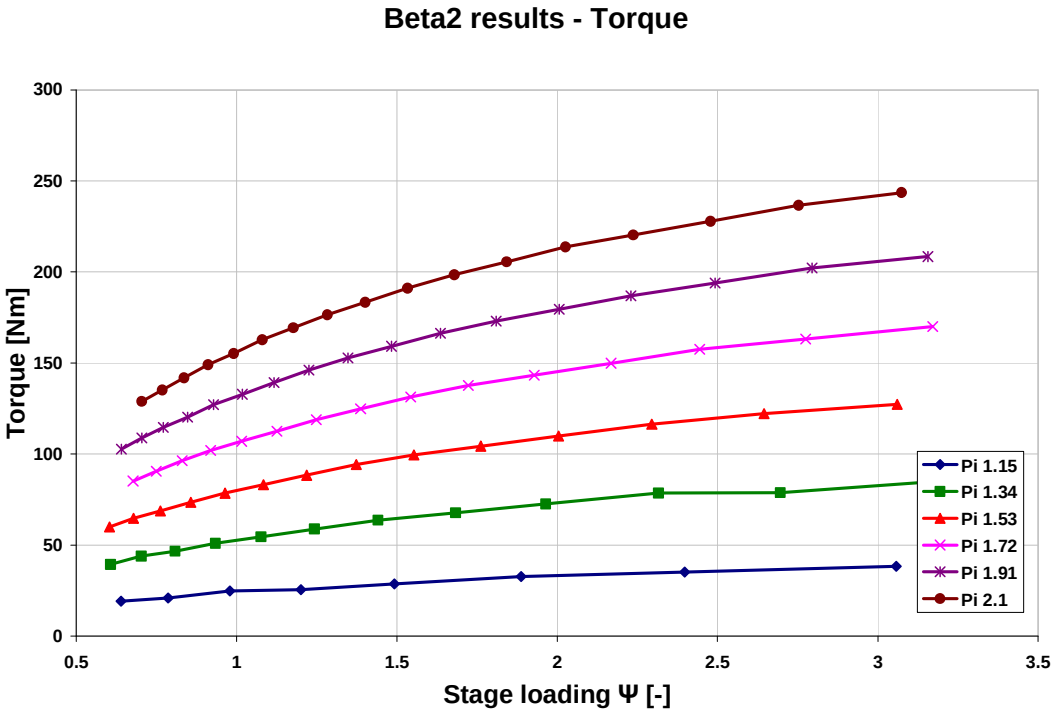

Figure 5-23 B6M -Torque against stage loading (Beta2)

5.4 Transition modelling

To evaluate the transition model used in CFX the skin friction coefficient was calculated along a surface line at mid span for the vane and the blade. The skin friction coefficient is a convenient parameter to consider when studying transition for different cases. A quick increase in skin friction indicates transition from laminar to turbulent boundary layer. The skin friction coefficient is defined as:

$$C_f \equiv \frac{\tau_w}{0.5 \cdot \rho_\infty \cdot C_\infty{}^2}$$

where the wall shear stress is defined as:

$$\tau_w = \mu \left. \frac{\partial u}{\partial y} \right|_w$$

The freestream values for the density and velocity was extracted at a distance of 0.75 - 1.5 mm from the wall surface outside the boundary layer and the wall shear stress is directly given by CFX at the surface. The result from the CFX cases with and without the transition model can be seen in Figure 5-24. In the full scale case transition occurs on the suction side at a distance about 45% from the leading edge for the vane whilst transition occurs almost immediately at blade leading edge according to the transition model. At model scale the transition model predicts completely laminar boundary layer on the suction side of the vane and transition at a distance about 55% from the leading edge at the suction side of the blade. The big difference between full and model scale is to be expected and is explained by the greater Reynolds number in the full scale case, which is about an order of magnitude greater, see Table 12. Table 10 shows the computed efficiencies for each case. In accordance with the skin friction coefficient calculation the predicted gain is greater at model scale.

A comment about the increase in skin friction for the model scale case close to the blade trailing edge has to be made. This is a local effect caused by a secondary flow vortex which interrupts the flow and increases the wall shear strain at the line from which the data is extracted. The vortex is still present in the Low-Re case but passes the blade at a greater radius, avoiding the mid span line.

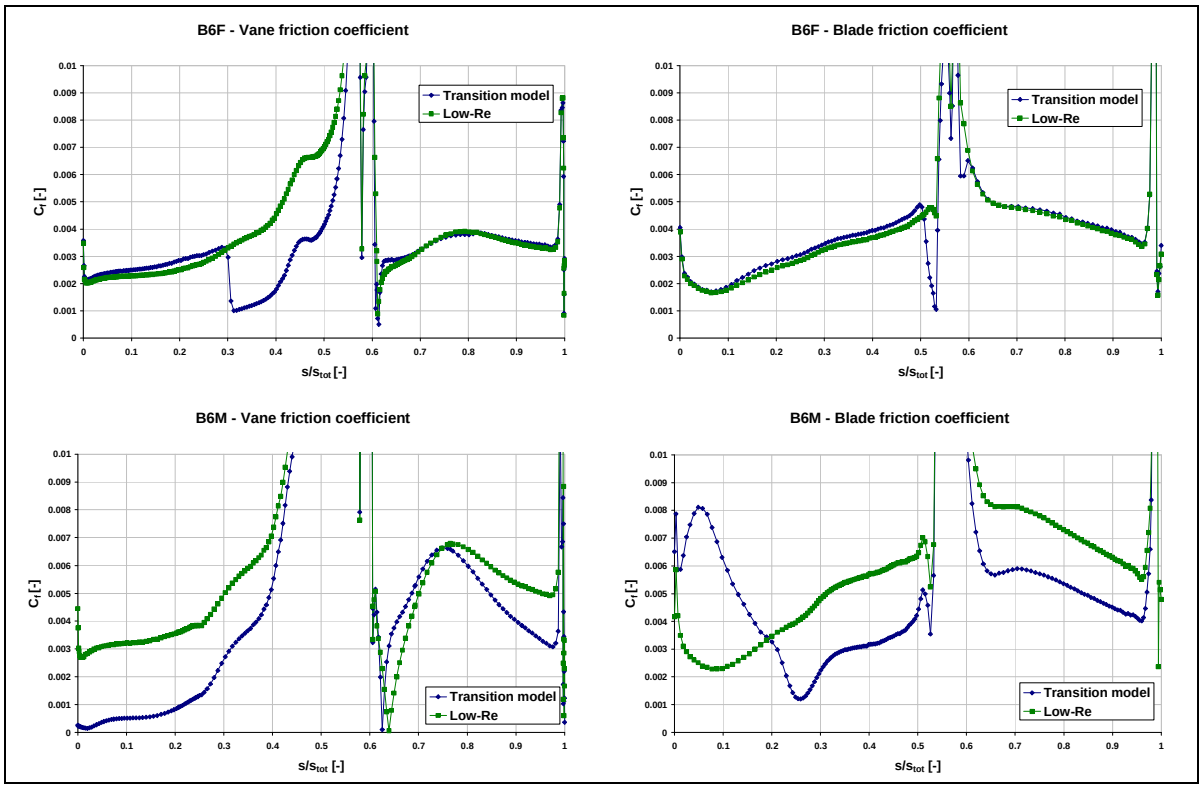

Figure 5-24 Skin friction coefficient at mid span

	B6F		B6M	
	Low-Re	**Transition**	**Low-Re**	**Transition**
η	0.8742	0.8754	0.8675	0.8722
η^*	0.9213	0.9232	0.9073	0.9190

Table 10 Transition model vs. Low-Re performance prediction

5.5 Result summary

A complete summary of B6F and B6M is shown in Table 11 to Table 13. The efficiency prediction differs between the codes as seen in Table 11. This is expected from previous experiences where 3D codes often give better performance. Without reliable experimental data the predictions are equally uncertain. Table 12 shows stage parameters as calculated by Beta2 for the reference stage, B6F, B6M and 4b at design load for corresponding turbine/stage. The task was to match the new design to the reference as good as possible and the B6F design accomplishes this as illustrated in Table 12. Comparing B6F and B6M the results are very similar and the main characteristics are maintained through the scaling back to model scale. The parameters for 4b at its design load are shown because of comparative reasons. Referring to stage loading and degree of reaction 4b has a considerably higher respectively lower value, typical of a steam turbine stage. The general aim to achieve characteristics more representative of an industrial gas turbine stage is accomplished via the B6M design.

	Beta2 1d	Multall	CFX Low-Re	CFX Tran
B6M η^* [-]	0.906	0.9141	0.9073	0.9190
B6F η^* [-]	0.904	0.9149	0.921349	0.923193

Table 11 Total to total efficiency code comparison

	Ref. stage	B6F	B6M	4b
Π [-]	2.139	2.138	2.138	1.23
ψ [-]	1.365	1.364	1.369	2.035
Φ [-]	0.407	0.428	0.425	0.396
$\Lambda_{p,mid}$ [-]	0.405	0.398	0.386	0.089
α_1 [°]	14.45	14.66	14.69	14.73
β_1 [°]	63.18	54.79	52.91	26.37
α_2 [°]	73.10	71.02	72.75	73.84
β_2 [°]	19.91	20.53	20.63	19.50
Ma_{1abs} [-]	0.794	0.797	0.781	0.532
Ma_{1rel} [-]	0.236	0.251	0.252	0.280
Ma_{2rel} [-]	0.812	0.811	0.78	0.323
Re_{1abs} [-]	30.3e5	29.3e5	6.9e5	3.1e5
Re_{2rel} [-]	16.0e5	20.7e5	4.9e5	2.1e5

Table 12 Stage parameters (Beta2)

	B6F			B6M		
Parameter:	**Hub**	**Mid**	**Tip**	**Hub**	**Mid**	**Tip**
r [mm]	430.44	462.21	493.97	177.50	190.60	203.70
d_1 [mm]	7.50	7.44	7.46	3.09	3.07	3.08
d_2 [mm]	2.80	2.80	2.80	1.15	1.15	1.15
β_{1m} [°]	56.18	61.83	66.36	56.19	61.83	66.36
β_{2m} [°]	18.96	18.93	18.88	18.95	18.93	18.88
ω_1 [°]	65.93	59.23	54.76	65.93	59.23	54.75
ω_2 [°]	9.75	9.66	9.60	9.73	9.66	9.61
δ [°]	22.27	22.53	23.20	22.28	22.53	23.20
t [mm]	60.10	64.54	68.97	27.78	26.61	28.44
b [mm]	75.65	76.46	77.46	31.20	31.53	31.94
B [mm]	61.13	57.72	54.48	25.21	23.80	22.42
t/b [-]	0.79	0.84	0.89	0.79	0.84	0.89
AR_{real} [-]	0.84	0.83	0.82	0.84	0.83	0.82
AR_{axial} [-]	1.04	1.10	1.17	1.04	1.10	1.17
d_2/b [%]	3.70	3.66	3.61	3.69	3.65	3.60
# of blades	45					
tip clearance [mm]	0.73			0.30		

Table 13 Section parameters (data from CATO)

6 Conclusions

A new blade design for the KTH test turbine has been presented in this thesis. The aerodynamic design of the blade is based on an industrial gas turbine, which acted as a reference. The design was performed at the reference scale and with similar gas conditions. A summary of the main conclusions:

- Full geometrical similarity between the reference blade and the B6M design was not possible because of manufacturing limitations and the chord had to be expanded. The aspect ratio is 0.83 for B6M which is considerable lower than for the reference. As a consequence the number of blades is much fewer for B6 compared to the reference.

- The metal angle was redesigned at full scale according to optimal incidence by Mamaev which resulted in a different blade twist compared to the reference blade, even though the meanline analysis indicated similar vane outlet flow angle. However, Beta2 and Multall06 predicted a great difference in blade inlet flow angel at relatively large regions near the hub and the tip due to lack of cooling flows. This resulted in a more uniform and almost linear twist compared to the reference blade. CFX predicted a similar result as Multall06 regarding blade flow angles and no redesign was considered due to the updated results.

- The final design at full scale B6F accomplishes the set target to mimic a reference stage although the test turbine vane geometry was maintained and no cooling was used. Both through flow and 3D calculations support this statement.

- At model scale the predicted result was very much similar and the general characteristics at full scale were well kept. However, since parameters as the Reynolds numbers and Mach numbers are smaller for a given load at model scale the predicted performance will differ in absolute values.

- According to the transition study in CFX both the vane and the blade at model scale experience laminar boundary layers to a much greater degree than at full scale. This effect must be considered when evaluating results from the test turbine.

7 Future work

The constraint of matching the axial chord at hub led to the reference blade profiles had to be enlarged in order to maintain the shape resulting in B6M. This design is the final result of this report complying with the requirement. During the work resulting in the final design no consideration has been taken to structural limitations. Regardless of design structural analysis must be performed considering the whole blisk (blade row and disc machined from one solid piece).

The scaling is based on the 4b geometry at cold conditions but was assumed to be at hot conditions, since the actual hot geometry of the blisk is not known. In reality centrifugal and thermal load will expand the dimensions somewhat. Even though conditions in the test turbine are far removed from what is normally expected in a gas turbine, some elongation will still occur. Of course this has to be investigated further before manufacturing can commence.

8 Appendix A

The mesh and y^+ statistics for B6F and B6M are shown in Table 14. In the full scale case the mesh had to be coarsened at the tip clearance region because of problem with numerical stability, resulting in larger y^+ values than desired. The effect of this is clearly seen in Table 14 where the maximum and average y^+ is considerable larger at full scale than small scale for the blade domain. According to a study regarding the effects of too large y^+ presented in the CFX Solver Guide [6], y^+ should be kept between 0.001 and 8 to effectively predict the transition point with the Gamma Theta transition model. This criterion could not be fulfilled at the tip in the full scale case but for the rest of the domain (values in parenthesis) the criterion is met. Since the flow at the tip clearance probably is fully turbulent anyway this compromise is not believed to have affected the transition model study in any major way. Figure 8-1 shows two computational domains in CFX for illustrative purposes. Only one passage is actually modeled and the result is mirrored to the other passages. The vane and blade mesh in the B6M case is shown in Figure 8-2 and Figure 8-3.

	Full scale			**Model scale**		
	Vane	**Blade**	**Outlet**	**Vane**	**Blade**	**Outlet**
# of elements	1943250	1551068	121720	1115400	2200581	153000
y^+ max	2.40	47.10 (7.60)	-	2.86	4.12	-
y^+ min	7.28e-3	8.69e-3	-	1.38e-2	1.42e-2	-
y^+ area averaged	0.98	3.66 (1.60)	-	0.84	0.54	-

Table 14 CFX mesh statistics

Figure 8-4 to Figure 8-7 shows contour plots of the total pressure at the vane and blade trailing edge for full and model scale respectively. Both the full and model scale result indicates that the vane is exposed to relatively small secondary flows while the main flow at the blade trailing edge is highly affected by secondary flows. In Figure 8-8 and Figure 8-9 is velocity vectors close to the surface and streamlines at the hub and tip shown. The figures clearly show the extent of the secondary flows in a low aspect ratio blade.

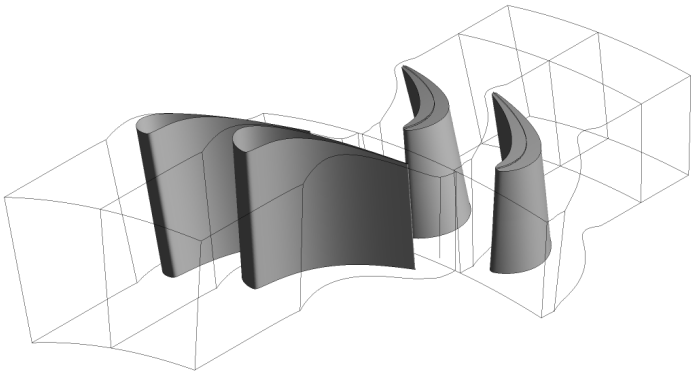

Figure 8-1 Domain overview

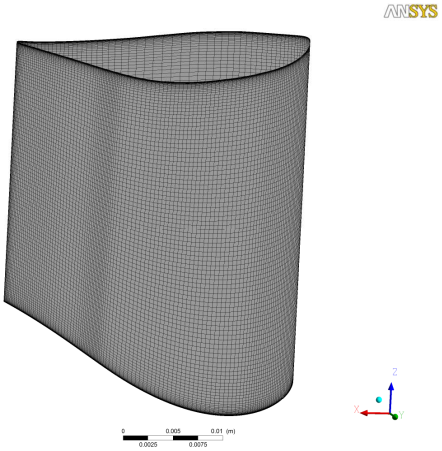

Figure 8-2 B6M Vane mesh

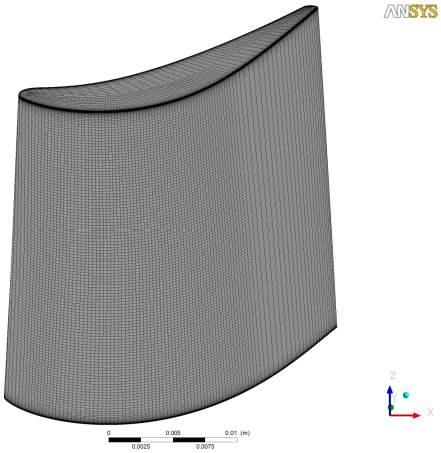

Figure 8-3 B6M Blade mesh

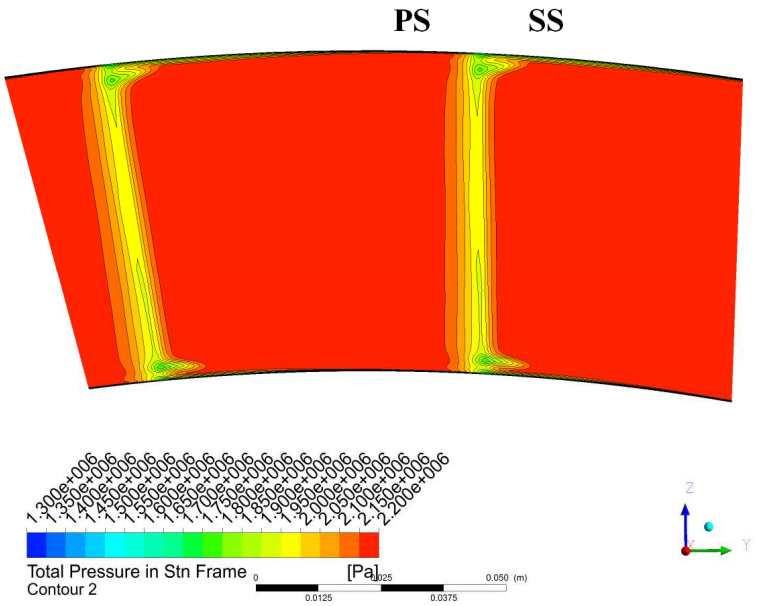

Figure 8-4 B6F - Vane TE looking upstream, total pressure

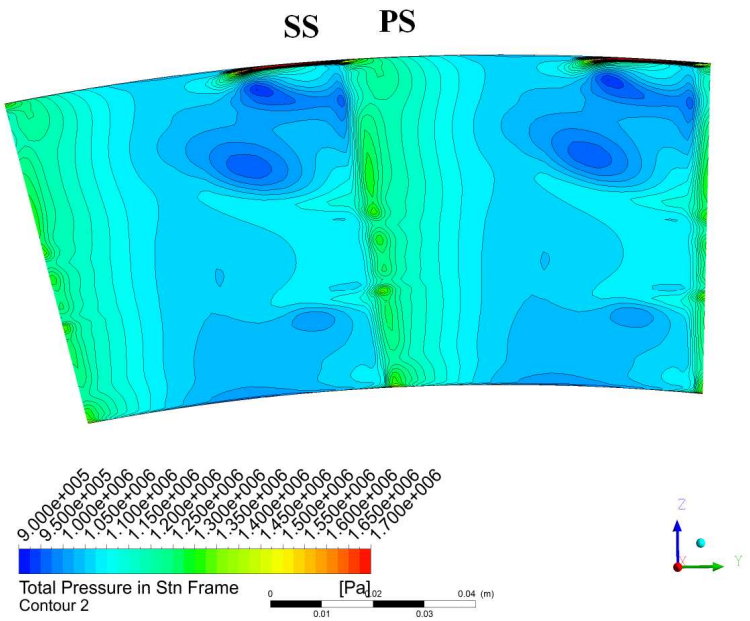

Figure 8-5 B6F – Blade TE looking upstream, total pressure

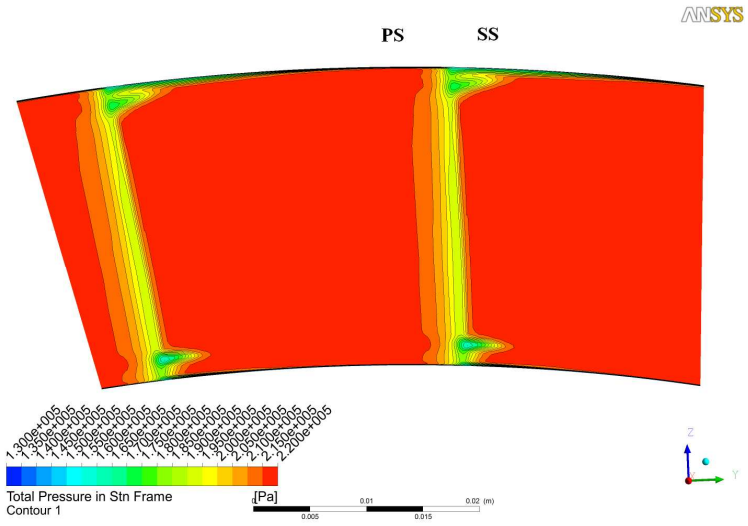

Figure 8-6 B6M - Vane TE looking upstream, total pressure

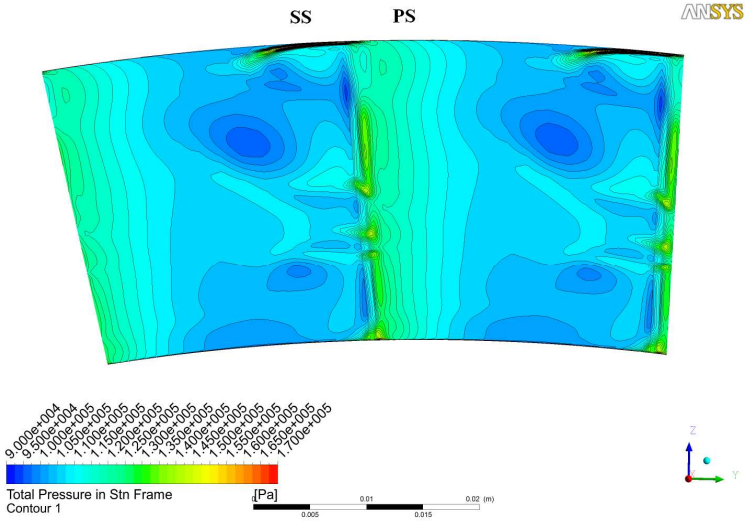

Figure 8-7 B6M – Blade TE looking upstream, total pressure

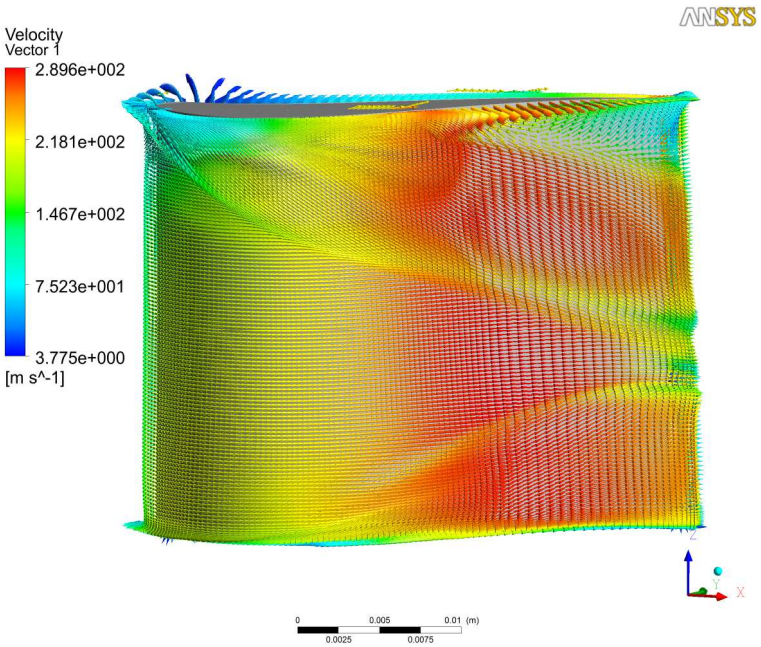

Figure 8-8 B6M – Blade, secondary flow vortices

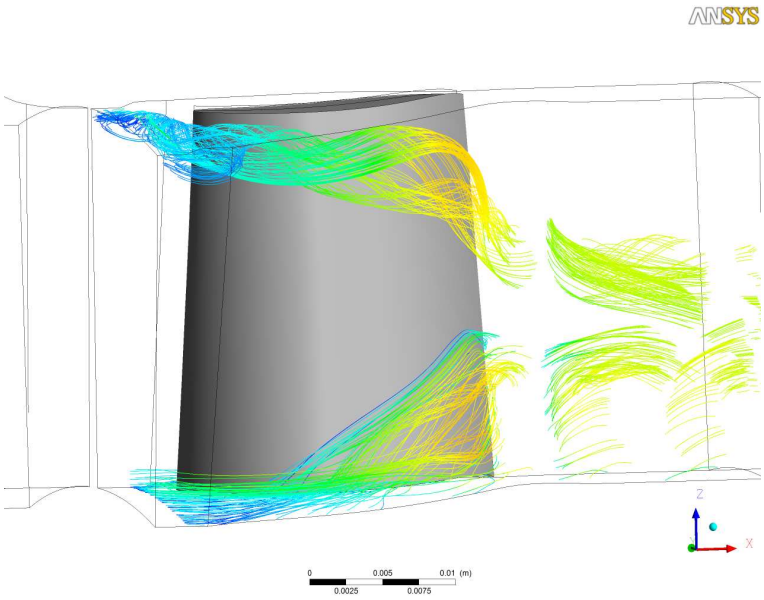

Figure 8-9 B6M – Blade streamlines

Bibliography

1) Saravanamuttoo, H.I.H., Rogers, G.F.C., Cohen, H., Straznicky, P.V *Gas turbine theory*. 6th Edition. London: Pearson Education Limited, 2009.

2) Moustapha, H., Zelesky, M.F., Baines, N.C Japikse, D. *Axial and radial turbines.* Vermont: Edwards Brothers Incorporated, 2003.

3) Dixon, S.L., Hall, C.A. *Fluid Mechanics and Thermodynamics of Turbomachinery*. 6th Edition. Burlington: Elsevier Inc., 2010.

4) Mamaev, B.I., Klebanov, A.G., *Loss model for vane/blade rows*. Moscow: Siemens Industrial Turbomachinery AB, 2007.

5) CFD-Online, 2012. Baldwin-Lomax model http://www.cfd-online.com/Wiki/Baldwin-Lomax_model (used 2013-03-03).

6) CFX-Solver Modeling Guide. *4.1.10. CFX Transition Model*. ANSYS, Inc, 2011.

7) Hedlund, L. *TurboAero Preliminary plan for Johan Dahlqvist's visit to Finspong in January 2013*. Finspong: Siemens Industrial Turbomachinery, 2013

8) Cengel, Y.A., Boles, M.A., *Thermodynamics: An Engineering Approach Sixth Edition (SI Units).* McGraw-Hill, 2007.

9) Genrup, M., Lecture notes from the courses MVKF05/MVK051 Lund: LTH Department of Energy Sciences 2012.

10) Hedlund, L., Li, Y.S., Mamaev, B.I., *On the aerodynamic design of turbines – Notes from meetings with Boris Mamaev*. Finspong: Siemens Industrial Turbomachinery, 2012.

11) Langtry, R.B., Menter, F.R., *Transition Modeling for General CFD Applications in Aeronautics*. Otterfing: ANSYS CFX, 2005.

12) Anderson, J.D., *Fundamentals of Aerodynamics.* 5th Edition. New York: McGraw-Hill., 2011.